On the acoustics of small partially open enclosures densely packed with active and passive installations

vorgelegt von
Dipl.-Ing. Jens Prager

Von der Fakultät V - Verkehrs- und Maschinensysteme
der Technischen Universität Berlin
zur Erlangung des akademischen Grades
Doktor der Ingenieurwissenschaften
Dr. Ing.

genehmigte Dissertation

Promotionsausschuss:

Vorsitzender: Prof. Dr. Ing. Paul Uwe Thamsen
Berichter: Prof. Dr. Ing. Michael Möser
Berichter: Prof. Henry Rice

Tag der wissenschaftlichen Aussprache: 08. 02. 2008

Berlin 2008

D 83

Declaration

I hereby declare that this thesis has not been previously submitted as an exercise for a degree at this or any other university. Except where otherwise acknowledged, the research is entirely the work of the author.

Contents

Declaration
Table of Contents
List of Symbols
Acknowledgements

ON THE ACOUSTICS OF SMALL PARTIALLY OPEN ENCLOSURES DENSELY PACKED WITH ACTIVE AND PASSIVE INSTALLATIONS 15

1 An introduction 17
2 References 24

WORK PACKAGE 1: ON THE SALIENT PHYSICS OF THE SOUND FIELD INSIDE SMALL FITTED ENCLOSURES 27

1 Introduction 31
2 Theoretical investigation 33
2.1 Modal synthesis for a rectangular enclosure 33
2.2 Modelling inserts 38
2.3 Simplifying the model 44
2.4 Velocity at the interface 49
3 Experimental investigation 52
3.1 Lab rig design 52
3.2 Transfer impedance measurement 54
3.3 Correlation between sources 58
3.4 Validity of the asymptotic results 60
4 Concluding Remarks 62
5 References 64

WORK PACKAGE 2: MODELLING THE SOUND FIELD BY USING NOVEL PROBABILISTIC APPROACHES 65

1 Introduction 69
2 Probabilistically distributed scattering objects 74
2.1 Volume effect 76
2.2 Scattering effect 77
2.3 Conversion schemes for the scattering behaviour 80
2.4 Illustration of the model 83
3 Probabilistically distributed wave guides 87
3.1 Modelling a system of coupled wave guides 87
3.2 Parameter variation 88
3.3 Illustration of the approach 91
4 Concluding remarks 93
5 References 95

WORK PACKAGE 3: IMPROVEMENTS ON THE STATISTICAL SOUND FIELD DESCRIPTION 97

1 Introduction 101
2 Interference patterns and SEA in rooms 102
2.1 Interference pattern 102
2.2 Statistical room acoustics 105
3 Interference patterns and SEA on plates 109
3.1 Interference Pattern 109
3.2 Statistical plate vibration 111
4 Concluding Remarks 115
5 References 116

WORK PACKAGE 4: CHARACTERISATION OF COMPLEX SHAPED SOUND SOURCES 117

1 Introduction 121
2 Modeling the test source 125
3 Reconstruction of an acoustic field 131
4 Shrinking of the reconstruction surface 135

5 Numerical example 140
6 Concluding remarks 145
7 References 146

CONCLUDING REMARKS 149

List of Symbols

Latin letters

a	length, radius
A	complex amplitude
$\mathbf{A}$	complex amplitude matrix
b	length
B	complex amplitude
$\mathbf{B}$	complex amplitude matrix
B'	bending stiffness
c	speed of sound
$C_n^{(\alpha)}$	Gegenbauer polynomial
d	diameter
E	energy
$\mathrm{Ei}(z)$	exponential integral function
∂f	modal spacing
F	force
$F(r)$	integral solution
g	complex number, damping coefficient
G	Greens function
$h(t)$	transfer function
$h_n^{(2)}(r)$	n-th order spherical Hankel function of second kind
$H_0^{(2)}(x)$	zero order Hankel function of second kind
I	sound intensity (in WP 2)
I	integer number (in WP 4)
$\mathbf{I}$	identity matrix
$j_0(x)$	zero order spherical Bessel function
J	integer number

k	wave number
Δk	wave number shift
l	length
l_m	mean free path
Δl	end correction term
L	sound pressure level
n	integer number (0, 1, 2,...)
$\vec{n}$	normal vector
∂n	deviation in normal vector direction
N	integer number
m	integer number (0, 1, 2,...)
m''	mass per unit area
p	sound pressure
$\mathbf{p}$	sound pressure vector
P	power
$P_n^m(x)$	associated Legendre function
$P_{mn}(r)$	complex amplitude (source strength)
q	volume velocity
$\mathbf{q}$	volume velocity vector
Q	scattering cross section
r	distance, radius
S	surface area
t	time
v	particle velocity
$\mathbf{v}$	particle velocity vector
V	volume
x	Cartesian co-ordinate
Δx	microphone distance
X	random variable
y	Cartesian co-ordinate
Y	mobility

Y^{∞}	input mobility of an infinite plate
$Y_n^m(\theta,\phi)$	spherical harmonic function
$\mathbf{Y}$	matrix of spherical harmonic functions
Y_{mn}^i	source strength of a multi pole component
z	Cartesian co-ordinate
$Z,\ Z'$	impedance, modified impedance
$\mathbf{Z}$	impedance matrix
Z_a	wall impedance
$Z_r = Z_r' + jZ_r''$	radiation impedance (real and imaginary part)

Greek letters

α	absorption coefficient
α	real positive number (in WP 4)
$\vec{\alpha}$	angular position
$\overline{\alpha}$	averaged absorption coefficient
β	length ratio
γ	modal overlap factor
$\Gamma(\alpha)$	Gamma function
δ	local variable
ε	local variable
η	dissipation loss factor
θ	latitude
λ	wave length
μ	mean value
ξ	local variable
ρ	density
σ	standard deviation
τ	impedance ratio
ϕ	longitude

$\mathbf{\Phi}$	position matrix
ψ_i	complex amplitude (source strength)
$\mathbf{\Psi}$	complex amplitude matrix
$\Psi,\ \Psi(S),\ \Psi(R)$	eigenfunction (on source and receiver position)
Ψ_n^{α}	normalisation constant
ω	angular frequency
Π	correction term

Acknowledgements

The research presented was undertaken during my employment as a research assistant at the Institute of Fluid Dynamics and Engineering Acoustics at the Technical University of Berlin and my EDSVS stay at the Department of Mechanical and Manufacturing Engineering at Trinity College Dublin. Most of the investigations were part of the EC-funded projects VISPeR (G1RD-99-00288) as well as SILENCE (TIP4-CT-2005-516288). The financial support received is gratefully acknowledged.

Fragments of this thesis are accepted for publication in the Journal of the Acoustical Society of America (JASA) and Acta Acustica united with Acustica (AAuA).

During the preparation of this work I have been assisted by numerous people. First and foremost, I wish to express my gratitude and appreciation to my supervisor Prof Björn Petersson. I wish to thank him for our many enlightening discussions, his boundless enthusiasm and his permanently open door. The assistance I have received was more than I had ever expected.

I wish to thank all postgraduates at TU Berlin, particularly Carsten Spehr, for their friendship, for the enjoyable collaboration, for always answering my questions and for helping me with their knowledge in acoustics and maths. I also wish to thank all technicians at the department for their assistance along the way. Special thanks to our secretaries.

Also I wish to thank Prof Henry Rice and all postgraduates at the Vibrations Lab for their warm welcome to Trinity College Dublin, Philip and Anton for their “legendary” hospitality in Dublin and Andreas for chatting incessantly.

My largest debt of thanks is owed to my parents for their willingness to sacrifice, for their support on my way to explore myself and for enabling my education and my academic career. Finally I wish to thank Torsten. Without his affection, understanding, encouragement and cheerfulness this PhD thesis would never have been written.

On the acoustics of small partially open enclosures densely packed with active and passive installations

1 An introduction

For a large class of technical artefacts, often several active and passive parts are enclosed by some structural casing. Such configurations can be found in, for example, manufacturing machines, white goods as well as in engine bays of passenger cars and trucks. More the rule then the exception, such units also constitute sources of sound. The sound generated by the active parts inside the casing partially couple to the exterior receiving field over the casing but above all, source and receiver are coupled at the apertures. For example, apertures are needed for air intake and outlet as well as for axle, pipe or cable passages. For appliances elevated some distance above the supporting structure, the bottom part of the casing is often completely open. A typical configuration of such a unit is sketched in Figure 1.

Although the characterisation of a source unit can be made experimentally on a prototype, the desire to shorten the lead time requires approaches for predictions.

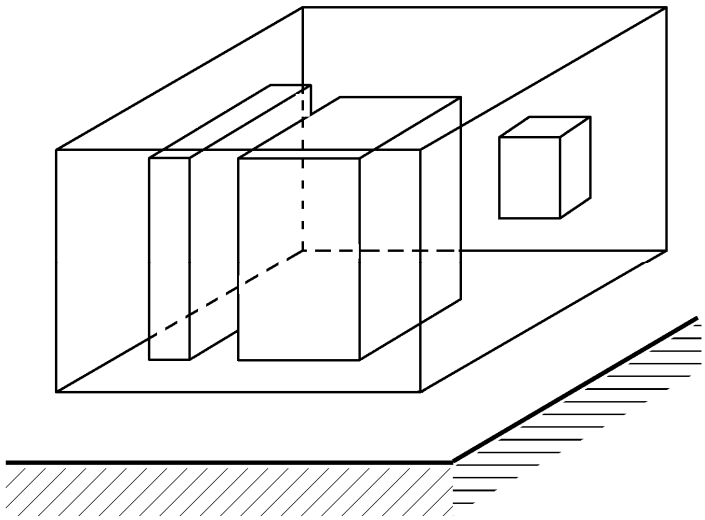

Figure 1: Simplified model of a machine configuration

To predict the sound radiation from such artefacts, the field inside the enclosure and the radiation problem can be handled separately by using different analysis methods. The result of this separation leads to an acoustic sub-grid-model approach. To couple the field inside the enclosure to that in the adjacent fluid, the complete sound field at coupling interfaces must be known. For this it is necessary to model the airborne sound

field inside the casing. The airborne sound field inside a small, partially or densely equipped enclosure, however, is problematic to describe in a deterministic way. The field varies radically with frequency because of the fact that the wavelength is either bigger, in the same dimension or smaller than the characteristic dimension of the source unit. This means among other things that several models are required to adequately handle the audible range.

Internally the source units can have a very complicated geometry consisting of complex shaped installations and appliances acting whether active as sound sources and/or as passive influences on the sound field. The surfaces of the installations as well as of the casing provide different surface impedances.

Further aggravating is that predictions are often requested already in the design stage, where the internal organisation and layout is not yet detailed. A numerical analysis, however, requires detailed information about the system under consideration, to obtain meaningful results. The results furnished by numerical methods can be to detailed to reveal the basic physical properties of the system and mask the insight into its salient physics. For these reasons precise numerical analyses establish no real alternative. Even if a numerical analysis is applicable, the requirements on exactness and complexity of the model geometry rise with increasing frequency. Additionally, with increasing frequency the number of nodes grows rapidly and with that also the calculation times and the requirements on calculation power. These requirements limit the applicability of the numerical methods.

The focus of the work presented is on developing approaches and methods for the analysis of the sound field inside small densely packed enclosures to complement the well known and widely used numerical methods. The work is featured by synthesis of existing knowledge supported by the presentation of novel approaches on different issues related with the underlying sound propagation problem. The methods presented should satisfy the requirements of the engineering practice with regard to flexibility, modelling effort and calculation time. Thereby the work is not aimed at an all-embracing and exact description of the complex system but rather at a collection of design guides and novel approaches applicable for the acoustic design.

The fundament of the investigations will be a deep insight in the salient physics of the underlying problem. This insight will be gained by analysing simplified geometries with

well known analysis tools. Concomitant the known analysis tools are investigated for their applicability on the given problem. For a wide range of applicability, however, appropriate analysis tools are not yet available. For those applications novel approaches are presented, designed by using probabilistic descriptions of the geometry inside the enclosure. The use of probabilistic approaches appears rather promising, particularly with a view towards the requirements of the design stage, as stated above. In the context of the development of novel approaches the knowledge of the salient physics is regarded to be very important. It enables the identification of the essential influences on the sound field which will be necessary for designing the probabilistic approaches.

The description of the sound field inside the enclosure is incomplete as long as the sound sources can not be included into the model. One possible scenario is that the characteristics of the sound source are available or at least determinable in a deterministic way. For most of the sound sources, however, their characteristics can only be determined by measurements. The measurement results have to be adapted to the requirements of the chosen sound field analysis tool. Hence, as part of the investigations, an approach is developed for determining a complete source description by using a weighted residuals method. Therein, the weighted residual method is extended for its applicability to complex shaped source geometries.

In the last few years a lot of work is published on the sound field prediction particularly with regard to application in automotive engineering and noise control. Approaches for analysing the sound field inside enclosures are suggested in [1]. In this textbook is shown the calculation of the sound field inside simply shaped, empty enclosures. For more complicated geometries the author recommends the use of Finite Element Methods (FEM). The usability restrictions of numerical methods like the recommended FEM, however, were already discussed in the previous paragraphs. Because the adaptation of FEM to the underlying problem is out of the scope of the work presented, no further publications on this method are discussed.

Various attempts have been made on the performance prediction of sealed and leaky acoustic enclosures (or hoods) used to reduce the noise emanating from machinery. The earliest attempts are made by Jackson [2] and refined by Junger [3]. Both Jackson and Junger only model the problem of coupling between machine and enclosure wall in

terms of two vibrating plates coupled via an air gap. Ver [4] presents a comprehensive and general analysis of the insertion loss of the enclosure at low and high frequencies. At low frequencies he describes the system in terms of coupled masses and compliances, whereas at high frequencies an energetic approach is used. At intermediate frequencies his approach is limited to empty and rectangular shaped enclosures. Lam and Hodgson [5] suggest a numerical method describing the sound field inside a cavity based on the Helmholtz integral and test its applicability in experiments for rooms with some 10 m³ volume. Byrne et al. [6] design a machine-mounted enclosure, describe its performance analytically and test it by experiments. Two models are presented by Oldham and Hillarby [7], [8] predicting the performance of enclosures for low and for high frequencies separately. Also in this investigation, the intermediate frequency region was considered inadequate. If any solutions are presented, then the results are only valid for empty rectangular enclosures. All attempts are limited to one source only and are focussed on the coupling between the source (machine) and the enclosure to predict the acoustic performance (insertion loss) of the enclosure.

The sound field inside an enclosure is experimentally investigated on simplified models of vehicle's passenger compartments by Gorman and Krylov [9]. Comparing different stages of simplification it is figured out a mode shift, possibly attributed to the increase in the effective length of the cavity due to the inserts. These results coincide with those found by Nefske et al. [10] using an FE model of the passenger compartment. The influence of enclosed equipment of rectangular shape can be calculated by the boundary perturbation theory described by Morse and Feshbach [11]. Smith et al. [12] validate the results experimentally. An approach for spherical inserts influencing the sound field is presented by Leung et al. [13]. Therein, a scattering approach is used for the approximation of the modal pattern. Also by Morse, Smith and Leung a resonance frequency shift is observed as result of volume exclusion and wave scattering. It is shown that this effect depends on the position of the inserted object.

Much work is published on the statistical treatment of the sound field inside enclosures and merged in the textbook by Lyon [14]. In all these descriptions a statistical distribution of the acoustical energy is assumed. As mentioned by Hodgson [15] this can not be argued valid e.g. if the absorption inside the enclosure is not equally distributed. In the 1950's Waterhouse [16], [17] published some papers on the efficiency of sound sources near reflecting walls. It is shown that interferences of the first order reflection can not

be neglected. This seems to be important especially for small enclosures where the sources likely are mounted close to the walls.

As an alternative to the well known numerical methods, different statistical approaches have been presented for predicting the sound field in large fitted rooms like factory halls. By using the concepts of a random diffusion process Kuttruff [18], Lindqvist [19] and Le Pollès et al. [20] have developed mathematical models describing the expected density of sound particles. Counting the particles passing a certain spatial position at a given time, an equivalent to the energy density is found. Ondet and Barbry [21] suggested a modified ray tracing approach. In this approach the probability density functions of fittings in the room is modelled by means of walls of varying degrees of reflectivity. Unfortunately, the approaches summarised are inappropriate for small enclosures. This is so since the condition that the wavelength must be much smaller than the characteristic size of the reflecting objects is not fulfilled. Nevertheless, the results of those statistical approaches are promising examples for the applicability of probabilistic approaches also for the intermediate frequency range.

The acoustical sub-grid technique which combines the use of different analysis methods for different spatial domains of the sound propagation problem has been studied in structural dynamics where deterministic models have been successfully interfaced with probabilistic [22], [23]. It is expected that the findings can be transferred to the underlying air-borne sound propagation problem.

All references discussed above, represent a solid fundament for the investigation presented in the following. For the investigation, the entire amount of work initially was subdivided in four separate work packages embracing the investigation of the salient physics of the sound field inside densely packed small enclosures and the development of extended or novel approaches for the sound field prediction. Accordingly, the results of each work package are presented in separate parts. The work packages are subdivided as follows.

Work Package One, concerns detailed investigations on the salient physics of the sound field inside small enclosures and provides the fundament for subsequent investigations. Therefore the complex geometry is simplified to those suitable with analytical methods. By using the analytical methods basic acoustical properties are extracted. Based on the analytical results theoretical models are developed to handle the low, intermediate and

high frequency region separately. The results of the analytical investigations will also be uses as a benchmark for further investigations and the assessment of the applicability of the novel approaches. In a second step, the analytical modelling is extended for the determination of influences of the enclosed equipment. Focus is on the influence of the installations to the modal pattern which mainly governs the physics at intermediate frequencies. The investigations will be complemented by the results of experiments for those issues not describable with the analytical methods. Thereby also the effect of interferences in a multiple source configuration will be regarded. The validity of the results from the simplified modelling is checked by comparing the results with those measured on a real technical device.

Starting from the validity and applicability limitations of the theoretical models developed in Work Package One, Work Package Two and Three concern approaches to overcome these limitations. Major concern is given the intermediate frequency range where the size of the enclosure is of the same dimension as the wavelength. Therefore, in Work Package Two, two different probabilistic approaches are suggested for handling complicatedly filled domains in this frequency range. These approaches model either the installations or the free fluid space. In the first approach a probability density distribution is assumed including the number and size of the objects installed. Depending on the wavenumber, the main physical effects of the scatterers and their probability distribution are combined to get a simplified description of the field. In a second approach the free fluid space is modelled as set of coupled one dimensional wave guides. The results are discussed together with the standard deviation and compared with FEM results.

Although in Work Package One, the Statistical Energy Analysis (SEA) was found to be appropriate for analysing, the diffuse field assumption employed in SEA and in statistical room acoustics is violated for source positions close to boundaries or discontinuities as shown in Work Package One. Thus, in Work Package Three, an approach is suggested to include the correction made by Waterhouse based on spherical Bessel functions in SEA-predictions. With this modification the SEA-results will be augmented by a position dependence and an additional frequency dependence. For the sake of completeness the approach is extended and demonstrated for plate-like structures. The validity of the approach is confirmed by means of comparisons with analytical results from Work Package One.

The fourth work package concerns the sound sources. An investigation is presented of the reconstruction of sound field parameters close to the surface of arbitrarily shaped sound sources. This provides the insertion of the sound sources into the sound field prediction. The field is reconstructed using Nearfield Acoustical Holography (NAH) in spherical co-ordinates. Of particular interest are source shapes where the Rayleigh hypothesis is violated. To overcome the limitation of the minimal sphere given by the validity restriction of the Rayleigh hypothesis, an algorithm is proposed for extracting local information from the non convergent NAH-solution. For the assessment of the results an appropriate virtual test rig is developed employing the Kirchhoff-Helmholtz-Integral-Theorem.

The separation of the work into work packages is mainly done to facilitate the findings of every sub task to be applied without reference and supplement of the other parts. This also provides the use of this work as a collection of design guides for the design engineer. Hence, the references are listed for each work package separately and overlapping of contents may occur.

2 References

[1] L. Beranek and I. Ver, Noise and Vibration Control Engineering. (John Wiley and Sons, Inc. New York, 1992).

[2] R. S. Jackson, "The performance of acoustic hoods at low frequencies," Acustica **12**, 139-152 (1962).

[3] M. C. Junger, "Sound transmission through an elastic enclosure acoustically coupled to a noise source," ASME Paper No. 70-WA/DE-12, (1970).

[4] I. L. Ver, "Reduction of Noise by Acoustic Enclosures. Isolation of Mechanical Vibration, Impact and Noise," Proceedings of the ASME Design Engineering Technical Conference, Cincinnati, 192-220 (1973).

[5] Y. W. Lam and D. C. Hodgson, "The prediction of the sound field due to an arbitrary vibrating body in a rectangular enclosure," J. Acoust. Soc. Am. **88**, 1993-2000 (1990).

[6] K. P. Bryne and H. M. Fischer and H. V. Fuchs, "Sealed, Close-Fitting, Machine-Mounted Acoustic Enclosures with Predictable Performance," Noise Control Engineering Journal **31**, 7-15 (1988).

[7] D. J. Oldham and S. N. Hillarby, "The acoustical performance of small close fitting enclosures, Part 1: Theoretical models," J. Sound Vibr. **150**, 261-281 (1991).

[8] D. J. Oldham and S. N. Hillarby, "The acoustical performance of small close fitting enclosures, Part 2: Experimantal investigation," J. Sound Vibr. **150**, 283-300 (1991).

[9] R. Gorman and V. V. Krylov, "Investigating the acoustic properties of vehicle compartments," Acoustic Bulletin, **Sept./Oct.**, 8-14 (2004).

[10] D. J. Nefske and J. A. Wolf and L. J. Howell, "Structural-Acoustic Finite Element Analysis of the Automobile Passenger Compartment: A review of Current Practice," J. Sound Vibr. **80**, 247-266 (1982).

[11] P. M. Morse and H. Feshbach, *Methods of Theoretical Physics, Part II*. (McGraw-Hill, New York, 1953).

[12] M. E. Smith and T. W. Moore and H. W. Nicholson, "Wave Phenomenon in an Acoustic Resonant Chamber," Am. J. Phys. **42**, 131-136 (1974).

[13] E. Leung and C. P. Lee and N. Jacobi and T. G. Wang, "Resonance frequency shift of an acoustic chamber containing a rigid sphere," J. Acoust. Soc. Am. **72**(2), 615-520 (1982).

[14] R. H. Lyon and R. DeJong, *Theory and application of statistical energy analysis*. (Second Edition, Butterworth-Heinemann, 1995).

[15] M. Hodgson, "When is the diffuse-field theory applicable?" Applied Acoustics **49**(3), 197-207 (1996).

[16] R. V. Waterhouse, "Interference Patterns in Reverberant Sound Fields," J. Acoust. Soc. Am. **27**(2), 247-258 (1955).

[17] R. V. Waterhouse, "Output of a Sound Source in a Reverberation Chamber and Other Reflecting Environments," J. Acoust. Soc. Am. **30**(1), 4-13 (1958).

[18] H. Kuttruff, "Über den Nachhall in Medien mit unregelmäßig verteilten Streuzentren, insbesondere in Hallräumen mit aufgehängten Streuelementen," Acustica **18**, 131-143 (1967).

[19] E. A. Lindqvist, "Sound Attenuation in Large Factory Spaces," Acustica **50**, 313-328 (1982).

[20] T. Le Pollès and J. Picaut and S. Colle and M. Bérengier, "Sound-field modelling in architectural acoustics by a transport theory Application to street canyons," Phys. Rev E **72**, 046609-1 – 046609-17 (2005).

[21] A. M. Ondet and J. L. Barbry, "Modelling of sound propagation in fitted workshops using ray tracing," J. Acoust. Soc. Am. **85**(2), 787-796 (1989).

[22] R.S. Langley and V. Cotoni, "Response variance prediction in the statistical energy analysis of built-up systems", J. Acoust. Soc. Am. **115**(2), 706-718 (2004).

[23] P.J. Shorter and R.S. Langley, "Vibro-acoustic analysis of complex systems", J. Sound Vibr. **288**, 669-699 (2005).

Work Package 1:

On the salient physics of the sound field
inside small fitted enclosures

Abstract:

The sound propagation inside a small partially open enclosure densely packed with active and passive installations is difficult to describe. For predicting the sound propagation from sound sources inside to an interface coupling the field to the adjacent fluid, appropriately simplified models are developed.

Emphasis is put on an analytical treatment to gain insight into the salient physics. Additional effects are included into the modelling to improve the validity of the prediction.

A lab rig model is developed for the assessment of the analytical approaches and for advanced investigations on the acoustic behaviour. Finally the reliability of the results is proven by comparison with those from dedicated experiments made on real technical devices.

1 Introduction

The focus of the work done in this work package is on gaining insight into the salient physics of the sound propagation inside densely packed small enclosures with complex geometry. Those configurations can be found in a considerable class of applications in engineering practice.

It is assumed a simplified configuration to have the same asymptotic behaviour as those, complex and fully equipped. It is expected, that the results of a modal expansion done for a simplified system reveal an asymptotic behaviour which will be found in a modified manner in any derived and rather complex configuration of the equipped enclosure. Further it is assumed that the salient physics exposes an asymptotic behaviour which is similar in any system with similar geometries.

Taking all these assumptions into account, the complex geometry of the system is initially simplified to those suitable for the investigations with analytical methods. The problem is reduced to an empty, hard walled enclosure of very simple shape. This means that all appliances inside the enclosure are removed and the complex wall impedances are neglected. This concerns the apertures and the opening at the bottom side as main perturbations in particular. Subsequently, the modelling is extended for the determination of the influences of different wall impedances and of the installations enclosed.

Finally a lab rig with geometry similar to those used for the analytical investigation is developed. The lab rig is used for complementing the findings of the analytical investigations with those influences not predictable with analytical methods. Additionally, the lab rig is used for the verification of the analytical results. The validity of the results found with the simplified modelling and therewith the validity of the assumptions regarding the applicability of the modelling results on derived, more complex geometries is proven by comparing with those measured on a real technical device.

In the following investigation the transfer impedance is chosen as an appropriate descriptor for the sound field. The transfer impedance thereby describes the coupling from a source position to a receiver point. Hence, it can be used to determine the sound pressure and velocity pattern at the surface of the openings and therewith on the inter-

face to the adjacent fluid. As the transfer impedances in two comparable systems are similar, the physics inside as well as the acoustic behaviour are assumed comparable. Thus, transfer impedances are also capable criterions for the assessment of the modelling.

2 Theoretical investigation

2.1 Modal synthesis for a rectangular enclosure

Firstly, the simple rectangular cavity as shown in Figure 1a) is investigated analytically. All walls are assumed rigid. The assumption of rigid walls can be argued valid at least for plates with a high mass per unit area with the exception of some narrow frequency bands at the first eigenfrequencies of the wall. For thin steel plates, however, the wall becomes flexible in abroad frequency range.

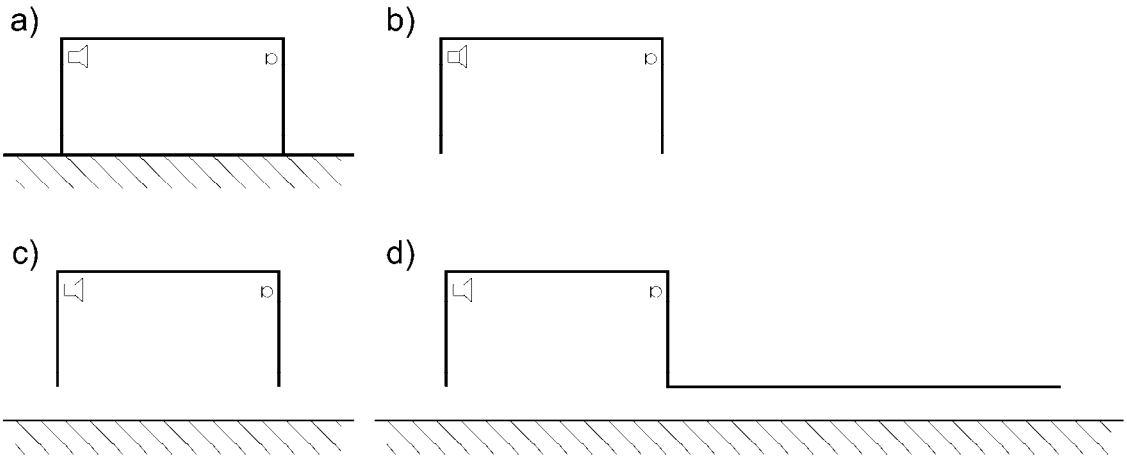

Figure 1: Investigated configurations of the enclosure. a) completely closed, b) bottom side open, radiation to free field, c) open with modified radiation impedance, d) partially open bottom side.

The transfer impedance of this simplified geometry can be calculated by means of a modal synthesis. With all walls rigid, the mode shape of the empty rectangular enclosure is simply given by e.g. [1.1]

$$\Psi_N = \cos\left(\frac{\pi n_x x}{l_x}\right)\cos\left(\frac{\pi n_y y}{l_y}\right)\cos\left(\frac{\pi n_z z}{l_z}\right), \tag{1}$$

where the enclosure dimensions are l_x, l_y and l_z respectively. The eigenvalues are given by

$$k_N^2 = \left(\frac{\pi n_x}{l_x}\right)^2 + \left(\frac{\pi n_y}{l_y}\right)^2 + \left(\frac{\pi n_z}{l_z}\right)^2; \qquad n \in N. \tag{2}$$

The transfer impedance, defined as the ratio of pressure to volume velocity, can be calculated from

$$\frac{p}{q} = jk\frac{\rho c}{V}\sum_N \frac{\Psi_N(S)\Psi_N(R)}{k_N^2 + jg_N k_N - k^2}, \tag{3}$$

where ρ is the density, V is the volume and c is the sound speed. S and R denote the source and receiver co-ordinates respectively. The losses inside the enclosure are included in the damping coefficient g_N.

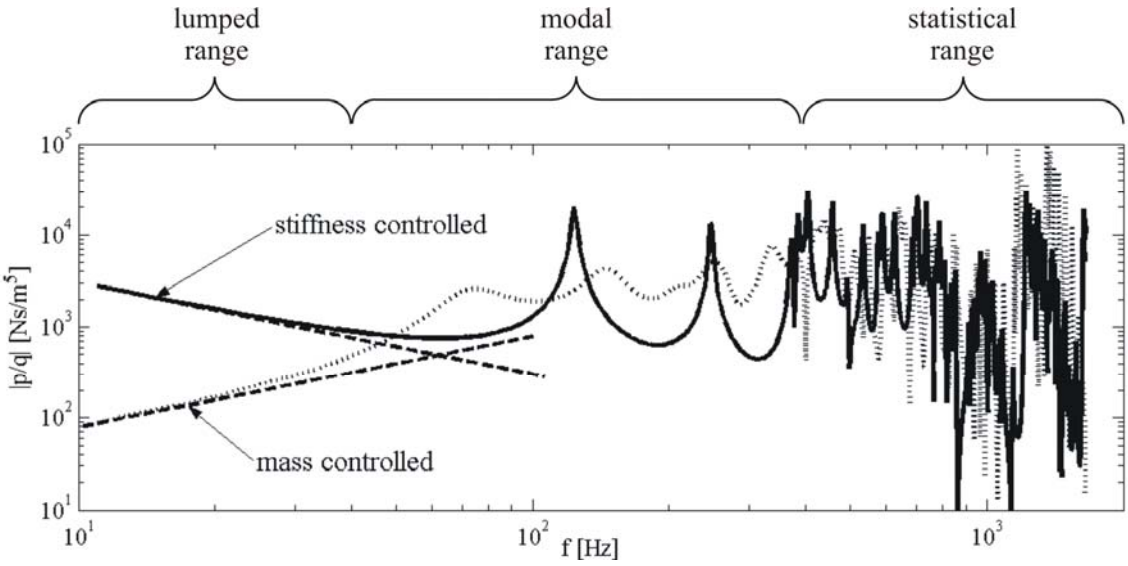

Figure 2: Transfer impedance for closed (—) and opened (·····) box and their ranges. The dashed lines indicate the approximation at low frequencies. The results are calculated for a box of 1.4 x 0.9 x 0.6 m³. Source and receiver are mounted in opposite corners.

The solid curve in Figure 2 shows an example of the calculated impedance for the simplified boundary conditions for a specific source and receiver position.

To simulate a more general case encompassing arbitrary surface impedances at the side walls of the cavity, the modal approach has to be modified. Due to the complex wall

impedances the eigenvalues become complex. This leads to an adapted modal synthesis [1.2]. Assuming complex wall impedances for one wall, the now complex eigenvalues are given by

$$k_N^2 = \left(\frac{\pi n_x}{l_x}\right)^2 + \left(\frac{\pi n_y}{l_y}\right)^2 + \left(\frac{\pi g_z}{l_z}\right)^2; \quad n \in N; \quad g \in C \tag{4}$$

and the modal function gets a complex component in z direction as well such that

$$\Psi_N = \cos\left(\frac{\pi n_x x}{l_x}\right)\cos\left(\frac{\pi n_y y}{l_y}\right)\cosh\left(\frac{\pi g_z z}{l_z}\right). \tag{5}$$

The modified transfer impedance therefore is

$$\frac{p}{q} = jk\frac{\rho c}{V}\sum_N \frac{\Psi_N(S)\Psi_N(R)}{k^2 - k_N^2}. \tag{6}$$

With the assumption that the damping of the system due to the complex impedance is much higher then the dissipation inside the enclosure initially contained in the value g_N in Eq. (3), the damping coefficient can be neglected.

To satisfy the boundary condition at $z = l_z$ the resulting complex eigenvalue problem can be described by [1.2]

$$\tanh(\pi g_z) = j\left(\frac{2\tau l_z}{\lambda g_z}\right), \tag{7}$$

wherein the wall impedance Z_a is introduced as the ratio

$$\tau = \frac{\rho c}{Z_a}. \tag{8}$$

The analytical solution of these equations is generally not an alternative. By application of a numerical routine the search for the eigenvalues can be simplified. In the numeri-

cal routine both sides of equation (7) are equated for real and imaginary part separately. In a second step the interception points between the resulting curves of the real and imaginary part are determined. The numerical routine developed for solving the problem performs a sequential eigenvalue search. Therefore the correct starting condition is needed. The starting condition, however, changes after an eigenvalue is found. The correct generation of the starting condition is essentially to ensure that all eigenvalues within a certain interval are found. The absence of some of the values will lead to serious errors in the impedance calculation. For the calculation process a visual cross-check of the validity of the results is helpful and also feasible because of the fact that the number of needed eigenvalues is limited due to the limited frequency range of interest.

The wall impedance Z_a of the open side of the box (see Figure 1b)) is given by its complex radiation impedance. Whereas at low frequencies the velocity is constant over the whole aperture, at high frequency a modal pattern appears. The modal pattern can be handled only with difficulties. Therefore, as an approximation the open side wall impedance Z_a is set to the radiation impedance Z_r seen by a baffled piston radiating into the free space [1.3].

The approximation neglects the modal pattern which appears above the first eigenfrequency and also adds a baffle. It is expected that both modification will limit the validity of the approach especially at low and intermediate frequencies. At low frequencies the baffle which does not exist in reality distorts the model. The influence of the baffle is shown in [1.3] by comparing the baffled and the flanged circular piston. There it is shown, that the error diminishes with increasing frequency. For high frequencies, where the modal pattern on the aperture comes into play, the radiation impedance of a piston converges to ρc. Therefore, the error resulting in neglecting the modal pattern is expected mainly in the frequency range where the first eigenfrequencies appear.

As at first presented by Burnett [1.4] and also published in [1.3] the real and imaginary parts of the radiation impedance of a piston $Z_r = Z_r' + jZ_r''$ with the side length ratio $\beta = b/a$ is given by

$$\frac{Z_r'}{\rho c} = 1 - \frac{2}{\pi\beta\left(ka\right)^2}\left[1 + \cos\left(ka\sqrt{1+\beta^2}\right) + ka\sqrt{1+\beta^2}\,\sin\left(ka\sqrt{1+\beta^2}\right) - \cos\left(ka\right) - \cos\left(ka\beta\right)\right] + \frac{2}{\pi\sqrt{\beta}}\cdot I_a\left(ka,\beta\right) \tag{9}$$

and

$$\frac{Z_r''}{\rho c} = \frac{2}{\pi\beta\left(ka\right)^2}\left[\sin\left(ka\sqrt{1+\beta^2}\right) - ka\sqrt{1+\beta^2}\,\cos\left(ka\sqrt{1+\beta^2}\right) + ka\left(1+\frac{1}{\beta}\right) - \sin\left(ka\right) - \sin\left(ka\beta\right)\right] - \frac{2}{\pi\sqrt{\beta}}\cdot I_b\left(ka,\beta\right) \tag{10}$$

with the integral expressions

$$I_a\left(ka,\beta\right) = \int_{\sqrt{\beta}}^{\sqrt{\beta+1/\beta}} \sqrt{1-\beta/x^2}\,\cos\left(xka\sqrt{\beta}\right)\cdot dx + \beta\int_{\sqrt{\beta}}^{\sqrt{\beta+1/\beta}} \sqrt{1-1/\left(\beta x\right)^2}\,\cos\left(xka\sqrt{\beta}\right)\cdot dx \tag{11}$$

and

$$I_b\left(ka,\beta\right) = \int_{\sqrt{\beta}}^{\sqrt{\beta+1/\beta}} \sqrt{1-\beta/x^2}\,\sin\left(xka\sqrt{\beta}\right)\cdot dx + \beta\int_{\sqrt{\beta}}^{\sqrt{\beta+1/\beta}} \sqrt{1-1/\left(\beta x\right)^2}\,\sin\left(xka\sqrt{\beta}\right)\cdot dx \tag{12}$$

which can be calculated numerically. For the open bottom side of the enclosure given by $a = l_x = 1.4$ and $b = l_y = 0.9$ the side length ratio is $\beta = 0.65$. The resulting transfer impedance is shown in Figure 3.

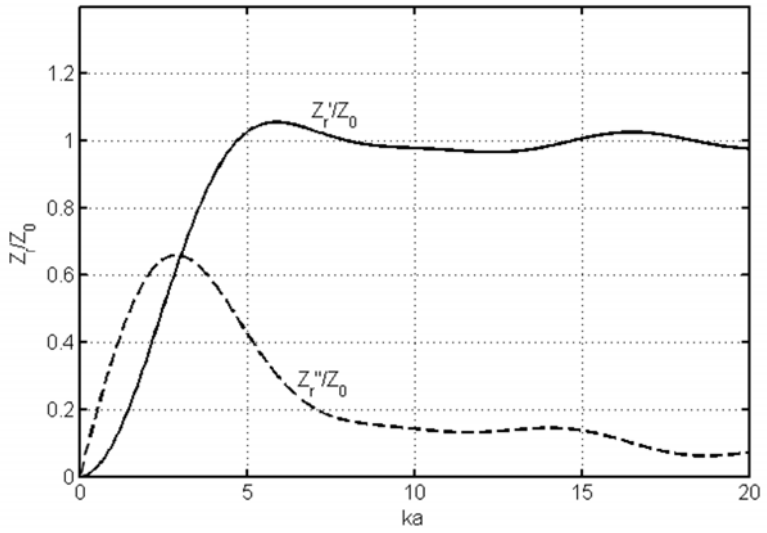

Figure 3: Real and imaginary part of the radiation impedance $Z_r = Z_r' + jZ_r''$ of a baffled rectangular piston normalised to $Z_0 = \rho c$.

Using these results the transfer impedance for the described configuration is depicted as dotted line in Figure 2. Comparing the completely rigid and the open case it is seen that essentially only the quasi-static range is affected from including the complex wall impedance Z_a into the model. The transfer impedance now exhibits a mass controlled behaviour. The eigenfrequencies become more damped, which confirms the assumption of additional damping due to the opening made for the damping inside the system. Due to the degeneration of the wave components perpendicular to the opening only a subset of modes remains.

2.2 Modelling inserts

The next step is to extend the modelling of the simplified empty enclosure by inserting installations. The installations, however, have to be simplified to ensure an analytical handling of the problem. Therefore, for the following investigations it is assumed, that the auxiliaries inside the enclosure can be taken to be rigid bodies. Their shape is restricted to be rectangular. According to [1.5] a volumetric and a scattering effect are expected due to the presence of such bodies in the sound field. It is expected that both effects perturb the modal pattern and shift the resonance frequencies.

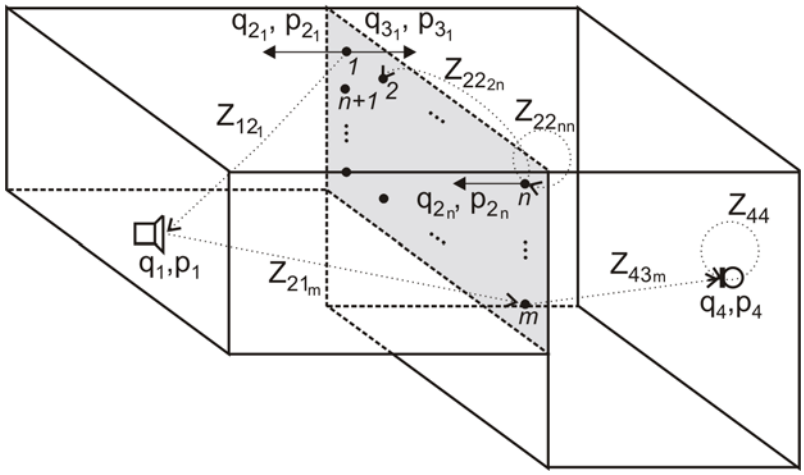

Figure 4: Underlying four-pole-problems for two coupled rooms with the coupling points 1...m. $\mathbf{p}_2$, $\mathbf{p}_3$, $\mathbf{q}_2$, $\mathbf{q}_3$, $\mathbf{Z}_{12}$, $\mathbf{Z}_{21}$, $\mathbf{Z}_{34}$ *and* $\mathbf{Z}_{43}$ *become m-row-vectors, whereas* $\mathbf{Z}_{22}$ *and* $\mathbf{Z}_{33}$ *become m-times-m-matrices, with m as the number of coupling points.*

By neglecting the volume and assuming rigid bodies of two-dimensional extent and a size at least at dimensions close to that of the wavelength, the inserts can be considered in a way, that they subdivide the cavity inside the enclosure into coupled subcavities. With these assumptions the shift of the resonance frequencies can be investigated.

The modal solution in each subcavity can be handled with the same analytical approach as described in Eq. (3) and (6). With an appropriate coupling condition at the interface between the subcavities, the transfer impedance for an arbitrary source and receiver position can be calculated. The coupling conditions at the interface are continuity in acoustic pressure and velocity. Both acoustical field variables are distributed over the interface area. To solve this problem the area has to be discretised. By discretising the interface and assuming a number of coupling points all impedances $\mathbf{Z}_{mn}$ and $\mathbf{Z}_{mm}$ of the underlying four-pole-problem become matrices as depicted in Figure 4. For the left subcavity the four-pole-equation is given by

$$\begin{pmatrix} \mathbf{p}_1 \\ \mathbf{p}_2 \end{pmatrix} = \begin{pmatrix} \mathbf{Z}_{11} & \mathbf{Z}_{12} \\ \mathbf{Z}_{21} & \mathbf{Z}_{22} \end{pmatrix} \begin{pmatrix} \mathbf{q}_1 \\ \mathbf{q}_2 \end{pmatrix} \tag{13}$$

and for the right subcavity with the indices 3 and 4 respectively. Therefore the coupling conditions at the interface area are $\mathbf{p_2} = \mathbf{p_3}$ and $\mathbf{q_2} = -\mathbf{q_3}$. Solving this set of equations and summing up all paths given in matrix $\mathbf{Z_{41}}$ the transfer impedance between source and receiver position can be determined from

$$\frac{p_4}{q_1} = \mathbf{Z_{41}} = \mathbf{Z}_{43} \cdot \mathbf{Z}_{21} \cdot \left(\mathbf{Z}_{22} + \mathbf{Z}_{33}\right)^{-1}. \tag{14}$$

For modelling a simply shaped, multi-dimensionally extended insert with a volume, a model of three coupled rooms can be used. Belonging to Figure 5, the transfer impedance from source position 1 to receiver position 6 can be calculated as

$$\frac{p_6}{q_1} = \mathbf{Z}_{65} \cdot \left[\left(\mathbf{I} - \mathbf{Z}_H \mathbf{Z}_{34}\right)^{-1} \mathbf{Z}_H \mathbf{Z}_{21} \right] \tag{15}$$

with

$$\mathbf{Z}_H = \left(\mathbf{Z}_{55} + \mathbf{Z}_{44}\right)^{-1} \mathbf{Z}_{34} \left(\mathbf{Z}_{33} + \mathbf{Z}_{22}\right)^{-1} \tag{16}$$

and $\mathbf{I}$ the unity matrix.

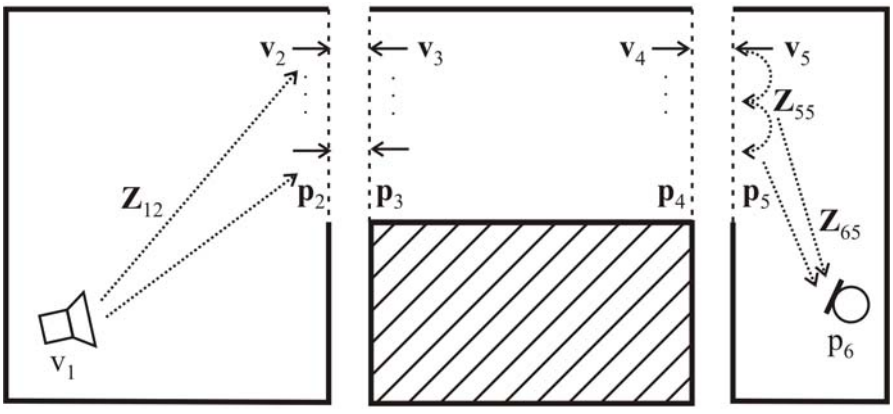

Figure 5: More-dimensional case of three coupled rooms. Some examples of the velocity-, pressure- and impedance-matrices are depicted. The marked range can be seen as an insert.

With Eq. (13) to (16) the sound field inside an enclosure can be investigated for different arrangements of inserts. In Figure 6 the result is depicted for a thin partition wall mounted at the centre of the widest box dimension and closing two-thirds of the cross sectional area. Comparing this result with those calculated for the empty box, the expected influence on the eigenmodes can be seen. The frequencies of the resonances are shifted downwards. Additional resonances appear and the modal density rises. The wavelength of the now downwards shifted, first eigenmode can be interpreted as the extension of the direct path between the parallel side walls of the enclosure due to the inserted partition wall. The additional resonances are generated between the enclosure walls and the newly inserted parallel wall.

In Figure 7 the position of the partition wall is varied along the x-axis within the first half of the box. As one can see, the spatial dependence of the resonance frequency shift of the perturbed first eigenmode follows a sinusoidal behaviour. This curve for the first eigenfrequency in x-direction is consistent with the results presented in [1.5] for a thin disk inside a rectangular box. Just as in [1.5], the effect of the inserted 2-D hindrance results only in a downward shift of the resonance frequencies.

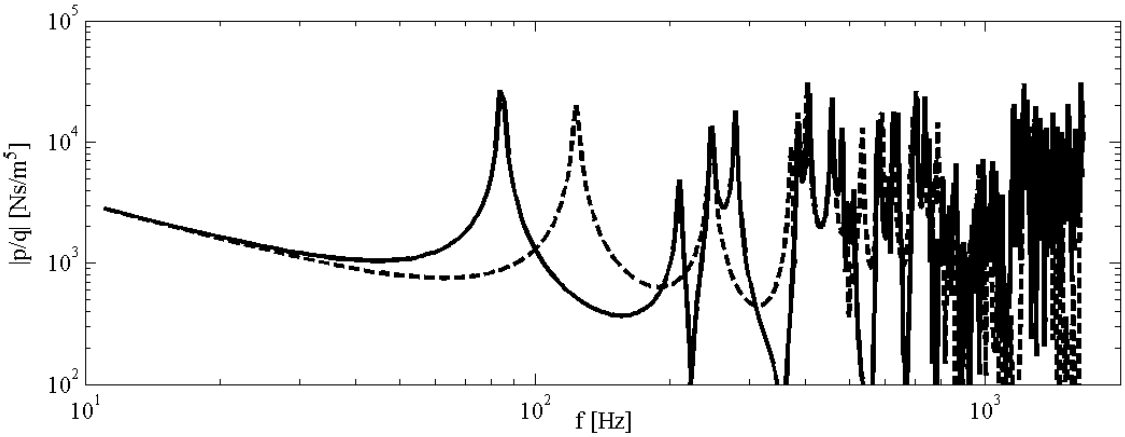

Figure 6: Transfer impedance measured inside the closed box; empty case (---) and with a partition wall mounted at the centre of the box closing two-thirds of the cross-section (—). The coupling interface between the two sub-cavities is discretized with 32 coupling points.

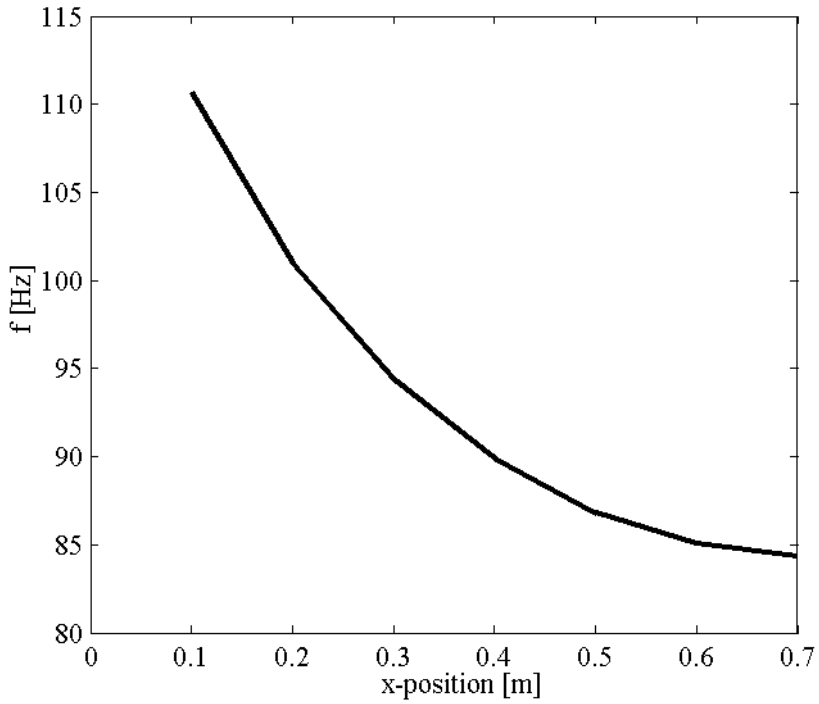

Figure 7: Shift of the resonance frequency for the first mode in x-direction due to a partition wall.

The results in [1.5] for three-dimensional extended spherical inserts show an increase of the resonance frequencies if the insert is placed close to an enclosure wall. For this case the modal density remains unaffected. In contrast to these results an increased number of eigenmodes can be seen in Figure 6. It is easily comprehensible that different sets of eigenfrequencies are generated due to the different shapes of the inserts.

It is obvious, that the knowledge about influence of the installations on the sound field inside the enclosure is essential for further investigations on alternative probabilistic approaches presented in Work Package Two. Hence, in the following the underlying physics should be investigated more detailed.

Figure 8a) and b) explain the influence of a hindrance on the modal pattern. In these plots the modal pattern for the second eigenmode in x-direction is shown. Strictly spoken, the system gets a completely new modal pattern due to the inserted hindrance. Nevertheless, as a simplification will be proposed assuming that only one wave component is influenced. By inserting a hindrance at an arbitrary position, the distance be-

tween two parallel side walls becomes longer and the first eigenmodes are shifted downwards in frequency Figure 8a).

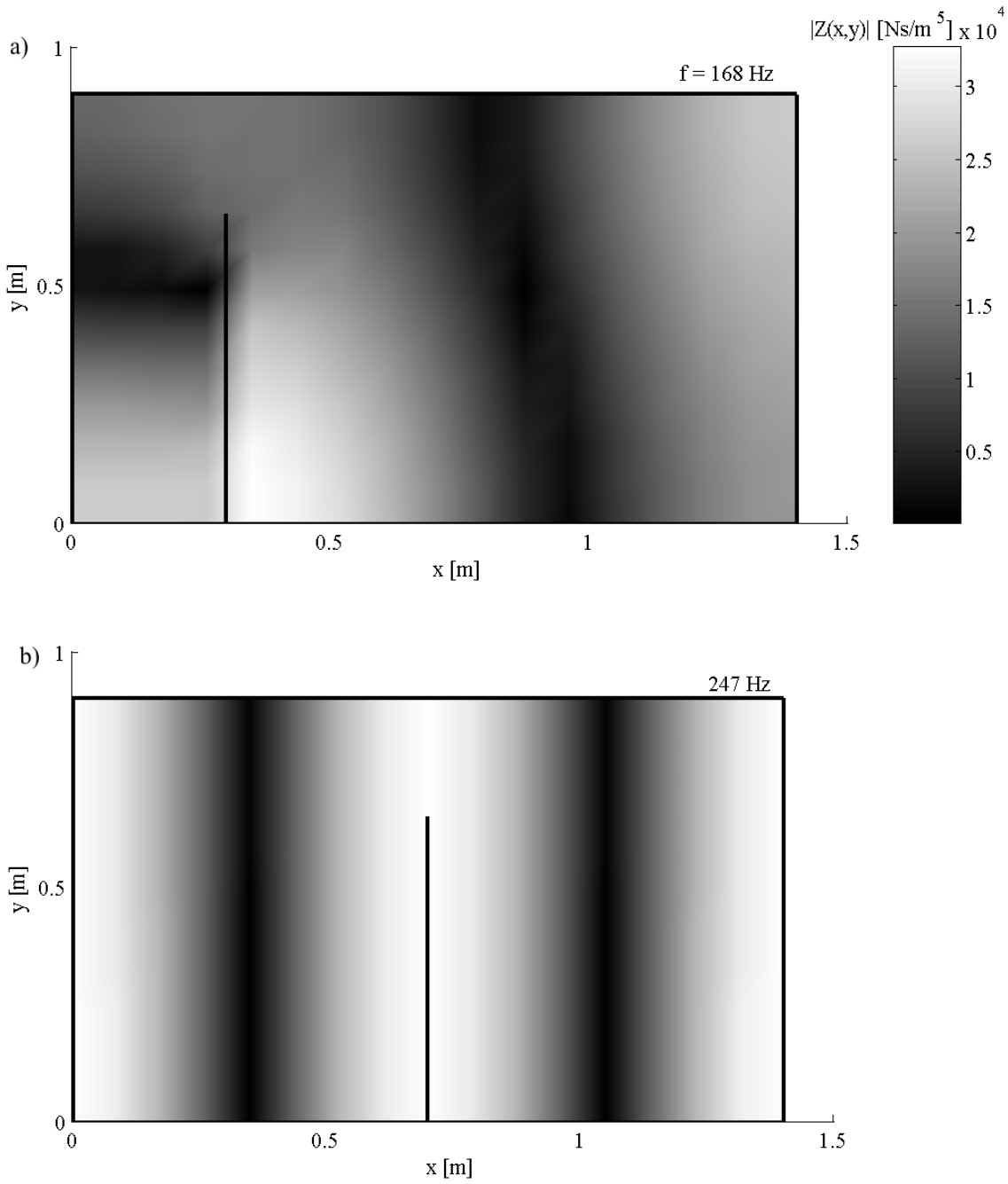

Figure 8: Variation in the modal pattern of the second mode in x-direction due to the influence of a partition. a) Modal pattern deformed and propagated in the longest sub-cavity dimension. b) Sound field unaffected.

For the special case where the hindrance is positioned at a velocity minimum, the modal pattern remains unaffected Figure 8b). Although there is no exact analytical description of the influence of partitioning the cavity, the resonance frequencies of the first eigenmodes can be approximated by measuring the free distance between two reflecting walls trough the system of sub-cavities flanked by the inserted objects.

Important for the propagation direction of the waves establishing the modal pattern is the relation between longitudinal and transversal dimension of the sub-cavity as can be seen by comparing the left and right side in Figure 8a). This insight has a bearing on a simplified analysis of an acoustical system introduced in the following paragraphs but especially on the probabilistic approaches presented in Work Package Two. It is obvious, that the modal pattern depicted in Figure 8a) suggests a possibility to model the sound field as system of coupled wave guides.

2.3 Simplifying the model

It is fundamental, that for analysing an acoustical system the ratio between wavelength and physical dimension of the structure is of particular importance and was also demonstrated by the results and findings of the previous analytical investigations. As the acoustical behaviour of the system changes with increasing frequency, the methods for analysing the physics become different. Although doable, the modal synthesis rapidly becomes time-consuming as the bandwidth of interest grows. For an effective and less time consuming calculation it can be necessary to subdivide the frequency range of interest and use the most appropriate analysis tool in each range. This is obvious, because the results of the modal analysis are not condensed enough to generate only the asymptotic behaviour. In the next paragraphs appropriate analysis tools for each frequency range will be suggested and investigated for their applicability. It may be necessary to simplify the system under consideration with regard to the used tool. For instance it can be helpful to neglect parts of the geometry which have no influence due to their ratio of size to wavelength.

Upon considering the curves in Figure 2, three different frequency regions in the calculated results are distinguished. These three frequency regions and their relating dominant physical behaviour are:

- Low frequencies – quasi-static behaviour
- Intermediate frequencies – modal behaviour
- High frequencies – statistical behaviour

Subsequently, models for each of the frequency regions are studied.

I. The lumped system

At low frequencies, the system behaves quasi-statically like a spring for the closed box and as a mass for the open box. In this region, a modal pattern for the sound field does not appear. The calculation of this simple lumped system will be easy because their main parameters of influence are the stiffness of the free volume and a mass plug formed at the openings. The lumped system is independent of the shape of the free fluid volume and therewith also of the configuration of the inserts inside the enclosure.

For a closed box the transfer impedance can be calculated by using the stiffness of the free fluid volume V inside the enclosure

$$Z = \frac{p}{q} = \frac{\rho c^2}{j\omega V}. \tag{17}$$

If the box is partially open and the opening is wide enough, the mass like behaviour becomes predominant. The mass is simply given by the air plug at the opening. For such a mass-controlled system the transfer impedance is readily given by

$$Z = \frac{p}{q} = \frac{j\omega m''}{S} \tag{18}$$

wherein S is the area of the opening and the mass per unit area

$$m'' = \Delta l \cdot \rho \tag{19}$$

is approximated by the end correction term for a rectangular opening given in [1.3]

$$\frac{2\cdot\Delta l}{l_x}=\frac{1}{3\pi}\left(1+\frac{1}{\beta^2}\right)\left(1-\sqrt{1-\beta^2}\right)+\frac{1}{\pi}\left[\frac{1}{\beta}\ln\left(\beta+\sqrt{1+\beta^2}\right)+\ln\left(\frac{1}{\beta}\left(1+\sqrt{1+\beta^2}\right)\right)\right] \quad (20)$$

with l_x and l_y being the dimensions of the box and

$$\beta = l_x/l_y \leq 1\,. \quad (21)$$

The resulting curves for a closed rectangular box and those with one side open are shown as dashed lines in Figure 2.

II. The modal range

The second range comprises the first few, distinct eigenfrequencies. In this region, the sound field is more complicated in nature. A detailed modal analysis seems to be necessary. Unfortunately, the applicability of the modal analysis is limited to simple shapes. Another possible way to investigate the system in the modal range is realized by the Finite Element Method with all the restrictions as stated previously.

In the modal range no asymptotic behaviour is identifiable. However, an average curve in conjunction with an uncertainty may be predicted. It is thus evident that an analysis tool is desirable, which essentially focuses on the salient physics. Those approaches are presented in Work Package Two.

III. The statistical range

At high frequencies, the field is increasingly diffuse in nature. With this it is evident to apply a statistical description of the field. Such a statistical method can be the Statistical Energy Analysis (SEA).

If the modal density is high enough, a crude SEA model leads to the required asymptotic behaviour for the transfer impedance. In this frequency range the sound field is mainly influenced by the absorption inside the enclosure as well as the coupling and therefore the energy losses to the environment. For the simplest case of a partially open box the SEA model consists of one room with dissipation. The energy inside the cavity is given by [1.6]

$$P_{in} = \omega \eta E \tag{22}$$

wherein P_{in} is the imparted power, η is the dissipation loss factor and E the energy inside. For a cavity, the dissipative loss depends on the absorption and the volume V. The absorption is composed of two parts. The first part is the equivalent absorbing surface $S_w \bar{\alpha}$, with the wall surface of the enclosure S_w and its mean absorption coefficient $\bar{\alpha}$. The second is the absorption of the openings. Owing to the fact, that the modal density outside the enclosure becomes infinite, the openings of the box can be assumed as total absorbing surface S_{open} with $\alpha = 1$. With this the dissipative loss inside the cavity is in the form

$$\eta = \frac{c\left(S_w \bar{\alpha} + S_{open}\right)}{4V\omega}. \tag{23}$$

For calculating the transfer impedance as a descriptor of the sound field inside the enclosure, the ratio of sound pressure p to volume velocity q is needed. The relation between energy and sound pressure in a cavity is given by

$$E = \frac{p^2 V}{\rho c^2}. \tag{24}$$

A monopole source with the radius a is assumed as source for the injected power. With a velocity v_a at its surface, the imparted power [1.7] is given by

$$P_{in} = 2\pi a^2 v_a^2 \rho c \frac{k^2 a^2}{1 + k^2 a^2}. \tag{25}$$

Combining these formulae and inserting the volume velocity of the source as $q = \pi v a^2$, the transfer impedance can be written as

$$Z = \frac{p}{q} = \frac{\rho c}{\pi a} \sqrt{\frac{8}{\pi\left(A_w \bar{\alpha} + S_{open}\right)} \cdot \frac{k^2 a^2}{1 + k^2 a^2}}. \tag{26}$$

For high wave numbers when ka becomes very large, the transfer impedance reaches a plateau governed by

$$Z_{k\to\infty} = \frac{\rho c}{\pi a}\sqrt{\frac{8}{\pi\left(A_w\bar{\alpha} + S_{open}\right)}}\,. \tag{27}$$

In Figure 9 the SEA result for the transfer impedance is compared with those from the modal analysis. The mean absorption coefficient of the walls is assumed to be 0.1 analogous to investigations presented in [1.8]. It can be seen that the SEA model reveals the "spine" of the transfer impedance. The results are calculated by assuming a volume velocity source with a surface of 57 mm² which corresponds to the sound source used for the subsequent experiments. Therewith the radius a is assumed as 4.2 mm.

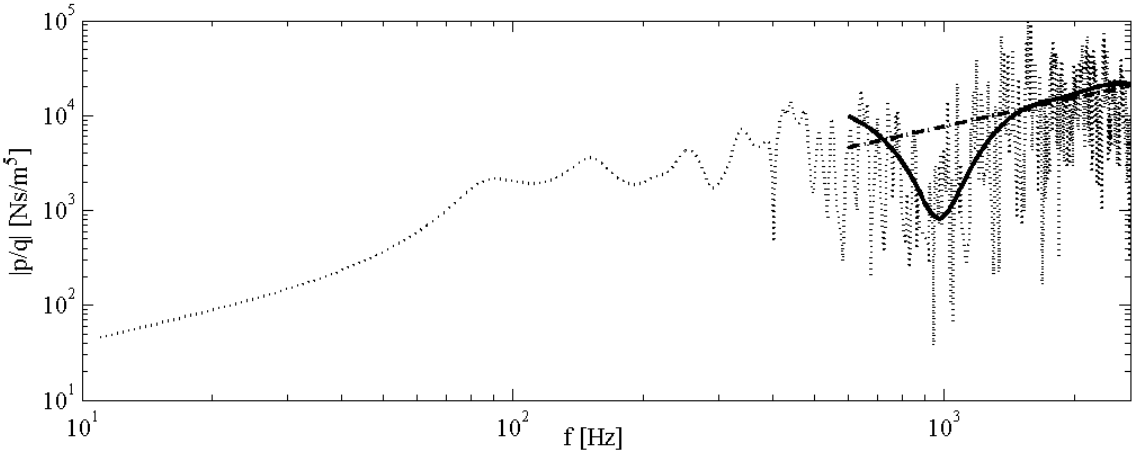

Figure 9: Transfer impedance for a box with one side open calculated by a modal analysis (---), a simple SEA model (·–·–) and a SEA model modified with the influence of the first order reflections of the side walls at source and receiver position (—).

At a frequency of 1 kHz a deviation is observable as dip in the analytically calculated result. By using the results published in the paper by Waterhouse [1.9], [1.10] this deviation is identified as a result interference effects. The interferences are generated by the first order reflections of the exposed side walls at the source and the receiver position. Sound waves incident on an a reflecting surface produce an interference pattern, also if they strike the boundary at all angles of incidence of random angle distribution and random phase. An approach for including this effect into the model presented in

Work Package Three. As anticipation the results of this approach are presented in Figure 9, too. Because of the fact that source and receiver are positioned at similar distances to the side walls only one dip is visible.

Another effect to be considered with regard to the assessment of the results is the overestimation of the efficiency of the absorbers due to the unequal spatial distribution of the absorbing surfaces [1.11].

Finally, a rough estimation of the boundaries between the three frequency ranges is defined to limit the ranges of validity of the suggested analysis tools. The boundaries between the three ranges can be defined as:

1. One octave below the first eigenfrequency for the limit between quasi-static and modal ranges.
2. For the limit between modal and statistical ranges, when the modal overlap factor exceeds unity, i.e., $\gamma \geq 1$, where $\gamma = \frac{\pi}{2} f \frac{\eta}{\partial f}$, with η as the loss factor and ∂f as the modal spacing.

With the asymptotic and generic assumptions presented above, it is revealed, that a detailed and time consuming analysis of a complex system can be avoided and sufficient results can be obtained with limited effort. Crucial is the selection of the appropriate analysis tool. Furthermore, it is shown that the acoustic transmission inside the enclosure can be calculated effectively by employing and combining different analysis methods which is conform to the idea of acoustic sub-grid modelling.

The results of the analyses contain information about the salient physics of the system rather than a detailed numerical method. For a refinement of the results additional effects can be added for each region separately.

2.4 Velocity at the interface

For the sake of completeness of the investigations a short excursion is presented for describing the sound field at the interface to adjacent fluid space by using the transfer impedance. By assuming sound sources $S_1 \ldots S_i$ inside the enclosure (see Figure 10) the

velocity distributions $\tilde{v}_1 \ldots \tilde{v}_r$ at the interfaces can be determined by using Green´s functions.

Each source therewith is defined by its surface sound pressure distributions and a corresponding surface velocity distribution. Using all sound pressure distributions p_1 to p_n and all velocity distributions v_1 to v_n at the surfaces S_1 to S_n of the sources S_1 to S_i the velocities $\tilde{v}_1$ to $\tilde{v}_r$ at certain points at the interface can be calculated as

$$\frac{\tilde{v}_r}{Z_r} = \sum_{S_1}^{S_n} \int_S \left[p_n \cdot \frac{\partial G}{\partial n} + j\omega\rho v_n G \right] dS \tag{28}$$

where Z_r is the impedance seen at the point r on the interface.

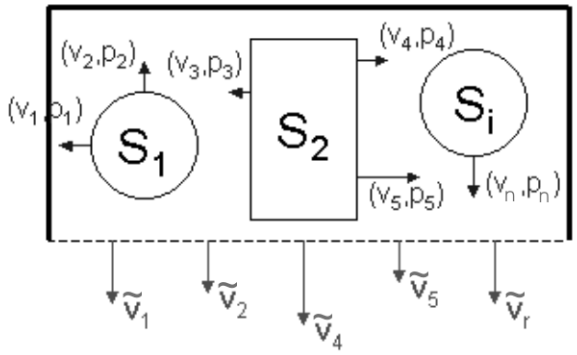

Figure 10: Sound propagation inside the enclosure from different sources to the interface

Moreover, imposing the condition that all sources can be expanded in term of spherical harmonics, a multipole synthesis technique [1.12] becomes applicable. An approach for decomposing complex shaped sound sources into multipoles of different order is presented in a subsequent work package. A corresponding modelling is schematically illustrated in Figure 11 where Y_{mn}^{i} represent the multipole terms for the *i*-th sound source. By only using monopoles, a similar scheme is developed and shown to be applicable in [1.13]. The summation of all terms weighted with the corresponding transfer impedance Z_{mn}^{ir}, determined from the frequency dependent modelling straightforwardly leads to the velocity distribution at the interface as

$$\tilde{v}_r = \sum Z_{mn}^{ir} Y_{mn}^{i} \,. \tag{29}$$

The multipole approach is applicable as long as the source behaves as an ideal velocity source. In reality, however, sources have finite source impedances. Additionally the source impedance will normally depend on the surface co-ordinate. For sources extended in space, therefore, the surface impedance has to be considered. For determining the surface impedance, sound pressure and velocity on the source surface are required. For solving this problem, the multipole approach presented in Work Package Four is extended for approximately determining the complete sound field on or at least close to the sound surface also for complex shaped sound sources.

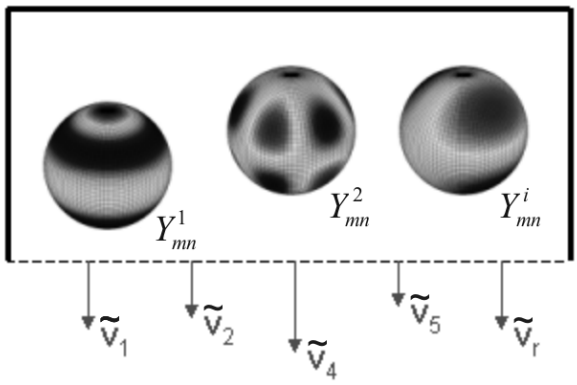

Figure 11: Approximating the sources as multipoles

3 Experimental investigation

3.1 Lab rig design

In the following the simplified results will be assessed by comparing with those from dedicated experiments. The most important aim of the experimental investigations is to prove the applicability of the simplified analytical results. Therefore, transfer impedances are measured between a source and receiver position inside a model-enclosure.

Additional to the assessment of the simplified modelling results, effects and influences are investigated experimentally which can not be described with the analytical model. All analytical models presented elsewhere in this study only include one single sound source. The real system, however, mostly consist of different sound sources, which can be either correlated or uncorrelated. Interference effects are expected if the sound sources are correlated. Beside this, those effects are expected to be frequency dependent and should be analysed in the presence of scattering objects.

In another experiment, the influence of the radiation impedance at the interfaces and its interaction with the adjacent air spaces should be investigated. An estimate of significance of those influences will be necessary for the design of novel approaches.

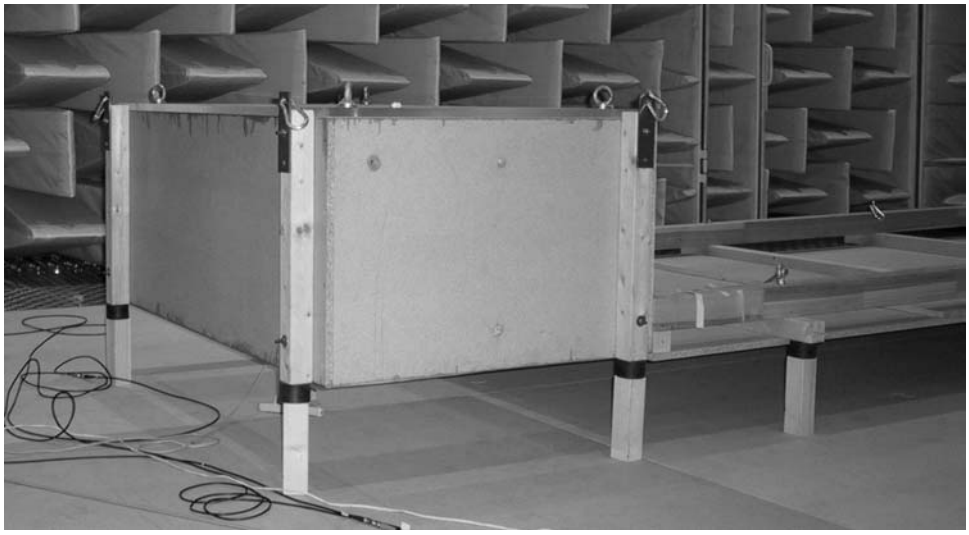

Figure 12: Lab rig design of the rectangular box elevated above the floor and with the attached panel.

The design of the experiment is derived from the simplified model used for the theoretical treatment. Therein the configuration was initially simplified to a rectangular box with rigid walls and one side open. Also for the experiments, a lab rig similar to the sketches shown in Figure 1 is designed. The dimensions of the box are also 1.4 x 0.9 x 0.6 m³. These dimensions are comparable with those of technical devices like the engine compartment of passenger cars or of white goods. As assumed, one side can be open. All walls are made of 20 mm chip-board except the top cover which is made of 20 mm Perspex. With the exception of some narrow frequency bands at the first few eigenfrequencies of the plates, the walls can be regarded as rigid in a wide frequency range. In contrast to the model, most of the systems in reality are enclosed by steel plates. At least at low and intermediate frequencies the impedances of such plates and the enclosed air volume are in the same order of magnitude so that a strong coupling between the fields of the enclosure and in the air may occur. This has to be considered for the assessment of the model validity.

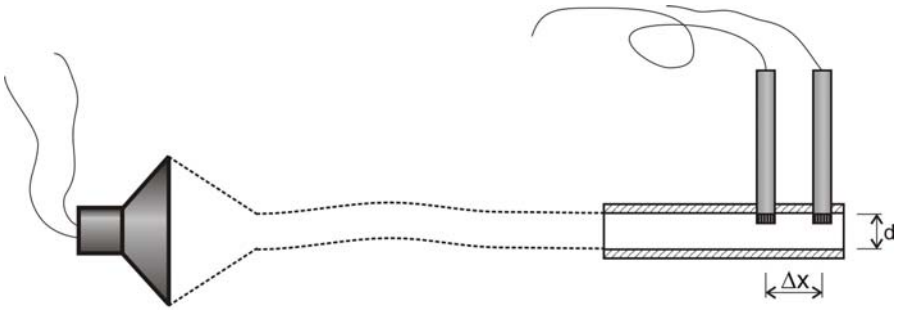

Figure 13: Design of volume velocity source. The orifice diameter $d = 12mm$ *and a microphone distance* $\Delta x = 32mm$ *allows applicability up to 3 kHz.*

Shown in Figure 1 are the different possible configurations of the experimental set-up, all walls rigid (a), one complex wall impedance due to a removed wall (b) and modified complex wall impedance (c) and (d). For simulating different radiation impedances at the open side, the lab rig can be elevated at various distances above a concrete floor. Additionally a 4 m² chip-board panel can be attached to simulate a semi opened bottom side of a machine or the car floor panel of a passenger car. The lab rig design is depicted in Figure 12.

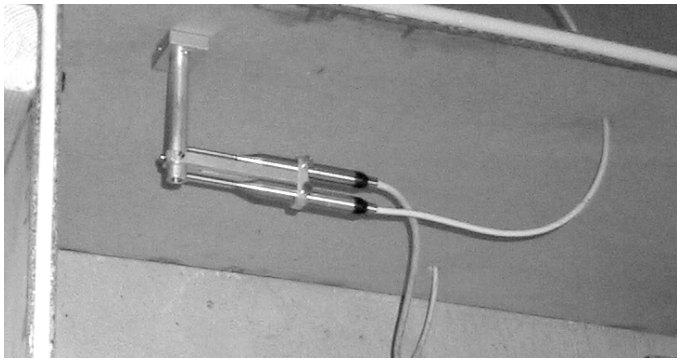

Figure 14: Volume velocity source installed close to a corner of the rectangular box. Two 1/8 inch microphones are used for determining the source strength.

Whereas a microphone simply can be used as receiver, the design of the volume velocity sound source is more complicated and requires a more detailed description. The orifice at one end of a flexible tube can be seen as a point source as long as the diameter of the orifice is much smaller than the wavelength. The volume flow in the tube is driven by a boxed loudspeaker assembled at the other end of the tube as sketched in Figure 13. The volume velocity at the orifice is determined indirectly by measuring the sound pressure difference inside the tube close to the orifice. From the sound pressure p_{Mic1} and p_{Mic2} measured at the microphones spaced by Δx, the volume velocity then is calculated as

$$q = \pi d^2 \frac{p_{Mic2} - p_{Mic2}}{4 j \omega \rho \cdot \Delta x}. \tag{30}$$

With the distance between the two measurement positions for the pressure difference measurement another upper frequency limit is given. The configuration of the sound source is shown on Figure 14.

3.2 Transfer impedance measurement

In the first investigations the transfer impedance between a source at the position $x_S = 0.1$ m, $y_S = 0.1$ m, $z_S = 0.5$ m and receiver at the position $x_R = 1.35$ m, $y_R = 0.1$ m, $z_R = 0.5$ m inside the enclosure is measured.

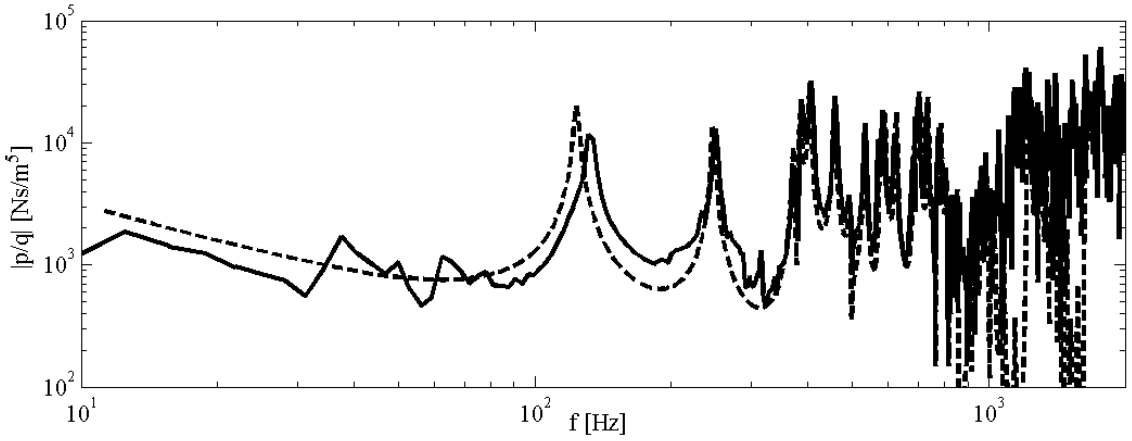

Figure 15: Measured (—) and calculated (---) transfer impedance with all walls rigid.

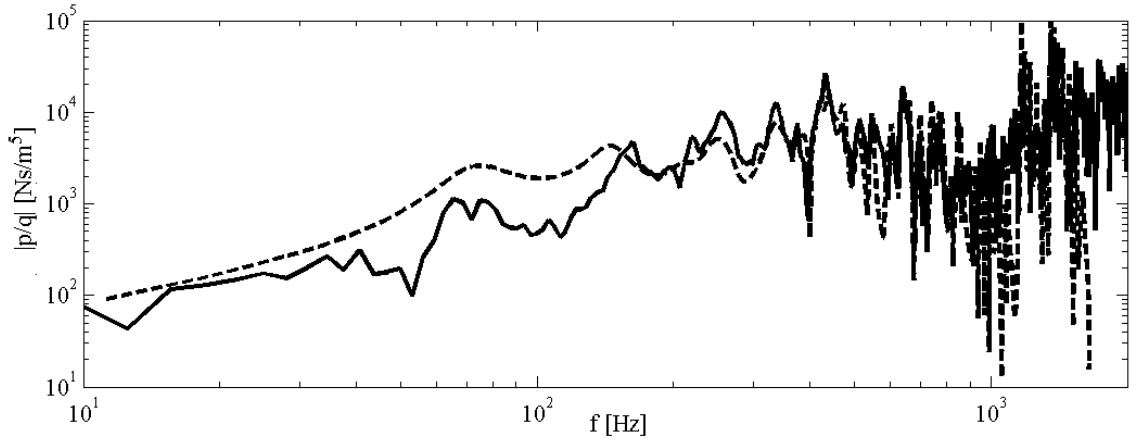

Figure 16: Measured (—) and calculated (---) transfer impedance with one wall removed (complex wall impedance).

As can be seen in Figure 15 and Figure 16, the experimental results follow the theoretical trends for the rigid boundary condition as well as for the case with one side fully open. It should be mentioned, that the calculated curve is limited at high frequencies due to calculation effort. For the open case there is a deviation between measured and calculated results at low frequencies around 80 Hz close to the first resonance. Taken into account that a baffled piston was assumed for the calculation of the radiation impedance at the opening, the difference can be explained. The validity limitations of the chosen approximation for the radiation impedance are explained previously. At 80 Hz the first eigenfrequency appears and the radiation impedance changes from those of a

piston to those of a field exited radiator. Nevertheless, at high frequencies the impedances of both cases reach the same asymptote. The error due to the approximation of the wall impedance seems to become secondary.

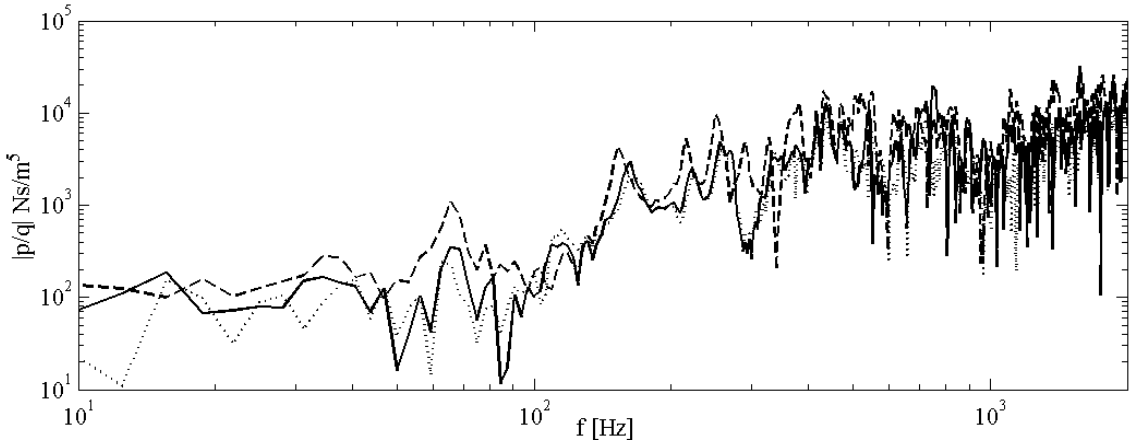

Figure 17: Transfer impedance with different air gaps. (---) 5 cm gap between open box and floor, (—) 25 cm gap between open box and floor, (···) open box without floor. Accuracy of the measured results is limited due to the limitations of the volume velocity source.

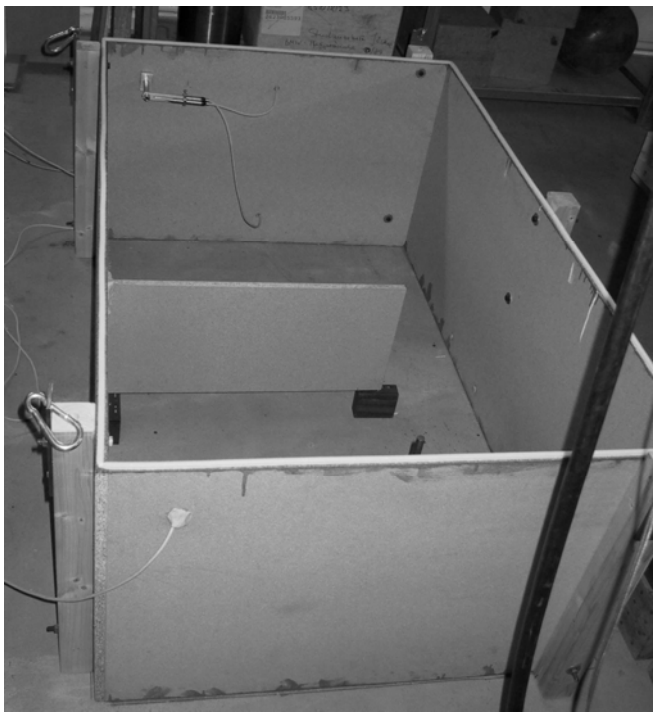

Figure 18: Partition wall inside the enclosure.

The significance of the radiation impedance into the adjacent air spaces for the sound field in the system under consideration is shown in Figure 17. For these investigations, additionally a 4 m² chip-board panel is mounted to the enclosure as shown in Figure 1d). It approximates the more general case of a semi-open bottom side and should influence the radiation impedance. In Figure 17 it is illustrated the configuration of the free field case without panel as reference, and the gap cases with additional panel. It is observed that beyond a certain height (say 25 cm) of the air gap there is a negligible influence on the radiation impedance of the opening and therefore an insignificant difference to a case with a free field. Also the influence of the attached panel on the radiation impedance is seen to be negligible which confirms the assumption made for the approximation of the radiation impedance in the theoretical model. Therein the radiation impedance was assumed to be that of a baffled rectangular piston, even though there is no baffle. The approximation therewith is proven to be valid.

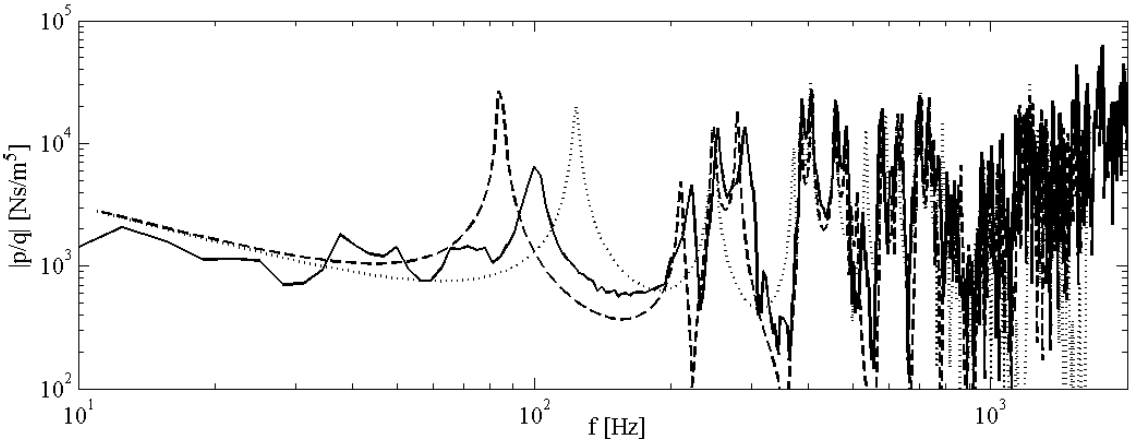

Figure 19: Transfer impedance for a closed enclosure with a partition wall (—) compared with the calculated results for the cases with (---) and without (···) partition wall.

For validating the calculated influence of the inserts, the coupled room problem is simulated by inserting a chip-board partition wall in the completely closed enclosure as depicted inFigure 18. The measured transfer impedance for a source position in one sub-room and a receiver position in the other sub-room is shown in Figure 19. Comparing the results for the empty and partitioned condition, the same trend can be observed as in the calculated results. The first eigenfrequencies are shifted downwards in frequency. Although all characteristics of the curves are the same, the resonances and

anti-resonances differ slightly from those calculated. The reason for this deviation is mainly founded in the finite number of coupling points on the interface between the sub-rooms and probably also in the calculation accuracy in the matrix inversion in Eq. (13) to (16).

3.3 Correlation between sources

In general, there will be several sound sources inside the enclosure. For equipped enclosures, the influence of different sound sources, however, can not be investigated analytically. The sources can be either correlated or uncorrelated. For correlated sources their phase relations as well as their positions in the cavity have a frequency dependent influence on the resulting sound field and therefore also on the velocity distribution at the interface to the exterior. At least at low frequencies where the dimensions of the system under consideration are comparable with the wavelength in air, spatial modulation effects become important. Due to the fact that scattering makes the sound field more diffuse, it is also expected, that there is dependence between the effect of correlation and scattering power e.g. the number of scattering objects in the sound field. This dependence should vary with frequency.

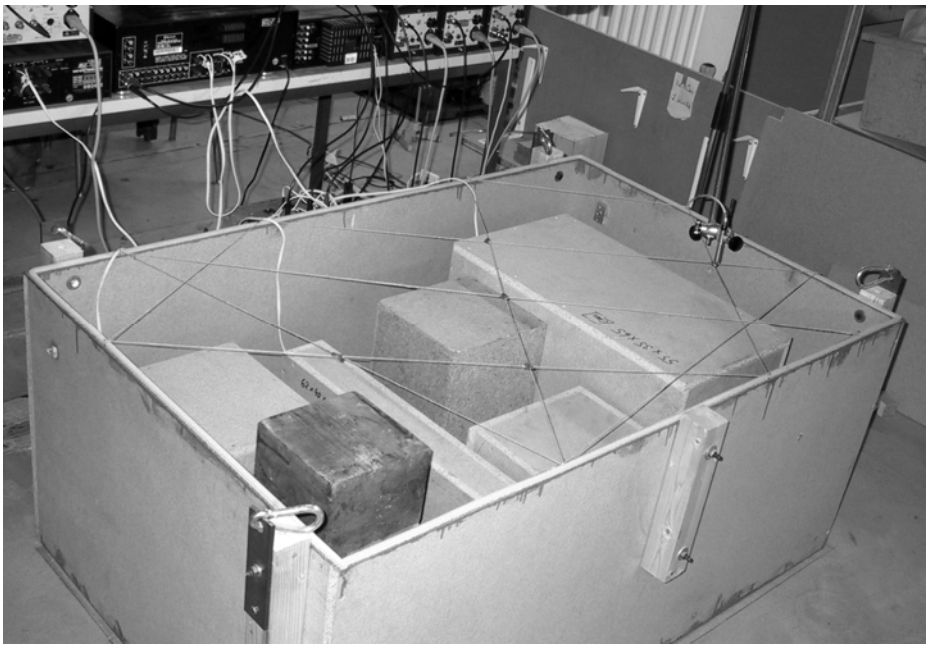

Figure 20: Lab rig design correlation measurement. Box is filled with scattering objects.

To examine these effects the lab rig design is modified in a way that three point sources were installed inside the closed box. The sources can be driven either with correlated or with uncorrelated noise signals. The recording of sound pressure levels at five random microphone positions is done for two different configurations of the cavity; the first with a dense package of additionally inserted scatterers and the second without scattering objects. The results for both configurations are compared. Several chip-board and Perspex parallelepipeds of different sizes are used as scattering objects. The set up of the experiment is shown in Figure 20.

To find an appropriate criterion for the assessment of the results, the difference is calculated between a fictitious analytical value obtained by summing all sources energetically and the measured values. Thus, this difference constitutes a quantitative measure of the diffusivity. The lesser the difference, the more diffuse is the field and the lesser is the influence of the correlation between the sources.

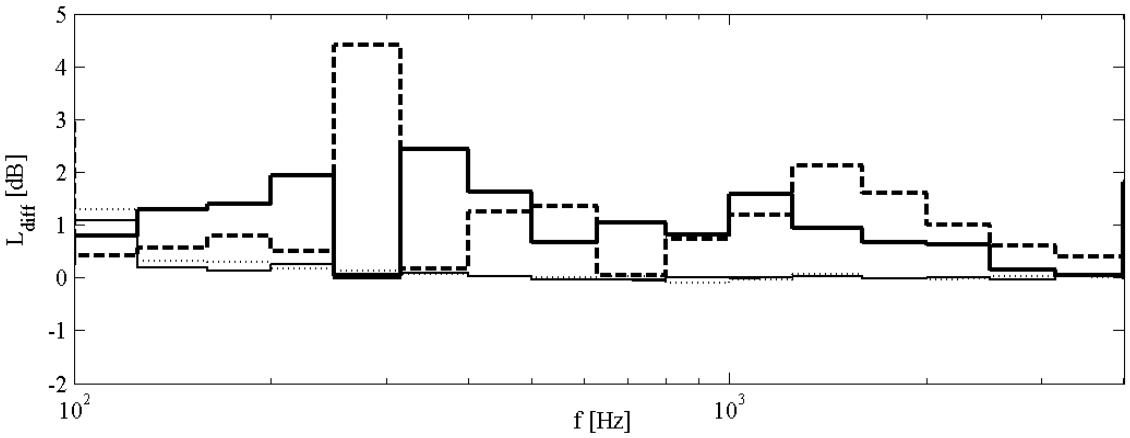

Figure 21: Spatially averaged error level due to correlation for three different sound sources (bold—) correlated with scattering, (bold---) correlated without scattering, (thin—) uncorrelated with scattering, (thin---) uncorrelated without scattering.

The result averaged over the five microphone position is plotted in Figure 21. From the figure it is seen that the deviation is close to zero for the uncorrelated case, independent of the amount of scattering objects, which means that the sound field is increasingly diffuse. As expected, the influence of correlation between different sources is marked, particularly at low frequencies. Because of the small number of receiver points the deviation is highly frequency dependent and exceeds in some 1/3-octave bands the 3 dB

difference. For a higher number of microphone positions it is expected that the results are smoother. At 1 kHz the wavelength is of the order of the dimensions of the scattering objects. Above this limit, the expected trend is recognisable. The influence of correlation between the sources is slightly reduced by the scattering. In most of the 1/3-octave bands, the deviation is lower with scattering objects than without. However, the significant result of this investigation is that the correlation between different source has to be taken into account at least as long as the wavelength is big compared with the geometrical dimensions.

3.4 Validity of the asymptotic results

All the described investigations assume a simplified model of the system under consideration. In reality machines and devices consist of complex structures, densely packed cavities and having complex surface impedances on the casing as well as on the installations. In the following the transfer impedances of an ordinary device is determined. As an example, the transfer impedances inside the engine compartment of various passenger cars are measured. For these measurements the same equipment as described previously for the lab rig experiments was used. A typical experimental set up is show in Figure 22.

Figure 22: Experimental set up for measuring a transfer impedance inside an engine compartment. The volume velocity source is marked black; the receiver microphone is marked white.

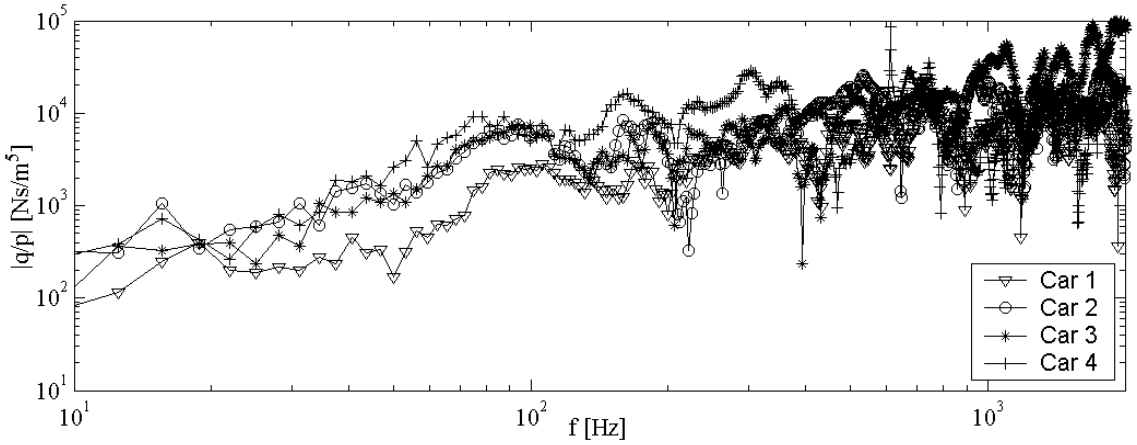

Figure 23: Measured transfer impedances of different engine compartments.

In Figure 23 a selection of measurement results is shown. Although the cars considered are different in dimensions and had different levels of packing density, there is no significant difference in transfer impedances recorded for similar source and receiver points in every car. The determination of the exact source and receiver position is problematic because of the complicated geometry of the system. Thus, the positions are assumed close to opposite corner locations to be comparable with the configurations for the theoretical and the lab rig investigations.

Compared with the calculated results (e.g. the dotted line in Figure 2 where the model has similar dimensions) the curves exhibit the same trends and the same distinct frequency ranges. As expected, the mass/spring, the modal and the statistical ranges can be distinguished. However the significance of the resonance frequencies in the modal range is lost due to the finite surface impedances, the damping effects and the scattering of the densely packed auxiliaries. The undulate curve especially at low frequencies is expected to result mainly from the frequency dependence of the surface impedances. Also at intermediate and high frequencies the influence of the surface impedances seems to be more significant than the modal structure. The modal density, however, is raised so that the distinct eigenfrequencies disappear.

Nevertheless, the comparison of the calculated results with those of the measurement example demonstrates the applicability of theoretical considerations. It shows that the salient physics of a small enclosure can be extracted with the methods suggested from the theoretical investigations developed for a simplified model approach.

4 Concluding Remarks

In Work Package One tools are presented which enable approximate characterisation of technical artefacts consisting of a small partially open enclosure densely packed with complicated shaped installations.

It is shown that depending on the relation between wavelength and the geometrical dimension, different tools have to be applied to reduce the calculation effort. Three main sub-ranges can be distinguished. For low frequencies where all dimensions are smaller than the wavelength, a lumped system description can be employed. This means the system can be analysed by dividing it in mass and spring components. For intermediate frequencies where the first distinct eigenfrequencies appear, a modal analysis can be established based on the major dimensions of the cavity. This approach, however, is limited to simple geometries. That poses the necessity for alternative approaches handling systems with complicated geometries. At high frequencies, where the modal density is high, the system characteristics can be obtained from statistical energy models augmented by the influence of the interferences from first order reflections.

For units with partially open walls, the influence of the radiation impedance at the interfaces to the adjacent fluid space is found to be of subordinate relevance for the sound field inside the enclosure.

The interior objects sub-divide the enclosed volume into sub-cavities which can be handled as coupled rooms. This mainly affects the first eigenfrequencies which are shifted due to changes in the propagation path of the standing waves. This sub-division of the free fluid space into coupled rooms provides the basis for a novel approach presented in the following work package.

The influence of correlation between different sound sources inside cannot be neglected. At high frequencies, however, the effect is found to be reduced owing to scattering. For statistical descriptions of the sound field at high frequencies influences due to reflections at the boundaries are found to be significant. These effects are investigated in more detail in Work Package Three.

Comparisons made with measurement results from full-scale automotive engine compartments indicate the wide-ranging applicability of the approaches outlined.

A scheme was presented for including the sound sources into the modelling. Approaches for the analysis and characterisation of sound sources with respect to the requirements of the modelling are considered in Work Package Four.

5 References

[1.1] L. Cremer and H. and Müller, *Die wissenschaftlichen Grundlagen der Raumakustik. Band II: Wellentheoretische Raumakustik*. (S. Hirzel Verlag, Stuttgart, 1976).

[1.2] P. M. Morse, *Vibration and Sound*. (Acoustical Society of America, 1995).

[1.3] F. P. Mechel, *Schallabsorber, Band I: Äußere Schallfelder, Wechselwirkungen*. (S. Hirzel Verlag, Stuttgart, 1989).

[1.4] D. S. Burnett, *Radiation Impedance Functions of Rectangular Pistons and their Applications to Sound Transmission through Finite Depth Apertures*. (Ph. Diss. Univ. Calif., Berkeley, 1969).

[1.5] E. Leung and C. P. Lee and N. Jacobi and T. G. Wang, "Resonance frequency shift of an acoustic chamber containing a rigid sphere," J. Acoust. Soc. Am. **72**(2), 615-520 (1982).

[1.6] R. H. Lyon and R. DeJong, *Theory and application of statistical energy analysis*. (Second Edition, Butterworth-Heinemann, 1995).

[1.7] L. Cremer and M. Heckl and B.A.T. Petersson, *Structure-Borne Sound*, (Springer, Berlin, 2005).

[1.8] E. A. Lindqvist, "Sound Attenuation in Large Factory Spaces," Acustica **50**, 313-328 (1982).

[1.9] R. V. Waterhouse, "Interference Patterns in Reverberant Sound Fields," J. Acoust. Soc. Am. **27**(2), 247-258 (1955).

[1.10] R. V. Waterhouse, "Output of a Sound Source in a Reverberation Chamber and Other Reflecting Environments," J. Acoust. Soc. Am. **30**(1), 4-13 (1958).

[1.11] M. Hodgson, "When is the diffuse-field theory applicable?" Applied Acoustics **49**(3), 197-207 (1996).

[1.12] E. G. Williams, *Fourier Acoustics, Sound Radiation and Nearfield Acoustical Holography*. (Academic Press, Inc., 1999).

[1.13] L. Chiesa and A. Grosso and I. Machetta and E.J.M. Nijman and G. Schellino, "Acoustical Source Characterisation of Automotive IC Engines: Further Developments of the Substitution Monopole Technique", Proceedings of Tenth International Congress on Sound and Vibration, Stockholm, 1781-1788 (2003).

Work Package 2:

Modelling the sound field by
using novel probabilistic approaches

Abstract:

The airborne sound field inside a small fitted enclosure is complex in nature and difficult to describe in a deterministic way. For describing the sound field different probabilistic approaches are suggested and investigated, modelling either the installations or the free fluid space. In the first approach a probability density distribution is assumed including the number and size of the objects installed. Depending on the wavenumber, the main physical effects of the scatterers and their probability distribution are combined to get a simplified description of the field. In a second approach the free fluid space is modelled as a set of coupled one dimensional wave guides. The results are discussed and compared with numerical model results.

1 Introduction

For predicting the sound radiation from devices, comprising many active parts enclosed by some machine casing, it is necessary to analyse the airborne sound field inside the enclosure. Thereby, the wavelength of the sound emitted is either larger than, of the same dimension as or smaller than the characteristic size of the system. Because of that, different analysis tools are required.

The presence of the active parts inside the enclosure, which can act as sound sources, as reflectors or scattering objects and the mixture of different surface impedances cause a highly complex sound field inside the enclosure. Due to the complexity of the sound field inside the fitted enclosure, analytical and numerical approaches cannot or only to limited extent be applied. Analytical solutions in terms of series expansions of normal modes [2.1] can only be achieved for simply shaped, empty enclosures with uniform wall impedances. Standard ray-tracing [2.2] and image-source [2.3] methods are limited to frequencies where the wavelength is much smaller than the characteristic dimension of the cavity. Particularly the image-source method is limed to simple geometries; else the calculation time rises drastically.

For the analysis of complex systems like those described previously, the Finite Element Method (FEM) is frequently used for low and intermediate frequencies [2.4]. Notwithstanding the advantages of FEM, some difficulties may arise at the design stage where details of the system are missing or unknown. For such situations, rather, an analysis tool is needed, which focuses on the salient physics and essentially requires generic information about the system to be analysed.

In Work Package One an approach was presented, which describes the physics inside a highly simplified design. This will be the starting point of the investigations described in the following. For an empty rectangular box with walls considered hard it was shown that the transfer impedance function as a descriptor of the sound field inside the enclosure can be approximated by using different analysis tools depending on frequency. Three frequency regions have been distinguished. For low frequencies, the system behaves quasi-statically like a spring or a mass. For a completely closed enclosure, the

acoustical behaviour is controlled by the stiffness of the enclosed fluid volume V with the impedance

$$Z = \frac{p}{q} = \frac{\rho c^2}{j\omega V}. \tag{1}$$

With an unobstructed aperture, the transfer impedance is dominated by the mass plug with a mass per unit area m'' on the aperture of area S_{open} as

$$Z = \frac{p}{q} = \frac{j\omega m''}{S_{open}}. \tag{2}$$

At intermediate frequencies, termed the modal range, the first few distinct eigenfrequencies occur. In this range a detailed modal analysis appears to be necessary. The transfer impedance is given by [2.1]

$$Z = \frac{p}{q} = jk\frac{\rho c}{V}\sum_N \frac{\Psi_N(S)\Psi_N(R)}{k^2 - k_N^2} \tag{3}$$

where Ψ describes the modal pattern, k_N are the wavenumbers for the eigenfrequencies and V the free volume inside.

At high frequencies, the field inside is increasingly diffuse in nature and statistical methods like Statistical Energy Analysis (SEA) are applicable. Assuming a monopole sound source with radius a the transfer impedance is governed by [2.5]

$$Z = \frac{p}{q} = \frac{\rho c}{\pi a}\sqrt{\frac{8}{\pi\left(A_w\bar{\alpha} + S_{open}\right)}\cdot\frac{k^2a^2}{1+k^2a^2}} \tag{4}$$

with the equivalent absorbing surface $A_w\bar{\alpha}$. In Figure 1 the result of such an approximate analysis is depicted for a partially open enclosure. The figure shows the curve calculated for the three frequency ranges separately. For comparison the measured transfer impedance for an engine compartment of a passenger car is shown. The dimensions and configuration of the modelled empty cavity and the real engine compartment filled

with appliances as well as the source and receiver position are similar except for the much higher absorption inside the real compartment at high frequencies. The difference in the absorption leads to the deviation observable at high frequencies. From this figure it can be seen that the analysis scheme proposed in Work Package One reveals the characteristics of the transfer impedance.

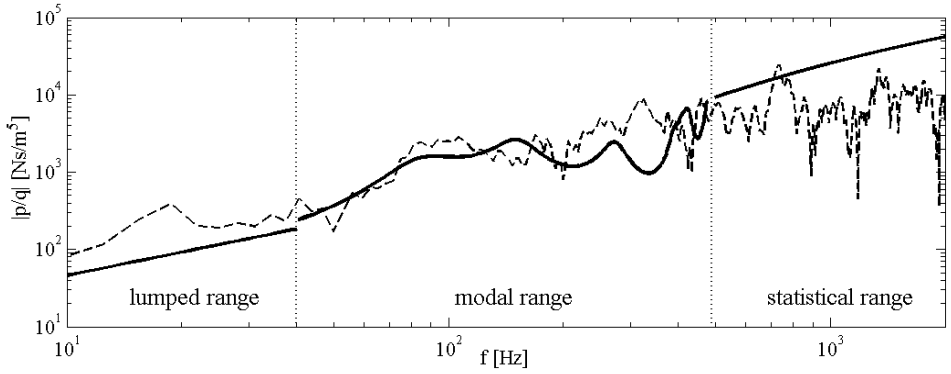

Figure 1: Calculated transfer impedance for an empty box (—) compared with the measured results of a real engine compartment (---) (see Work Package One). The calculated results are for a box of 1.4 x 0.9 x 0.6 m³ with the bottom side open. Source and receiver positions are similar.

Like the examined example of an engine compartment, most of the real machine casings relevant for this investigation are densely packed with auxiliaries. It was already mentioned that those auxiliaries can be either active when they are sound sources or passive appearing only as scattering objects. Above all, the auxiliaries subdivide the free volume. The free volume becomes a complex system of coupled sub spaces. It is expected that all the installations will passively influence the sound field and therefore the transfer impedance.

Because of the complex shape and the large number of fitted objects, their influence can only with great difficulty be taken into account in a strict sense. Especially with regard to a product line, the treatment of an ensemble of identical machines or units becomes important rather than the appearance of a single realisation. With this, a statistical spread of the mechanical as well as the acoustical properties comes into play. Consequently, a statistical treatment seems appropriate rather than an analytical one. In various publications, different statistical approaches have been presented for predicting the sound field in large fitted rooms like factory halls. By using the concepts of random

diffusion processes Kuttruff [2.6], Lindqvist [2.7] and Le Pollès et al. [2.8] have developed mathematical models describing the expected density of sound particles. Counting the particles passing a certain spatial position at a given time, an equivalent to the energy density is found. Ondet and Barbry [2.9] suggested a modified ray tracing approach. In this approach the probability of fittings in the room is modelled by including walls of varying degrees of reflectivity. Unfortunately the presented approaches do not work properly for smaller enclosures not fulfilling the condition that the wavelength is much smaller then the characteristic size of the room.

Following the requirements for a statistical treatment, in this work package two different probabilistic approaches are presented modelling the influence of the inserts. Both approaches are mainly aimed at treating the behaviour at intermediate frequencies. With some restrictions, however, their applicability ranges can be extended for high and low frequencies.

In the first approach the inserts are simply considered as scattering objects. A probability density is assumed for the number and size of objects and their geometrical arrangement. Therefore, the influence of the probability density of the inserts on the transfer impedance is investigated. It is expected that the scattering objects influence the sound in different manners depending on frequency. Hence, this investigation is made for each of the three frequency regions separately. Because simply shaped scatterers should be used for the modelling, conversion schemes are developed to transfer the real, complex shaped objects to simple scatterers with similar acoustic behaviour. Two different conversion schemes seem to be appropriate, either via the same scattering cross section or via the same volume. This implies that the required geometric or acoustic properties of the complex shaped objects are known. Whereas the volume is easily determined, different methods for measuring the scattering cross section for complex shaped objects are discussed.

Another approach is based on modelling the free space. It is assumed that the subspaces of the cavity can be modelled as a system of coupled one-dimensional wave guides. Of course, this assumption is applicable only for frequencies below the cut-on frequency of the wave guides. It can be argued that this condition is satisfied at least in a limited frequency range where the first eigenfrequencies of the system under consid-

eration appear. At the current state of the investigations the results are limited to those of completely closed systems with rigid boundaries.

2 Probabilistically distributed scattering objects

By means of this approach the influence of enclosed scattering objects on the sound is investigated. Two main influences can be distinguished, a) shifts of the eigenfrequencies and b) a higher apparent absorption, which results from an enhanced effectiveness of the absorbers inside due to the scattering. For a sphere as the simplest object shape, the scattering behaviour is analytically describable [2.10]. Owing to this it is suggested that all installations should be appropriately transformed to spherical objects.

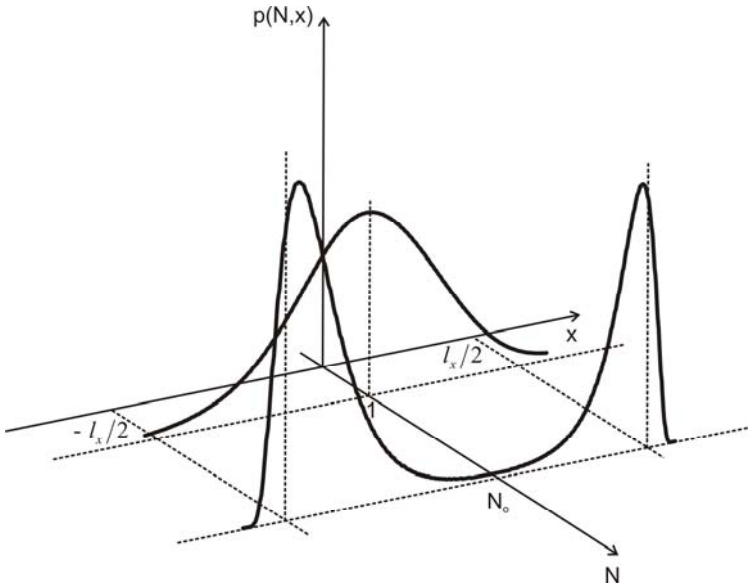

Figure 2: Fictional probability density distribution. For lucidity the surface curve is depicted only for two distinct numbers of scattering object in x-direction.

For a given configuration of auxiliaries in the enclosure, a probability density is developed as a five-dimensional distribution, including the three dimensional Euclidian space, the number and sizes of the objects installed. In the resulting function the main properties of each distinct configuration of installations are contained. For sake of simplicity, the parameters governing the distribution are assumed statistically independent.

For illustrating the concept of describing the geometry probabilistically, in Figure 2, a hypothetic probability density distribution is shown. In this illustration only the prob-

ability of the number of the objects over one spatial dimension is shown as an example. The curve is based on the assumption that a high number of the auxiliaries, mostly with small dimensions, are mounted near the side walls of the enclosure whereas only one big object, e.g. the engine block, is placed at the centre of the cavity.

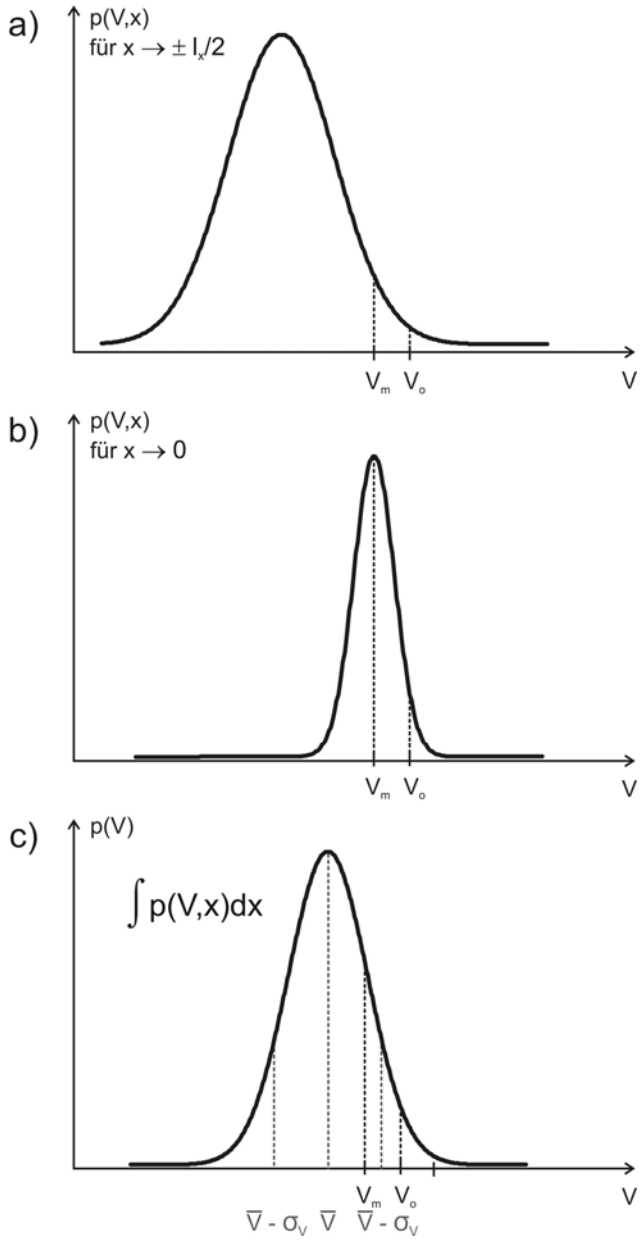

Figure 3: Fictional probability density for the volume of the installations. a) and b) for different positions in x-direction. c) integrated over x. V_0 is accumulated volume of all installations. V_m is the volume of the large appliance in the centre of the cavity. $\overline{V}$ is the mean value and σ_V its standard deviation.

A possible probability density function for the volume of the installations is depicted in Figure 3. After integrating the density function over each direction in space, mean values and variances for the number and size depending on the direction can be determined (see Figure 3c).

2.1 Volume effect

From the findings presented in equations (1) to (4), it is expected that the objects inside the enclosure have different influence depending on frequency. At low frequencies, the free volume in the enclosure is affected by the installations. Due to this volume change, the mass or stiffness governing the acoustic behaviour in this range will change. The free volume can be calculated as

$$V_{free} = V_{empty} - \sum_i N_i \cdot V_i \tag{5}$$

wherein V_i is the volume of the *i*-th object and N_i the number of objects with that volume within the enclosure V_{empty}. It is assumed that scattering has only a negligible influence at low frequencies below the cut-on frequency of the enclosure. For calculating the transfer impedance, the free volume V_{free} together with its uncertainties can be inserted in equation (1) which yields

$$Z' = \frac{\rho c^2}{j\omega\left(V_{empty} - \sum_i N_i \cdot V_i\right)}. \tag{6}$$

Because the result is statistically based the calculation of the variance is required. Starting with the known error function

$$\sigma_{Z'}^2 = \sum_{i=1}^{n}\left(\frac{\partial Z'}{\partial x_i}\right)^2 \sigma_i^2 \tag{7}$$

the variance of the transfer impedance is given by

$$\sigma_{Z'}^2 = \frac{\partial Z'}{\partial V}\sigma_V^2 + \frac{\partial Z'}{\partial N}\sigma_N^2. \tag{8}$$

2.2 Scattering effect

Beginning at frequencies where the wavelength is of the same dimension as the enclosure, the objects installed mainly influence the sound field by scattering. In the modal range as well as in the statistical range, the distinct eigenmodes are frequency shifted and additional absorption results. Because of the different underlying mechanisms, both effects will be treated separately. The frequency shift of the eigenmodes is important mainly in the modal range where the modal density is low. In the statistical range with high modal density the frequency shift of an eigenmode becomes secondary and is neglected. The most important effect of the auxiliaries, however, is the enhanced absorption due to scattering.

The influence of the scattering of one sphere on the eigenfrequencies is treated in [2.11]. The formulae given in [2.11] can be applied to an eigenmode with the wavenumber $k = \pm\sqrt{k_x^2 + k_y^2 + k_z^2}$. For the wavenumber component in x-direction, the wavenumber shift of the eigenmodes Δk_x due to a sphere of radius a at the position *x* inside a rectangular enclosure is given by the equation

$$\Delta k_x = k\frac{4\pi a^3}{3V_{empty}}\left[\left(1-\frac{2}{5}(k_x a)^2\right)\cos(2k_x x)+\ldots \left(\frac{1}{4}-\frac{17}{72}(k_x a)^2\right)\cos(2k_x x)-\left(\frac{1}{4}+\frac{67}{360}(k_x a)^2\right)\right] \tag{9}$$

with

$$0 \le x \le l_x\,. \tag{10}$$

wherein l_x is the length of the box in x-direction. As shown in [2.11] equation (9) is reasonably applicable even when the sphere is fairly large ($k_x a \le 1$) or fairly close to a side wall of the enclosure ($x = 0$ or $x = l_x$). In Figure 4 the normalised wavenumber shift is shown for the first and second eigenmode. The shift can be calculated for y- and z-wavenumber components respectively.

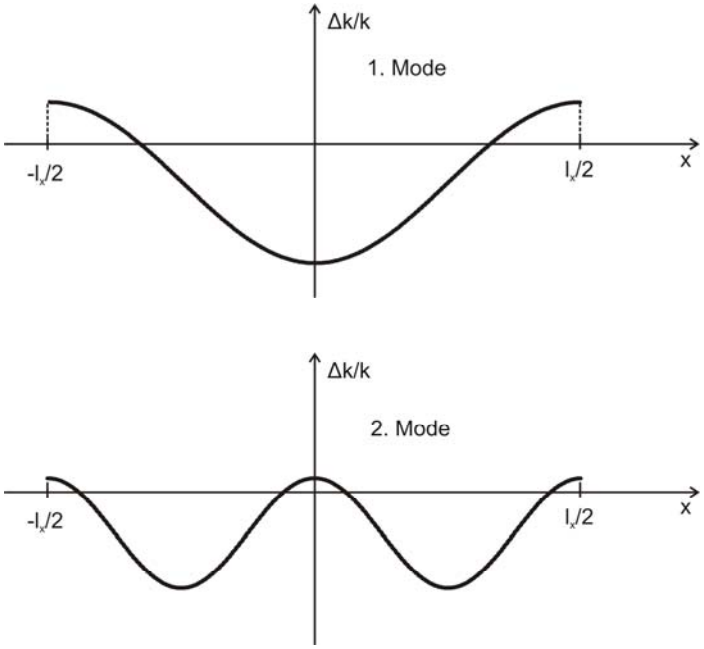

Figure 4: Normalised wavenumber shift of the first and second eigenmode in a rectangular box containing a rigid sphere as function of its position.

Using the information about the number and sizes of the contained spheres from the probability density function, a mean value of the wavenumber shift

$$\mu_{\Delta k} = \Delta k\left(\mu_V, \mu_x\right) \cdot \mu_N \tag{11}$$

can be determined. By inserting this value in the modal equation (3) a modified transfer impedance

$$\overline{Z'}(k) = \frac{jk\rho c}{V_{free}} \sum_N \frac{\Psi_N(S)\Psi_N(R)}{k^2 - \left[\left(k_x^{(N)}\left(1+\mu_{\Delta k_x^{(N)}}\right)\right)^2 + \left(k_y^{(N)}\left(1+\mu_{\Delta k_y^{(N)}}\right)\right)^2 + \left(k_z^{(N)}\left(1+\mu_{\Delta k_z^{(N)}}\right)\right)^2\right]} \tag{12}$$

can be calculated.

Starting from the error function

$$\sigma_{\Delta k}^2 = \sum_{i=1}^{n}\left(\frac{\partial k}{\partial x_i}\right)^2 \sigma_i^2 \tag{13}$$

the variance of the wavenumber shift in x-direction is

$$\sigma_{\Delta k_x}^2 = \left(\frac{\partial \left(N \cdot \Delta k \right)}{\partial V} \right)^2 \sigma_V^2 + \left(\frac{\partial \left(N \cdot \Delta k \right)}{\partial x} \right)^2 \sigma_x^2 + \left(\frac{\partial \left(N \cdot \Delta k \right)}{\partial N} \right)^2 \sigma_N^2 . \tag{14}$$

With this the variance of the transfer impedance function yields

$$\sigma_{Z'}^2 = \left(\frac{\partial Z'(k)}{\partial k_x} \right)^2 \sigma_{\Delta k_x}^2 + \left(\frac{\partial Z'(k)}{\partial k_y} \right)^2 \sigma_{\Delta k_y}^2 + \left(\frac{\partial Z'(k)}{\partial k_z} \right)^2 \sigma_{\Delta k_z}^2 . \tag{15}$$

The eigenfrequency shift mainly stems from the elongation or contraction of the path between the boundaries determining a modal pattern due to the inserted scatterer. This leads to the assumption that the volume is the appropriate conversion parameter between the real object and the sphere. This can be argued valid at least for compact objects of similar spatial dimension in every direction.

In addition to the eigenfrequency shift, the scattering leads to a higher absorption than would be the case for the field without scatterers. The reason for this is that the sound field in an enclosure becomes increasingly diffuse if scattering occurs. This leads to an enhanced efficiency of the absorbers in the enclosure. In the statistical range where the modal density is high this effect is more prominent than the eigenfrequency shift. From a basic ray-tracing approach the sound intensity I is

$$I_n = I_O \left(1-\alpha\right)^{\frac{ct}{l_m}} = I_O e^{\frac{ct}{l_m}\ln(1-\alpha)} \tag{16}$$

after the *n*-th reflection of a sound ray at an obstacle and the additional absorption can be determined as

$$\overline{\alpha} = 1-\left(1-\alpha_s\right)^{\frac{S \cdot l_m}{4V}} . \tag{17}$$

The absorption resulting from the scattering object α_s e.g. can be set to *0.1* analogous to investigations presented in [2.12].

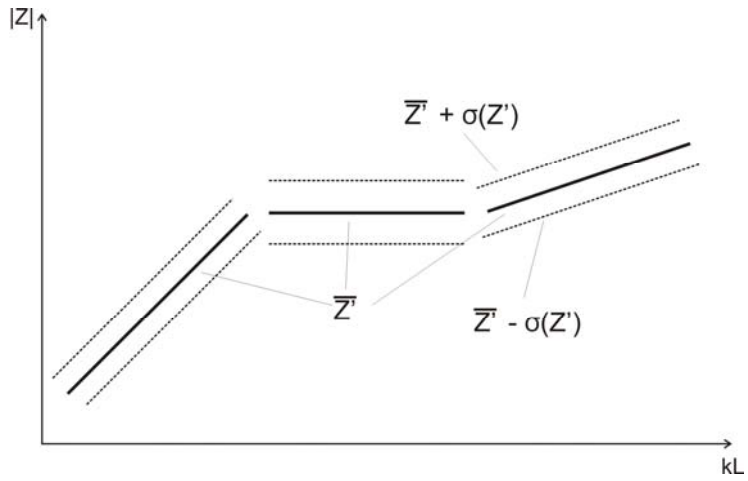

Figure 5: Simplified transfer impedance function with the associated standard uncertainties.

The mean free path l_m can be derived according to [2.12] from the scattering cross-section Q of each of the N objects inside the volume V with an equivalent absorption area of S by

$$l_m = \frac{V}{\sum_i N_i \cdot Q_i} \,. \tag{18}$$

From this equation one can see that the scattering cross section is the leading property of the scattering object. Therefore the conversion from the real object to the spherical scatterer is performed with respect to the scattering cross section. Such a conversion leads to a frequency dependence. The variance herein depends on the variance of the number of objects σ_N^2 and those of the scattering cross section.

Compiling the results for each of the three frequency ranges, a transfer impedance function for the open enclosure is obtained as sketched in Figure 5.

2.3 Conversion schemes for the scattering behaviour

For handling the eigenfrequency shift the conversion scheme is simply geometrical with respect to the volume. Contrary to this for the additional absorption approach the scattering cross section was found as appropriate conversion parameter. Thus, for converting the real complex shaped installations to the spherical scattering objects, the scatter-

ing cross section has to be determined. For illustrating the scattering cross section, in the following the concept is described more detailed.

By using its scattering cross section the scattering efficiency of any object in a sound field can be described. The scattering cross section is defined as the ratio of the acoustical power P_S scattered at an obstacle to the intensity I_0 of the incident wave front. For an obstacle of dimension a, bigger or as big as the wavelength λ, the scattered power P_S consists of two parts: one scattered more or less uniformly in all directions, and a second part as big as the first, which is scattered in the propagation direction of the incident wave and creating the shadow due to the interferences with the incident wave field. If the obstacle is small compared to the wavelength as it is often the case for the problem considered, the scattered wave is propagated in all directions and no sharp shadow occurs [2.13]. With respect to the deflected acoustic power, in [2.6] the scattering cross section Q is

$$Q = \frac{P_S}{2I_O} \text{ for } \lambda \ll a\,. \tag{19}$$

The scattering cross section is a function of frequency and direction of the incident wave. At high frequencies and in a reverberant environment, where an almost diffuse field can be assumed, the directivity of the scattering can be neglected.

Several publications deal with the analytical treatment of the scattering cross section of simply shaped obstacles.

Detailed results for solid cylinders and spheres are given in [2.14]. In [2.15] many formulas relating to problems of scattering of waves from objects are contained. Even if the calculation of scattering pattern is feasible for simple shaped bodies, the obstacles associated with the present problem are generally of complicated shape and an analytical description appears difficult.

To determine the scattering cross section of arbitrarily shaped devices and auxiliaries, an easy to use measurement scheme is required. A simple test rig as suggested in [2.14] is depicted in Figure 6. By this technique a sound source irradiates the scatterer with sound. A microphone array scans a circular or spherical surface concentric with the

scatterer. After integration over the angular distribution of the scattering pattern, the scattering cross section can be calculated as shown in equation (19).

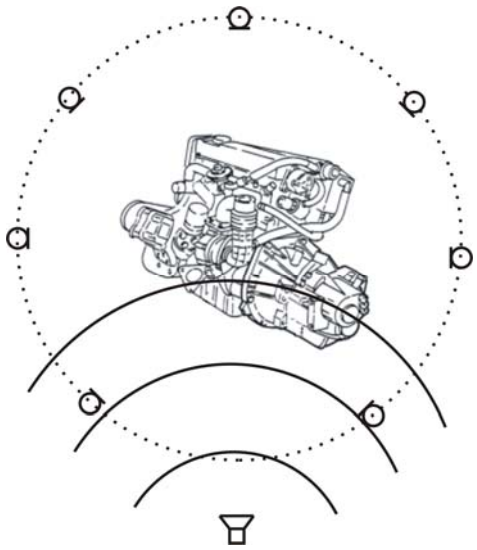

Figure 6: Test rig for the direct measurement of the scattering wave pattern.

In most of the publications, this method is used for analysing the scattering properties of obstacles in fluids, e.g. ultrasonic waves in water. For measurements in air, the method is limited to frequencies, where the wavelength is smaller than or comparable with the dimensions of the scatterer and the test rig.

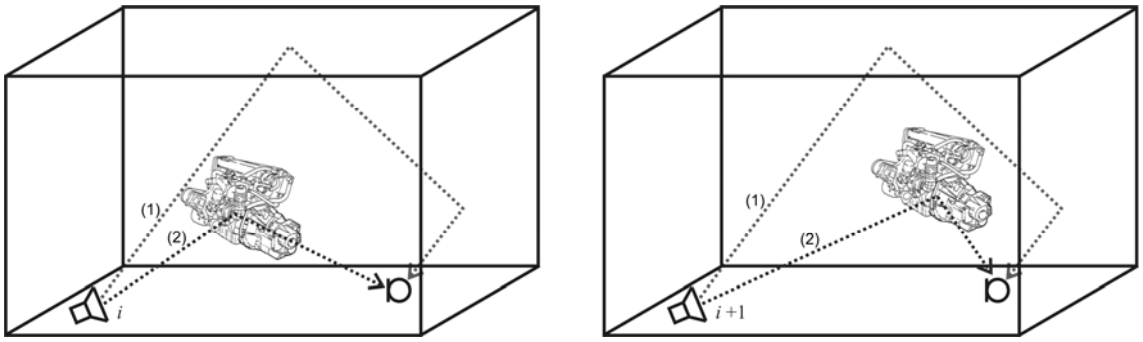

Figure 7: Experimental set up for the DRAWS-technique with different contributions to the echo: (1) Coherent part of the cavity walls; (2) Incoherent part of the moving scatterer.

As an alternative, the diffusing reverberant acoustic wave spectroscopy (DRAWS) [2.16] was developed. Aim of this technique, depicted in Figure 7, is the characterisation of

one or more moving objects in a stationary reverberant cavity with fixed source and microphones. In this method, a number i of sound pulses are emitted into the cavity. The reverberation over time $h_i(t)$ resulting from the *i*-th pulse consists of two parts. First the echoes from the boundaries of the reverberant chamber and second those from the moving scatterers. Between pulses i and $i+1$ the contribution of the chamber boundaries remain steady, whereas the contribution due to the moving objects changes in an uncorrelated way. Therefore, the displacement of the scatterer can be either continuous or stepwise between two pulses. By averaging over a series of N pulses, the coherent contribution of the room remains whereas the incoherent parts of the mobile scatterers are attenuated due to the destructive interference. As shown in [2.16], the mean free path l_m and the scattering cross section Q can be estimated by

$$\frac{\overline{h_i(t)}^2}{\overline{h_i(t)^2}} \approx e^{\frac{-ct}{l_m}} \approx e^{\frac{-ctQ}{V}} \tag{20}$$

wherein V is the volume of the reverberant chamber. The equation is valid as long as the cavity reflections are present. The result should be averaged over different microphone positions. Initially the method has been applied for determining the scattering behaviour of moving objects in water. In [2.17] the method is successfully proven for a rigid sphere in a water tank. Measurements of the scattering cross section of a moving human body in a reverberant room are published in [2.18].

Although the publications applying the DRAWS-method in the airborne sound context are sparse at this moment, the method will be suitable for the present problem. Because of the fact, that the measurements are made in a diffuse sound field, no directivity of the scattering can be determined.

2.4 Illustration of the model

In a first step the applicability of equation (9) and (12) to the given problem will be investigated. Assuming a completely closed, hard walled rectangular box of the size 1.4 x 0.9 x 0.6 m³ and an also hard walled cube with an edge length of $l = 0.2$ m inserted at the centre of the box. The transfer impedance Z from a source position close to one corner of the box to a receiver position close to the opposite corner is calculated by a

commercial FE software tool. For the analytical handling, the inserted cube is converted to a sphere of same volume. The radius a of the sphere is given by

$$a = \sqrt[3]{\frac{3}{4\pi}} l \,. \tag{21}$$

For a configuration with only one sphere equation (12) is modified to

$$Z(k) = \frac{jk\rho c}{V_{free}} \sum_N \frac{\Psi_N(S)\Psi_N(R)}{k^2 - \left[\left(k_x^{(N)}\left(1+\Delta k_x^{(N)}\right)\right)^2 + \left(k_y^{(N)}\left(1+\Delta k_y^{(N)}\right)\right)^2 + \left(k_z^{(N)}\left(1+\Delta k_z^{(N)}\right)\right)^2\right]} \,. \tag{22}$$

The wavenumber shift Δk is calculated using equation (9) for the x-, y- and z-directions separately. In Figure 8 the results of both calculations are compared. The wavenumber shift of the eigenmodes is excellently represented by the analytical approximation. Therewith the approximation of the eigenfrequency shift is demonstrated to be applicable.

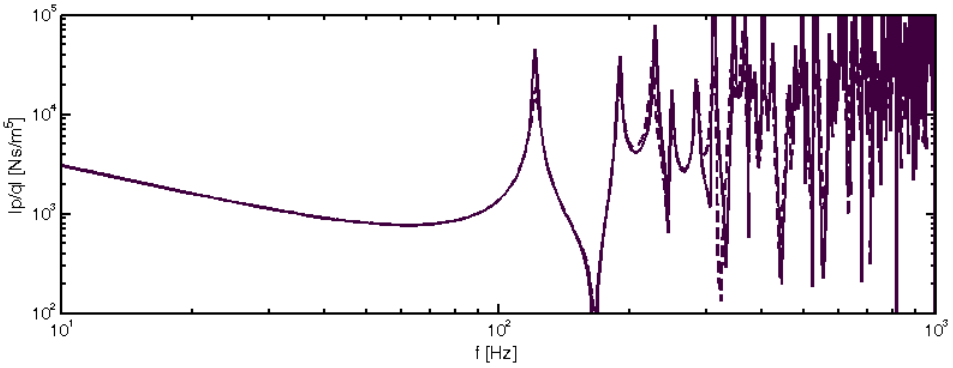

Figure 8: FEM model results of a cube in a box (—) compared with analytical approximation of the eigenfrequency shift due to a sphere with equivalent volume (– – –).

In the next step the validity is checked for the probabilistic approach. Now it is assumed that the closed, hard walled rectangular box of size 1.4 x 0.9 x 0.6 m³ is partially filled with rigid walled cubes of different sizes. Inserted are 40 cubes with an edge length $l = 0.1\,\text{m}$, 8 cubes with $l = 0.2\,\text{m}$ and one with $l = 0.4\,\text{m}$. The cubes are arranged as shown in Figure 9. The arrangement is related to the hypothetic probability density distribution shown in Figure 2. Again, the transfer impedance Z from a source posi-

tion close to one corner of the box to a receiver position, close to the opposite corner, is calculated using FEM. In various test runs with different arrangements it has been shown that a perturbation of the symmetric arrangement presented here does not lead to significant alterations.

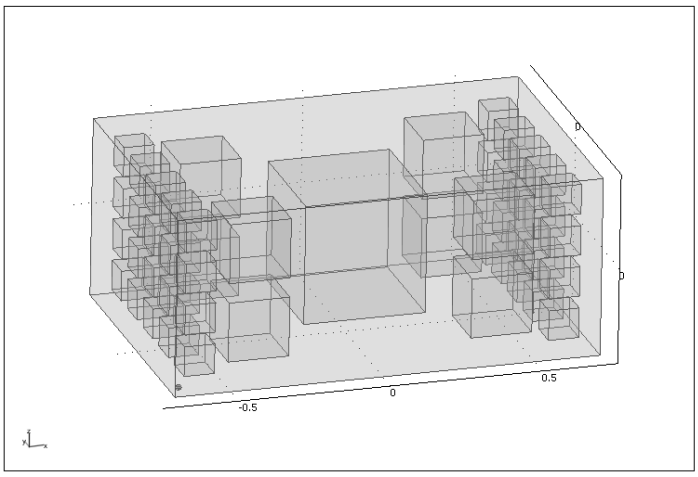

Figure 9: FEM model for the scattering objects approach. The parallelepiped of $(1.2\text{x}0.9\text{x}0.6)m^3$ *is filled with differently sized cubes.*

To analyse the model probabilistically, at first, the cubes have to be converted to spheres with the same volume as described in equation (21). The mean value for a discrete random variable is given by

$$\mu = \sum_{i=1}^{n} X_i p(X_i). \tag{23}$$

X_i can be either the volume V, the number N or the position in x-, y- or z-direction respectively. For the volume the probability distribution $p(V_i)$ is given by

$p(V_i)$	N_i	l_i	a_i	V_i
0.82	40	0.1	0.062	0.001
0.16	8	0.2	0.124	0.008
0.02	1	0.4	0.248	0.064

which leads to $\overline{V} = \mu_V = 0.00338$. The probability distribution for the position in x-direction is determined by using the concentrated volume at the centre of each sphere.

$p(x_i)$	N_i	V_i	N_iV_i	x_i
0.12	20	0.001	0.02	0.1
0.19	4	0.008	0.032	0.3
0.38	1	0.064	0.64	0.7
0.19	4	0.008	0.032	1.1
0.12	20	0.001	0.02	1.3

With the origin of the coordinate system at the centre of the box, $\overline{x} = \mu_x = 0.5$. The mean value of the position in y- and z-direction is 0.5 as well. The probability distribution for the number is given by $p(N_i) = 1/3$ for every i which leads to $\overline{N} = \mu_N = 16.3$.

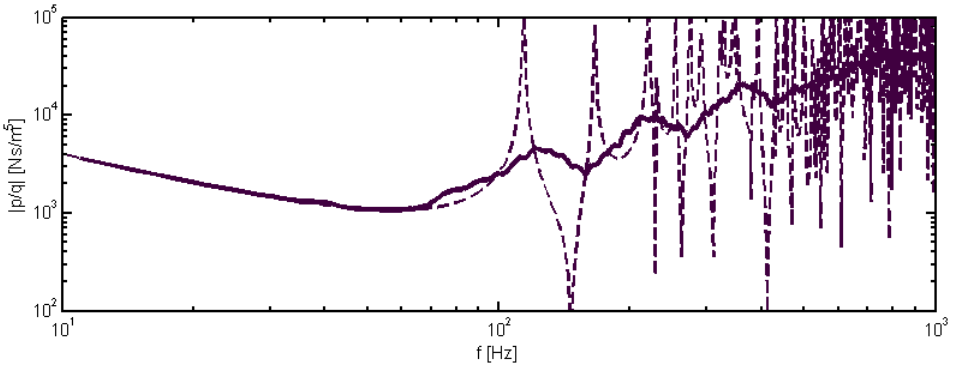

Figure 10: Results of statistical scattering objects model (——) compared with result of a FEM model configuration (– – –).

For the statistical treatment in a Monte Carlo process the probability density distributions for each random variable are required. In the process the random variables will be varied following the probability density distribution. For this primary test the random variables for the position are assumed equally distributed over the whole range within the box. Also the random variables for volume and number of spheres are equally distributed in a domain of $\pm 50\%$ around the mean value.

By using the randomized variables in equations (9) and (12) the Monte Carlo simulation can be performed. The result of the simulation is compared in Figure 10 with the FEM result for the model. As expected, the result of the probabilistic approach captures the main trend of the transfer impedance but not the distinct eigenmodes. As the distributions are assumed fictive, the calculation of variance is not in scope of this investigation.

3 Probabilistically distributed wave guides

In contrast to the scattering method described previously, this approach considers the free fluid volume enclosed in the system. The free volume is subdivided into coupled sub spaces by the installations. It is assumed that the sub spaces can be modelled as a system of coupled one dimensional wave guides. The wave guides vary in length and cross section. The assumption can be argued valid at least for the frequency range below the cut-on frequency of the wave guide with the widest cross section. Further it is assumed that the wave guides are statistically distributed with respect to length and cross section. The coupling points between the wave guides are selected randomly which neglects the space dependency of the model. With these preparations a Monte Carlo simulation can be performed.

3.1 Modelling a system of coupled wave guides

A system of coupled wave guides should be modelled by using the four-pole description. Two types of wave guides are chosen; the tube coupled at both ends and the one-sided coupled tube, terminated acoustically hard at the other side. The element matrix for the tube coupled at both ends is given by [2.19]

$$\begin{pmatrix} p_1 \\ q_1 \end{pmatrix} = \begin{pmatrix} \cos kl & j\frac{\rho c}{S}\sin kl \\ \frac{jS}{\rho c}\sin kl & \cos kl \end{pmatrix} \begin{pmatrix} p_2 \\ q_2 \end{pmatrix} \tag{24}$$

and for the one-sided coupled tube as

$$\begin{pmatrix} p_1 \\ q_1 \end{pmatrix} = \begin{pmatrix} 1 & 0 \\ \frac{jS}{\rho c}\tan kl & 1 \end{pmatrix} \begin{pmatrix} p_2 \\ q_2 \end{pmatrix}. \tag{25}$$

l is the length of the tube and S its cross section. The transfer matrices can be easily transformed to impedance matrices. In this manner, the element impedance matrix for each element e is given by

$$\mathbf{p}_e = \mathbf{Z}_e \mathbf{q}_e \,. \tag{26}$$

For a system of coupled wave guides the transfer impedances between any coupling points can be calculated by assembling the four-pole matrixes of each element together in a topology matrix [2.4]. Therefore the matrices $\mathbf{\Phi}$ are required which describes the position of the element in the assembly, satisfying

$$\mathbf{q}_e = \mathbf{\Phi}_e \mathbf{q} \,. \tag{27}$$

The global impedance matrix assembled by a summation over all N elements is obtained as

$$\mathbf{Z} = \sum_{e=1}^{N} \left[\mathbf{\Phi}_e\right]^T \mathbf{Z}_e \left[\mathbf{\Phi}_e\right]. \tag{28}$$

With this the transfer impedance between any pair of coupling points can be determined.

For a statistical description of a population of realisations, an averaged transfer impedance is required as

$$\overline{Z} = \frac{1}{N} \sum_{i=1}^{N} Z_i \,. \tag{29}$$

This means that no information about any distinct source or receiver position is included. Thus, the transfer impedance is given for an “average” source-receiver-distance. For determining the averaged transfer impedance of the system under consideration, additionally, it has to be averaged over a large number of randomly created realisations. In this Monte-Carlo-simulation the parameters influencing the realisation are varied following a uniform probabilistic distribution.

3.2 Parameter variation

Selecting appropriate parameters influencing the approach is necessary for a reliable statistical model. Finding those parameters is the aim of the investigations described in the following. It is required that the selected parameters represent the main properties

of the considered system. Parameters linking the real system to the statistical model are: the free fluid volume, the maximum length and the maximum cross section of the wave guides in the set. For the statistics, probability density functions are required for each parameter.

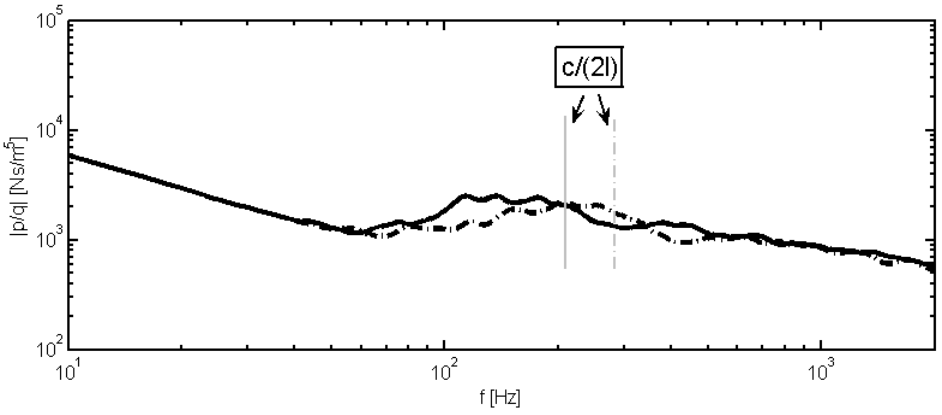

Figure 11: Averaged transfer impedance with varied maximum wave guide length $l = 0.7m$ *(——) and* $l = 0.5m$ *(– · – · –). Free volume* $V = 0.378m^3$ *. Corresponding frequencies* $f = \frac{c}{2l}$ *marked with vertical grey lines respectively.*

As given in equation (1), the free fluid volume governs the characteristics of the system at low frequencies. From equation (3) it is evident that also the order of magnitude of the transfer impedance at intermediate frequencies is influenced by the free volume. An influence is expected of maximum length and maximum cross section of the wave guides on the characteristics of the transfer impedance at intermediate frequencies.

The maximum length should govern the frequency of the lowest mode and the cross section influences the amplitude of the modes. Since the influence cannot be described analytically, different sets of wave guides are simulated using the Monte-Carlo-method to investigate this relation. In the different simulations are varied either the maximum length or the maximum cross section dimension. For the statistic process, the lengths and cross sections are uniformly distributed up to a maximum. To analyse the influence of length and cross section, only one parameter is varied at a time. Hence, it is necessary to keep the other parameter as well as the free volume constant. This means that the number of wave guides included will differ. The magnitudes of two averaged transfer impedances are shown in Figure 11 and Figure 12. From the figures it is seen that

there is a stiffness dominated range at low frequencies. Further, a weak local maximum can be found where the first distinct eigenfrequencies occur.

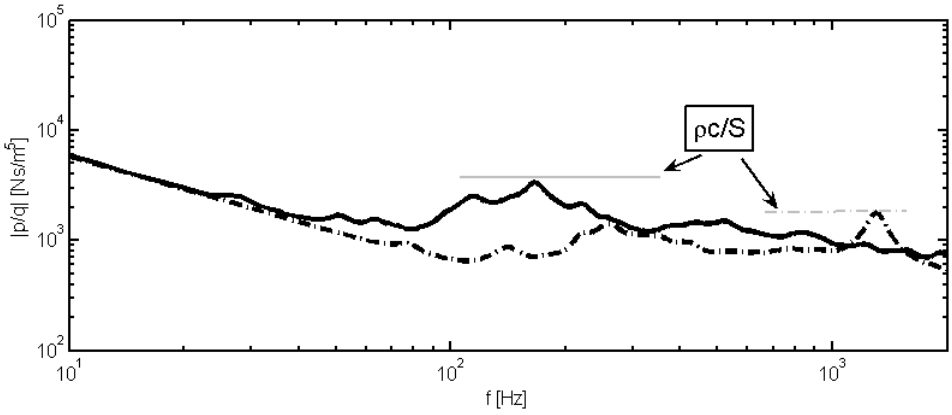

Figure 12: Averaged transfer impedance with varied maximum wave guide cross section $S = 0.1m^2$ *(——) and* $S = 0.2m^2$ *(– · – · –). Free volume* $V = 0.378m^3$. *Corresponding impedance* $Z = \frac{\rho c}{S}$ *marked with horizontal grey lines respectively.*

As an example is shown in Figure 13 the unwrapped phase corresponding to the $S = 0.1\,\mathrm{m}^2$ magnitude curve in Figure 12. From this phase curve it becomes evident that the phase at a receiver position only depends on the shortest distance between source and receiver. It is worth mentioning that magnitude and phase are averaged separately. This is necessary because the system is not minimum phase.

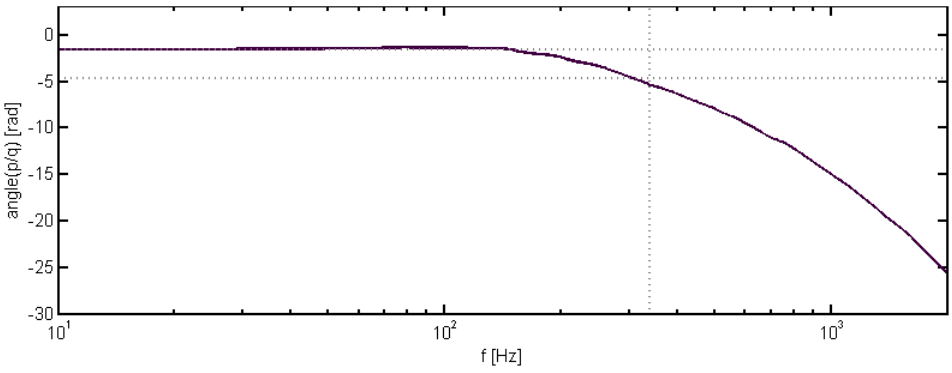

Figure 13: Averaged phase of the transfer impedance to the configuration with $S = 0.1m^2$ *as shown in Figure 12.*

As can be expected, the location of the local transfer impedance maximum depends on the length of the wave guides and is governed by $c/2l$ (see Figure 11). At this value the phase is rotated by $(-\pi)$ in addition to the start value of $(-\pi/2)$ governed by the stiffness of the enclosed fluid. The maximum cross section governs the magnitude of the impedance in this frequency range through the relation $\rho c/S$ as can be seen from Figure 12.

3.3 Illustration of the approach

As an illustration of the approach the results have been compared with those of a Finite-Element calculation. Different FEM models are assembled by filling a rectangular box with different sets of parallelepipeds. An example is shown in Figure 14 with one of the designs used in the investigation. All walls are assumed rigid. The installations subdivide the free volume into a complex system of coupled sub spaces. For all realisations of the model the installations are chosen such that a free volume of 0.378 m³ remains. The parameter for translating the FE-model to the statistical one are determined as follows:

- The free volume V is determined directly from the FE-model.
- The maximum length is set to $l = \sqrt[3]{V}$.
- The maximum cross section is estimated from the FE-model.

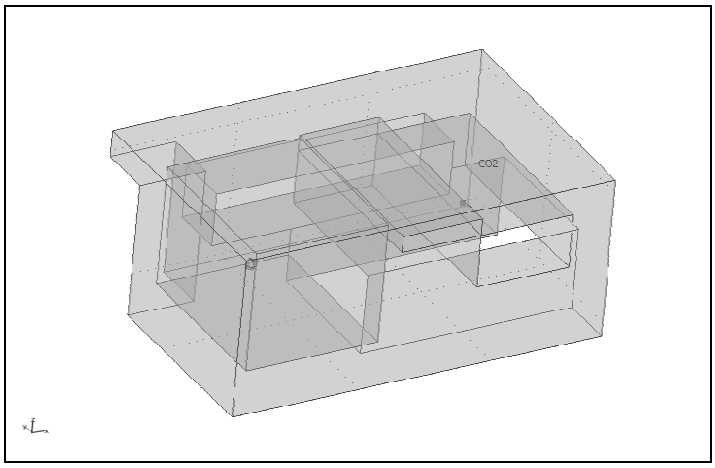

Figure 14: Free volume of the FEM model. The parallelepiped of $(1.4\text{x}0.9\text{x}0.6)m^3$ *is filled with installations.*

The result of the Monte-Carlo process is shown in Figure 15 together with the transfer impedance calculated from two different realisations of the FE-model. The source and receiver positions for the FE calculation have been set arbitrarily.

As expected, the statistical result captures the reality in the lumped range at low frequencies. In a limited frequency domain where the first eigenfrequencies occur the Monte-Carlo results can be seen as a “spine” curve demonstrating the applicability of the suggested method. At high frequencies the models loses its validity. This is also to be expected because of the violation of the plane wave propagation condition for the wave guides.

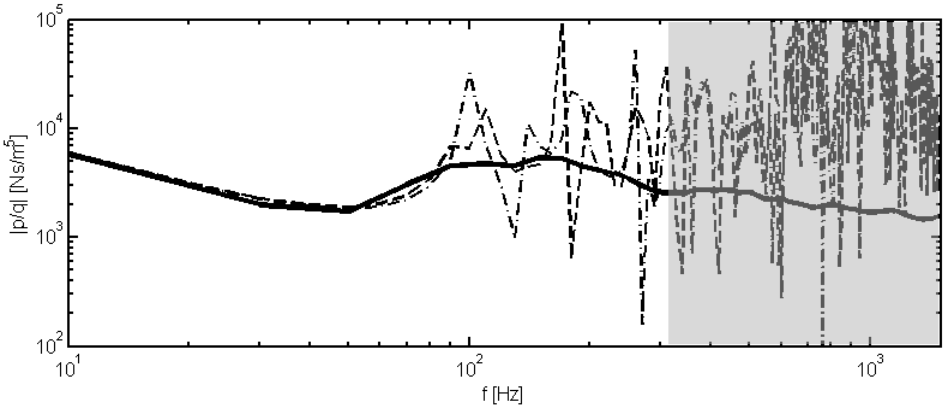

Figure 15: Results of statistical wave guide model (——) compared with results of two different FEM model configurations (– · – · –), (– – –). In the greyed region the validity of the statistical approach is violated.

4 Concluding remarks

Two different probabilistic approaches have been presented for modelling the sound field inside an enclosure densely filled with installations. The approach of probabilistically distributed scattering objects relies upon a modal synthesis whereas the approach of probabilistically distributed wave guides relies upon a wave guide model. Both approaches comply with the salient physics of the system considered. The applicability of the approaches has been investigated.

Both methods offer strategies for engineering practice to obtain reliable results without having detailed information about the geometry and the acoustical properties of the system under consideration. In contrast to deterministic methods, the presented schemes deliver a mean which can be seen as a “spine” of the behaviour. Additional information about the confidence of the results can be extracted.

Taking into account, that mostly the input parameters like geometry or boundary conditions are statistically distributed and therefore also the behaviour, the specification of a confidence interval is necessary. Particularly with regard to series production e.g. in automotive industry, a statistical treatment of the acoustical behaviour becomes important. Depending on the accuracy of the underlying probability assumed, the analysis can be performed either for a group of products, e.g. a type series or for a specific product configuration. Manufacturing tolerances will be averaged. In this context the exact prediction of the eigenmodes often becomes secondary, particularly as long as broadband excitations are investigated.

It is shown that a probabilistic approach is feasible modelling the inserts as well modelling the free fluid space. The phase of the transfer impedance is shown to be only dependent on the shortest distance between source and receiver position. With this knowledge wave interferences can also be predicted.

Consistently, the results of both approaches show a local maximum at frequencies where the first eigenmodes of the system are assumed. As can be seen from the curves presented, the validity range is extended up to higher frequencies for the scattering objects approach. At the time, neither of the approaches includes absorption. As can be observed from a detailed analysis of the behaviour in Work Package One, however, ab-

sorption plays an important role for the real systems. From the measured curve in this figure no distinct eigenmodes are identifiable. The exact prediction of the eigenmodes, however, is of subordinate significance in a highly damped environment.

Although further investigations are required to clarify the limitations of the approaches suggested, it is established that the probabilistic formulations keep the computational effort comparatively low.

5 References

[2.1] L. Cremer and H. A. Müller, Die wissenschaftlichen Methoden der Raumakustik. Vol. 2: Wellentheoretische Raumakustik, (S. Hirzel Stuttgart, 1976).

[2.2] A. Krokstad and S. Strøm and S. Sørsdal, "Calculating the acoustical room response by the use of a ray tracing technique," J. Sound Vibr. **8**, 118-124 (1968).

[2.3] S. Borish, "Extension of the image model to arbitrary polyhedra," J. Acoust. Soc. Am. **75**, 1827-1836 (1985).

[2.4] M. Petyt, *Introduction to finite element vibration analysis*, (Cambridge University Press, 1990).

[2.5] R. H. Lyon and R. DeJong, *Theory and application of statistical energy analysis,* (Second Edition, Butterworth-Heinemann, 1995).

[2.6] H. Kuttruff, "Über den Nachhall in Medien mit unregelmäßig verteilten Streuzentren, insbesondere in Hallräumen mit aufgehängten Streuelementen," Acustica **18**, 131-143 (1967).

[2.7] E. A. Lindqvist, "Sound Attenuation in Large Factory Spaces," Acustica **50**, 313-328 (1982).

[2.8] T. Le Pollès and J. Picaut and S. Colle and M. Bérengier, "Sound-field modelling in architectural acoustics by a transport theory Application to street canyons," Phys. Rev E **72**, 046609-1 – 046609-17 (2005).

[2.9] A. M. Ondet and J. L. Barbry, "Modelling of sound propagation in fitted workshops using ray tracing," J. Acoust. Soc. Am. **85**(2), 787-796 (1989).

[2.10] A. D. Pierce, *Acoustics: An Introduction on Its Physical Principles and Applications*, (McGraw Hill, 1981).

[2.11] E. Leung and C. P. Lee and N. Jacobi and T. G. Wang, "Resonance frequency shift of an acoustic chamber containing a rigid sphere," J. Acoust. Soc. Am. **72**(2), 615-520 (1982).

[2.12] E. A. Lindqvist, *Design Curves for Estimating Sound Pressure Levels in Factories*, Chalmers University of Technology, Swedish Council of Building Research, Stockholm (1982).

[2.13] P. M. Morse and K. U. Ingard, *Theoretical Acoustics*, (McGraw Hill 1968).

[2.14] J. J. Faran, "Sound scattering of solid cylinders and spheres," J. Acoust. Soc. Am. **23**, 405-418 (1951).

[2.15] J. J. Bowman and T. B. A. Senior and P. L. E Uslenghi, *Electromagnetic and acoustic scattering by simple shapes*, (North-Holland Publishing Co. 1969).

[2.16] J. De Rosny and P. Roux, "Multiple scattering in a reflecting cavity: Application to fish counting in a tank," J. Acoust. Soc. Am. **109,** 2587-2597 (2001).

[2.17] D. Dremer and S. Conti and J. De Rosny and P. Roux, "Absolute measurement of total target strength from reverberation in a cavity," J. Acoust. Soc. Am. **113**, 1387-1394 (2003).

[2.18] S. Conti and P. Roux and D. Dremer and J. De Rosny, "Measurement of the scattering and absorption cross sections of the human body," Applied Physics Letters **84,** 819-821 (2004).

[2.19] M. L. Munjal, *Acoustics of Ducts and Mufflers*, (John Wiley & Sons., 1987).

Work Package 3:

Improvements on the statistical sound field description

Abstract:

The diffuse field assumption employed in Statistical Energy Analysis (SEA) and in statistical room acoustics is violated for positions close to boundaries or discontinuities. An approach is suggested to include the correction made by Waterhouse based on spherical Bessel functions in SEA-predictions. With this modification the SEA-results will be augmented by a position dependence and an additional frequency dependence. The approach is extended and demonstrated for plate-like structures. The validity of the approach is confirmed by means of comparisons with modal analysis.

1 Introduction

The use of Statistical Energy Analysis (SEA) usually assumes multi-resonant or diffuse field condition. Therefore, a uniform distribution of sound energy is assumed and random phase relations between different wave field components converging at one point. It is shown in Work Package One that this assumption is not valid unrestrictedly for real systems. These results coincide with those published by Waterhouse [3.1]. Waterhouse predicted that the assumption of a uniform sound field distribution is violated at least close to reflecting surfaces. This is due to the fact that the phases of the reflected wave trains near to reflecting surfaces are not entirely random. Interference pattern occur and the energy density is not uniform. For his investigations Waterhouse assumes an arbitrary oblique incidence of the sound waves averaged over all angles as is the case for a reverberant sound field.

With this in mind it is expected, that an error occurs in the SEA calculation for the case that the source is situated near to a reflecting surface. Because of reciprocity this error also occurs for similar receiver positions. Especially for the considered small enclosures those positions are very probable.

In the following an approximation is presented to calculate a correction term to account for the influence of the interference pattern in an SEA calculation. As in the paper by Waterhouse a mirror image method is employed.

It is conceivable, that the effect of reflecting surfaces is expandable to any wave field discontinuities. Hence, in the second part of the work done within this work package the method developed for air borne sound is adopted to a structural acoustics problem. For a plate it is shown that depending on the boundary condition interference pattern occur as well. For the case of a simply supported plate the correction term is developed by using the results of Petersson [3.2], [3.3]. In the papers the spatial variation of the significance of force excitation are investigated in the proximity of discontinuities on beam and frame-like structures as well as on plate-like structures.

At the end of each section, the modified statistical results are compared with those from a modal analysis.

2 Interference patterns and SEA in rooms

2.1 Interference pattern

In his investigations Waterhouse [3.1] observes that the energy in an air borne sound field is not equally distributed. For the case of oblique incidence of the wave on reflecting surfaces as it is the case in a reverberant sound field he calculates the mean square sound pressure $\langle p^2 \rangle$ which is an equivalent of the potential energy. This is done for the wall, edge and corner position of the observer point by using one, three and seven reflected wave components respectively with an averaged angular incidence. For the corner case Waterhouse derives

$$\begin{aligned}\langle p^2 \rangle \sim 1 &+ j_0(2kx) + j_0(2ky) + j_0(2kz) + j_0\left(2k\sqrt{x^2+y^2}\right) \\ &+ j_0\left(2k\sqrt{x^2+z^2}\right) + j_0\left(2k\sqrt{y^2+z^2}\right) \\ &+ j_0\left(2k\sqrt{x^2+y^2+z^2}\right)\end{aligned} \tag{1}$$

where x, y and z are the distances from the reflecting surface and k is the wave number. The function $j_0(x)$ is the zero order spherical Bessel function. The interference pattern for the potential energy is plotted in Figure 1. As expected, the amplification is 9 dB close to the corner for low frequencies. A dip can be observed for the first destructive interference.

For an SEA calculation commonly, the input impedance for the power injection is assumed to be that of a corresponding infinite system. This can be argued valid for high frequencies where the energy is equally distributed or for random excitation points. If the system under consideration has distinct points where the energy is injected, the input impedance at these points become important. As has been shown, the impedance will deviate from that obtained for free field conditions. Contrary to Waterhouse, who employed an energetic approach for correcting the sound pressure, a wave propagation approach is used in the following to find a correction term for approximating the input impedance.

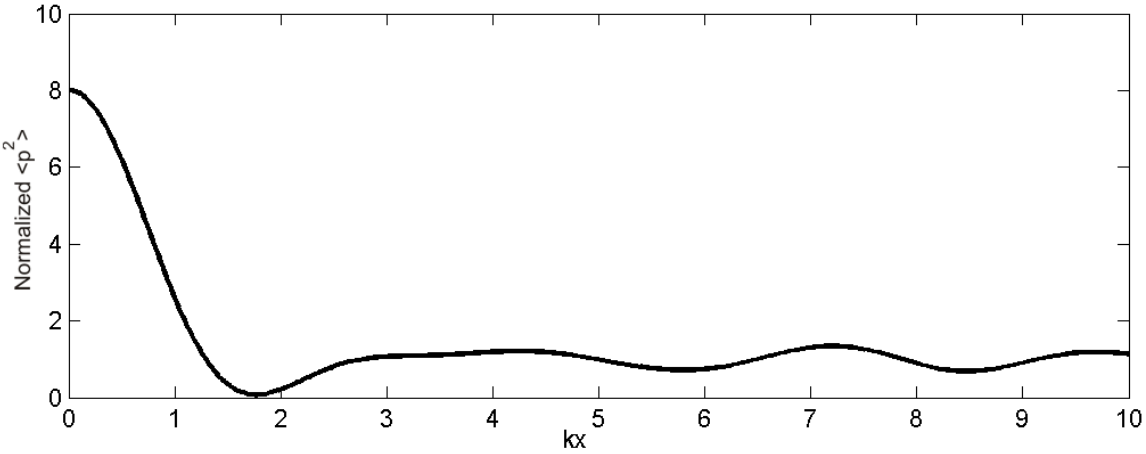

Figure 1: Interference pattern in reverberant sound fields at reflecting corners [3.1]. The source is on the symmetry axis.

For a corner position, as depicted in Figure 2, the infinite system becomes semi-infinite by inserting semi-infinite reflecting surfaces in the xy-, yz- and xz-plane. With the reflectors, mirror image sources can be constructed. Due to the infinite extent of the model only images with either one, two or three reflections appear. Each image can be seen as source of a propagating spherical wave field. The phase as well as the amplitude of the wave is influenced by the reflection. For reasons of simplicity all surfaces are assumed rigid and the reflection factor is 1.

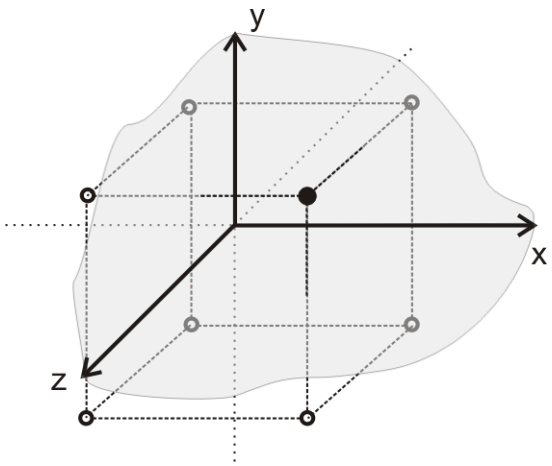

Figure 2: Image sources for corner case in a semi-infinite room.

The acoustic potential at a distance *r* for a harmonically radiating monopole with the complex amplitude A amounts to

$$\phi(r,t) = A\frac{e^{i\omega(t-r/c)}}{r} \tag{2}$$

and the sound pressure is given by the relation

$$p(r,t) = -\rho\frac{\partial\phi}{\partial t}, \tag{3}$$

which yields

$$p(r) = -\frac{j\omega\rho A}{r}e^{-jkr}. \tag{4}$$

With the Euler equation

$$p(r) = k^2\rho cA\left(\frac{\sin(kr)}{kr} - j\frac{\cos(kr)}{kr}\right) \tag{5}$$

the pressure can be expressed in terms of spherical Bessel functions of first and second kind

$$p(r) = k^2\rho cA\left(j_0(kr) - jy_0(kr)\right). \tag{6}$$

Assuming that the pressure at the source is $p_n = k^2\rho cA$, the pressure at a distance r_n is given by

$$p(r_n) = p_n\left(j_0(kr_n) - jy_0(kr_n)\right). \tag{7}$$

For the investigated model (Figure 2) the polar co-ordinate

$$r_n = \sqrt{(x_n - x)^2 + (y_n - y)^2 + (z_n - z)^2} \tag{8}$$

can be interpreted as the distance between the n-th image and the response point (x, y, z). By inserting

$$p_n = Z_0 v = Z_0 \frac{q}{4\pi a^2} \tag{9}$$

in (7) and summing the contributions of all sources, the image sources with $n = 1 \ldots 7$ and the actual excitation point for $n = 0$, the input impedance is given by

$$Z(x,y,z) = \frac{p(x,y,z)}{q(x,y,z)} = \frac{Z_0}{4\pi a^2} \sum_{n=0}^{7} \left(j_0(kr_n) - j y_0(kr_n) \right). \tag{10}$$

The sum in this impedance formula can be seen as a correction term for the input impedance in an elementary SEA calculation

$$\Pi_{air}(x,y,z) = \sum_{n=0}^{7} \left(j_0(kr_n) - j y_0(kr_n) \right), \tag{11}$$

from which the real and imaginary part can be separated easily.

2.2 Statistical room acoustics

The simple SEA model investigated consists of one room with dissipation. The energy inside the room is given by [3.4]

$$E = \frac{P_{in}}{\omega \eta}, \tag{12}$$

wherein P_{in} is the imparted power, η is the loss factor and E the energy inside, and is therefore equally distributed. For a cavity, the dissipation depends on the absorption and the volume V. The absorption inside is given by the equivalent absorbing surface $S_w \bar{\alpha}$, with the wall surface of the enclosure S_w and its mean absorption coefficient $\bar{\alpha}$. With this the loss factor of the cavity is of the form

$$\eta = \frac{c S_w \bar{\alpha}}{4 V \omega} \tag{13}$$

For calculating the transfer impedance as a descriptor of the sound field inside the enclosure the ratio of sound pressure p to volume velocity q is required. The relation between energy and sound pressure in a room is

$$E = \frac{p^2 V}{\rho c^2}. \tag{14}$$

A monopole source of radius a is assumed as source for the power injection. With a velocity v_a at its surface, the imparted power [3.5] is given by

$$P_{in} = 2\pi a^2 v_a^2 \rho c \frac{k^2 a^2}{1 + k^2 a^2}. \tag{15}$$

Combining these formulae and inserting the volume velocity of the source as $q = 4\pi v_a a^2$, the transfer impedance can be written as

$$Z_{SEA} = \frac{p}{q} = \frac{\rho c}{\pi a} \sqrt{\frac{8}{\pi \left(A_w \bar{\alpha} \right)} \cdot \frac{k^2 a^2}{1 + k^2 a^2}}. \tag{16}$$

By introducing the correction term $\Pi_{air}\left(x_s, y_s, z_s\right)$ and $\Pi_{air}\left(x_r, y_r, z_r\right)$ for the source and receiver position respectively in the assumption that the imparted power can be evaluated as

$$P_{in} = \frac{1}{2} |p|^2 \, \mathrm{Re}\{Z_0\} \tag{17}$$

the modified transfer impedance is obtained as

$$Z_{SEA\_corr} = Z_{SEA} \cdot \mathrm{Re}\left\{\Pi_{air}\left(x_s, y_s, z_s\right)\right\} \cdot \mathrm{Re}\left\{\Pi_{air}\left(x_r, y_r, z_r\right)\right\}. \tag{18}$$

In Figure 3, the results calculated by means of an elementary SEA model and those modified by the influence of the interferences at source and receiver position are compared with those from a modal synthesis of a rectangular room with all walls rigid. There the mode shape is simply given by e.g. [3.6]

$$\Psi_N = \cos\left(\frac{\pi n_x x}{l_x}\right)\cos\left(\frac{\pi n_y y}{l_y}\right)\cos\left(\frac{\pi n_z z}{l_z}\right), \tag{19}$$

where the room dimensions are l_x, l_y and l_z respectively. The eigenvalues are given by

$$k_N^2 = \left(\frac{\pi n_x}{l_x}\right)^2 + \left(\frac{\pi n_y}{l_y}\right)^2 + \left(\frac{\pi n_z}{l_z}\right)^2; \quad n \in N. \tag{20}$$

The transfer impedance, defined as the ratio of pressure to volume velocity, can be calculated from

$$Z = \frac{p}{q} = jk\frac{\rho c}{V}\sum_N \frac{\Psi_N(S)\Psi_N(R)}{k_N^2 + jg_N k_N - k^2}, \tag{21}$$

where ρ is the density, V the volume and c the sound speed. S and R denote the source and receiver co-ordinates respectively. The losses inside the enclosure are included in the damping coefficient g_N.

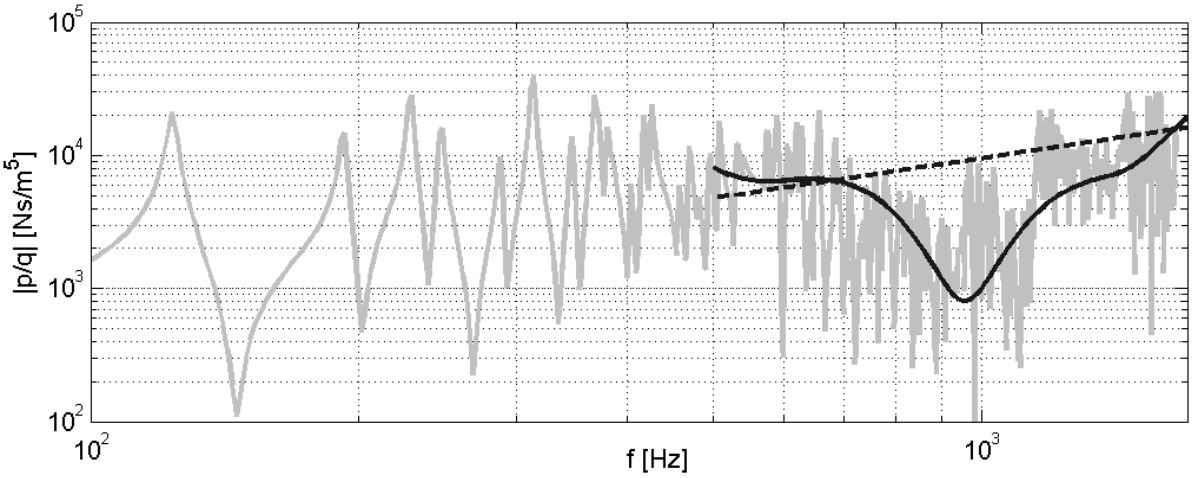

Figure 3: Transfer impedance for rectangular room. (grey: analytical result, dashed black: elementary SEA result, solid black: corrected SEA result).

From the graphs of the transfer impedance in Figure 3, calculated analytically for a rectangular room with source and receiver position close to corners, 'global' dips and troughs can be found in the high frequency range. Thus, the signature of the analyti-

cally calculated curve deviates noticeably from the results predicted with the straightforward SEA model.

Bearing the Waterhouse results in mind, such deviations are also expected and, hence, the dips observed are associated with destructive interferences. Especially those from the first reflection around 1 kHz are prominent. In the curve calculated with the elementary SEA formula these interferences are not captured. Modifying the SEA results by means of the interference correction term (eq. (18)), the predictions are brought in better agreement with the analytical results. However, because higher order reflections are neglected in the approach, not all of the subtleties will be captured.

3 Interference patterns and SEA on plates

3.1 Interference Pattern

The effect of a discontinuity on a plate is to reflect the incident wave. The reflection factor of the plate boundary depends on the boundary condition and can either be real or complex whereas the complex value indicates a phase shift between incident and reflected wave. For the elementary case of a simply supported plate boundary, the reflection factor is –1. For this case the interference pattern can be developed by the method of image sources as suggested in [3.3] and depicted in Figure 4.

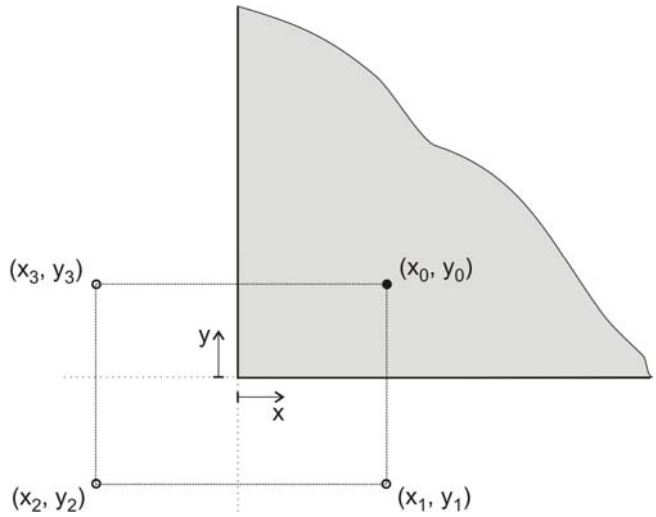

Figure 4: Image sources for a corner position of the excitation on a simply supported semi-infinite plate.

Assuming a time base of $e^{j\omega t}$, the transfer function from the *n*-th mirror image source to the response point (x, y) is given in terms of the Hankel-functions of second kind and zero order $H_0^{(2)}(x)$ by [3.7]

$$v(r_n) = v_n\left(H_0^{(2)}(kr_n) - H_0^{(2)}(-jkr_n)\right), \tag{22}$$

where the distance between excitation and response point is

$$r_n = \sqrt{\left(x_n - x\right)^2 + \left(y_n - y\right)^2} \,. \tag{23}$$

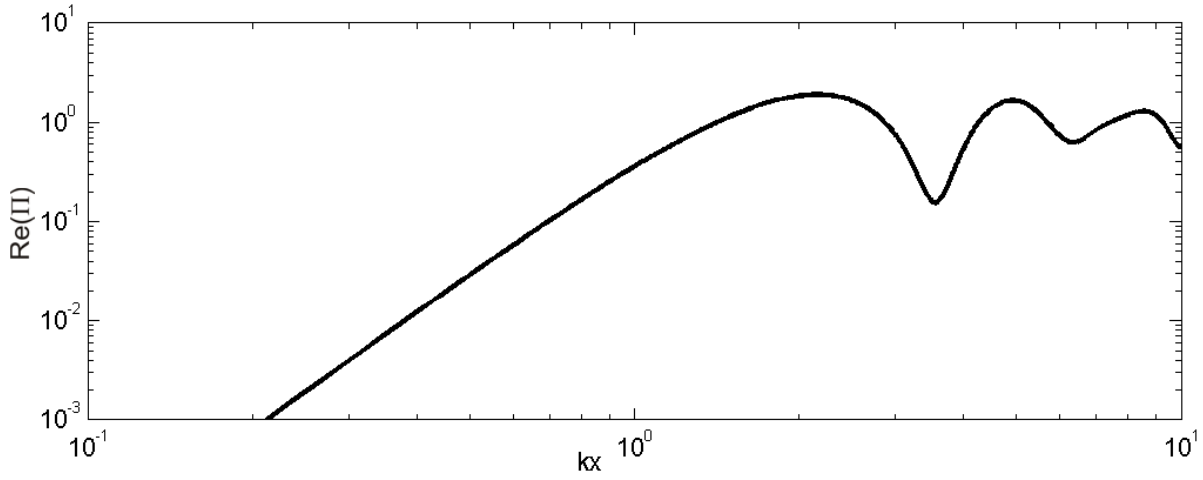

Figure 5: Real part of the correction factor on a plate for corner position with distance x = y from corner

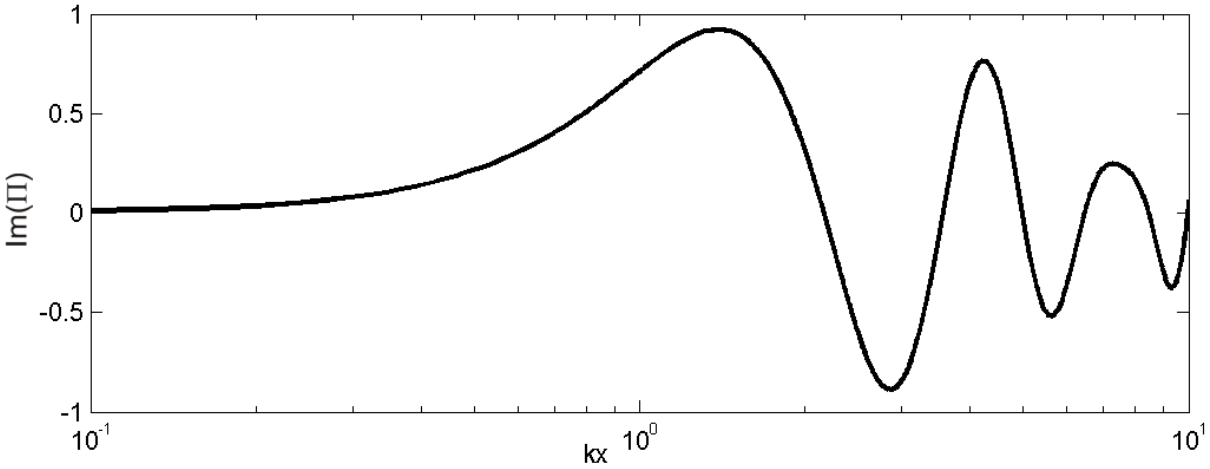

Figure 6: Imaginary part of the correction factor on a plate for corner position with distance x = y from corner

Exciting the fully infinite plate with the force *F,* the velocity at any image source is

$$v_n = Y^{\infty} F \tag{24}$$

wherein Y^{∞} is the input mobility of the infinite plate in terms of the bending stiffness B' and the mass per unit area m'' given by

$$Y^{\infty} = \frac{1}{8\sqrt{B'm''}}. \tag{25}$$

Summing up the contributions of all first and second order images, regarding their reflection factors at the discontinuities leads to

$$Y = \frac{v}{F} = Y^{\infty}\sum_{n=0}^{3}(-1)^n\left(H_0^{(2)}(kr_n) - H_0^{(2)}(-jkr_n)\right), \tag{26}$$

from which

$$\Pi_{plate}(r_n) = \sum_{n=0}^{3}(-1)^n\left(H_0^{(2)}(kr_n) - H_0^{(2)}(-jkr_n)\right) \tag{27}$$

is the correction factor for corner positions of excitation or receiver. The real and, for the sake of completeness, the imaginary parts can be separated as

$$\mathrm{Re}\left\{\Pi_{plate}(r_n)\right\} = \sum_{n=0}^{3}(-1)^n J_0(kr_n) \tag{28}$$

and

$$\mathrm{Im}\left\{\Pi_{plate}(r_n)\right\} = -\sum_{n=0}^{3}(-1)^n\left[N_0(kr_n) + \frac{2}{\pi}K_0(kr_n)\right]. \tag{29}$$

In the Figure 5 and Figure 6, the normalized mobility for the corner position is depicted.

3.2 Statistical plate vibration

Statistically, the energy on the plate is given in [3.4] by

$$E = \frac{P_{in}}{k^2\eta}\sqrt{\frac{m''}{B'}}. \tag{30}$$

On a plate with the area *S*, the kinetic energy

$$E = \frac{1}{2} m'' S v^2 \tag{31}$$

results from the injected power P_{in} calculated by the exciting force and the real part of the input mobility as

$$P_{in} = \frac{1}{2} |F|^2 \operatorname{Re}\{Y\}. \tag{32}$$

For high frequencies the input mobility can be taken to be as that of an infinite plate given by

$$\operatorname{Re}\{Y^{\infty}\} = \frac{1}{8\sqrt{B' m''}}. \tag{33}$$

Combining equation (30) to (33), the averaged transfer mobility from the statistical consideration can be written as

$$Y_{SEA} = \frac{v}{F} = \frac{1}{2k\sqrt{2B' m'' \eta S}}. \tag{34}$$

By introducing the correction factor for the exciter and receiver position, the effect of interferences is incorporated in the statistical model. By modifying (32) into

$$P_{in} = \frac{1}{2} |F|^2 \operatorname{Re}\{Y^{\infty} \cdot \Pi_{plate}(x, y)\} \tag{35}$$

and invoking reciprocity for the exciter and the receiver position marked with the indices *e* and *r* respectively, the transfer mobility changes to

$$Y_{SEA\_corr} = Y_{SEA} \cdot \operatorname{Re}\{\Pi_{plate}(x_e, y_e)\} \cdot \operatorname{Re}\{\Pi_{plate}(x_r, y_r)\}. \tag{36}$$

To compare the results with those from the modal analysis, the modal description of the sound field of a simply supported rectangular plate is given by [3.7]

$$Y = \frac{v}{F} = \frac{4jk^2}{S\sqrt{m''B'}} \sum_{n=1}^{\infty} \frac{\sin\left(\frac{n_x \pi x}{l_x}\right)\sin\left(\frac{n_y \pi y}{l_y}\right)\sin\left(\frac{n_x \pi x_q}{l_x}\right)\sin\left(\frac{n_y \pi y_q}{l_y}\right)}{k_n^4 - k^4} \tag{37}$$

with the eigenvalues

$$k_n^2 = \left[\left(\frac{\pi n_x}{l_x}\right)^2 + \left(\frac{\pi n_y}{l_y}\right)^2\right]; \qquad n \in N\,. \tag{38}$$

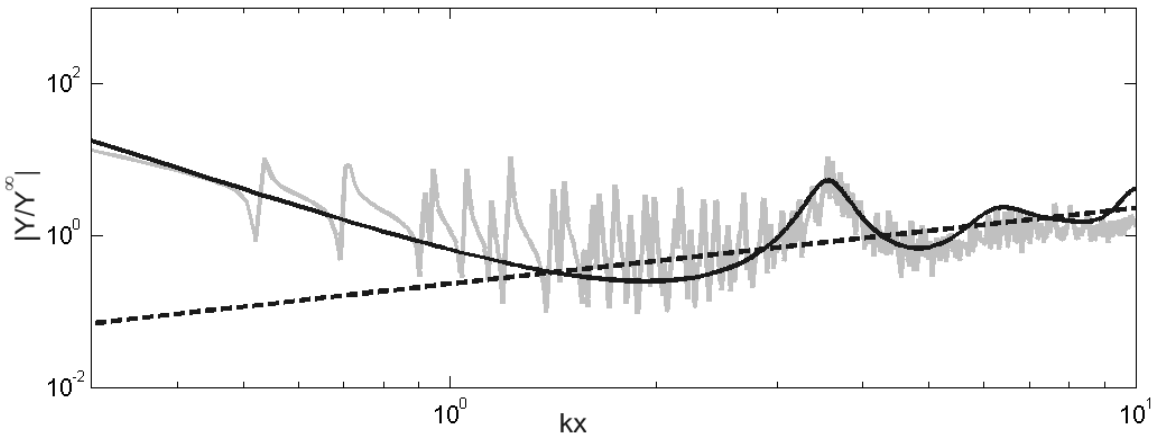

Figure 7: Normalized point mobility for a simply supported rectangular plate ($x_r = x_e = y_r = y_e = x$); (grey: analytical result, dashed black: elementary SEA result, solid black: corrected SEA result).

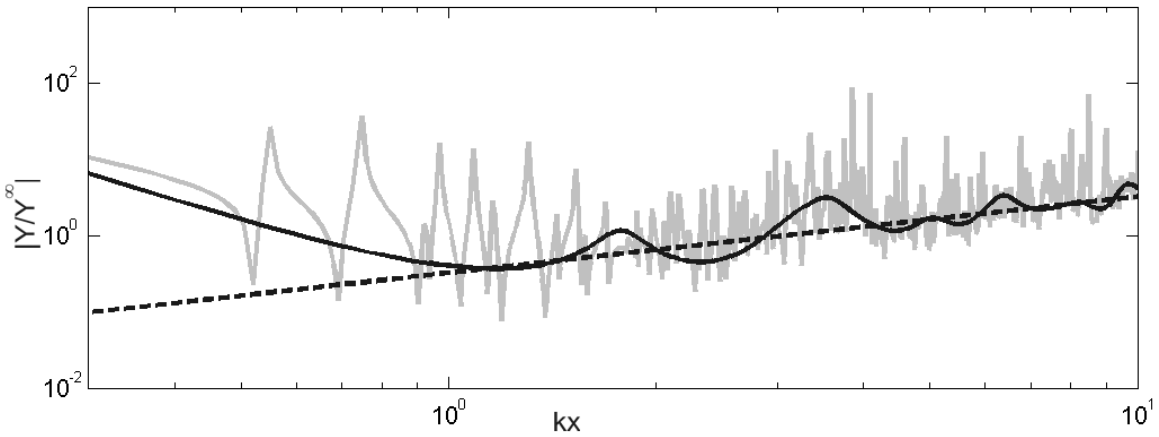

Figure 8: Normalized transfer mobility ($x_r = 2x_e = y_r = 2y_e = x$); (grey: analytical result, dashed black: elementary SEA result, solid black: corrected SEA result).

As expected the same results can be observed for the structural acoustic case as for the airborne sound case. In Figure 7 and Figure 8 the curves for a point and a transfer mobility are displayed respectively. It is seen that the modified SEA curve renders an improved approximation for the behaviour of the transfer mobility at high frequencies. The unexpectedly good agreement also at low frequencies should be observed. In this frequency range SEA is usually not applicable because the modal density is not high enough.

For the investigation only simple discontinuities with real reflection coefficients were taken into account. It is expected that the method works well also for more complex structures. The reflected sound field components than can be determined by using the work [3.8]. The resulting reflection coefficients than can be inserted in equation (26).

4 Concluding Remarks

In this work package a simple method is presented to improve the accuracy of an SEA calculation when the exciter and receiver position are known. The method suggested takes the effect of primary interferences of a sound field into account in the SEA description. It is shown that those interferences are particularly important if source and receiver position are close to sound field discontinuities. Two cases are investigated, a corner position of source and receiver in a reverberant room and on a simply supported plate. In both cases the input impedance of an infinite system is substituted by those of a semi-infinite one. This means the highly reverberant sound field is simplified by considering only the influence of the first order reflections by including the corresponding image sources. The effect of higher order reflections is neglected. Although the scheme presented is approximate, the results are radically improved compared with the elementary SEA calculation.

Even though, the method is developed for known exciter and receiver positions, it is also applicable to assess the spatial deviation of an SEA result.

5 References

[3.1] R. V. Waterhouse, “Interference Patterns in Reverberant Sound Fields,” J. Acoust. Soc. Am. **27**(2), 247-258 (1955).

[3.2] B. A. T. Petersson, “Structural acoustic power transmission by point moment and point force excitation; Part 1: Beam- and frame-like structures,” J. Sound Vibr. **160**, 43-66 (1993).

[3.3] B. A. T. Petersson, “Structural acoustic power transmission by point moment and point force excitation; Part 2: Plate-like structures,” J. Sound Vibr. **160**, 67-92 (1993).

[3.4] R. H. Lyon and R. DeJong, *Theory and application of statistical energy analysis*. (Second Edition, Butterworth-Heinemann, 1995).

[3.5] A. D. Pierce, *Acoustics - An introduction to its physical principles and applications*. (McGraw-Hill, 1981).

[3.6] P. M. Morse, *Vibration and Sound*. (Acoustical Society of America, 1995).

[3.7] L. Cremer and M. Heckl and B.A.T. Petersson, *Structure-Borne Sound*, (Springer, Berlin, 2005).

[3.8] B. A. T. Petersson, “Transfer mobilities of stiffened plates,” Proceedings of Ninth International Conference on Recent Advances in Structural Dynamics, Southampton, (2006).

Work Package 4:

Characterisation of complex shaped sound sources

Abstract:

The Nearfield Acoustical Holography (NAH) in spherical co-ordinates can be used for the reconstruction of sound field parameters close to the surface of an arbitrarily shaped sound source. It is known that depending on the shape of the source the applicability of this reconstruction method is limited by the validity restrictions of the Rayleigh hypothesis. To overcome the limitation of the minimal sphere given by the validity restriction an algorithm is proposed for extracting local information from the non convergent NAH-solution. For the assessment of the results an appropriate virtual test rig is developed employing the Kirchhoff-Helmholtz-Integral-Theorem.

1 Introduction

The analysis and characterisation of sources of sound and vibration remains a challenging area of research. In this pursuit also simplifications are required making proposed methods applicable in engineering practice. As shown in recent text books, the methods of weighted residuals offer appropriate tools for source characterisation. The basic idea is the expansion of the sound field in terms of outgoing wave components radiated from a set of discrete theoretical sources always located inside the vibrating body. Those sets of theoretical sources e.g. a number of distributed monopole and/or dipole sources establish the field at a predefined, continuous interface, simulating that of the actual source sufficiently accurately [4.1]. Alternatively this is achieved by a single multipole. There the pseudo sources of different order are concentrated in one point. This model can be seen as an analogy to a wave field expansion in spherical co-ordinates. Although the expansion is infinite in theory it is truncated in any practical realisation and, hence, errors are introduced. The expansion coefficients can be considered as the complex strengths of the pseudo sources (poles). By knowing the expansion coefficients the field can be reconstructed on any point where the expansion is valid. This means that also the surface impedance of the source can be determined which is essential for including the sources into the sound propagation models.

One possibility to determine the expansion coefficients is the Nearfield Acoustical Holography (NAH). A goal of the NAH in the given context can be to reconstruct the velocity and the sound pressure of the vibrating source surface by simply measuring the sound pressure on a hypothetical surface at an accessible distance from the source. Because of the advantage of the closed, compact analysis surface, the NAH in spherical co-ordinates is desirable for this analysis. The periodicity of the analysis surface removes the requirement of spatial windowing and introduces no low frequency limit. Further it provides a way to measure the source as one entity rather than at different time steps. This might be pivotal for transient processes. For the spherical NAH, however, it is required that the sound source is completely enclosed by the analysis surface.

This condition can be easily fulfilled if the shape of the source is nearly spherical. The velocity can be calculated directly on or close to the source surface. In engineering

practice, the sound sources usually have complicated shapes. For arbitrarily shaped sources the limitation of the minimal sphere becomes important.

Consider the radiating body as a bounded domain $D \subset \mathbb{R}^3$, bounded by the surface Γ. Denote the exterior domain $D' = \mathbb{R}^3 \setminus D$. For all spheres B with the origin inside D completely enclosing D and accordingly not intercepting it at any point, the NAH approach is always valid and the field can be reconstructed for any point on the sphere. It should be mentioned that the field is represented entirely in terms of outgoing wave functions.

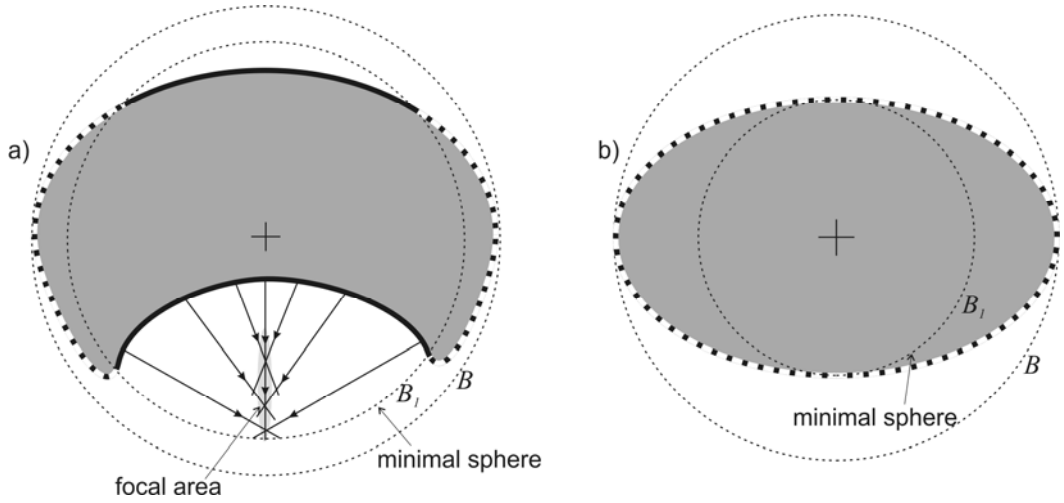

Figure 1: The minimal sphere B_1 limits the validity of the sound field reconstruction. The sound field can be reconstructed only on the dashed white marked surface segments of the sound source (grey). a) Sound field singularities occur in the focal area. b) The field is free of singularities.

One century ago Rayleigh [4.2] conjectured that the representation can also be applied unrestricted to the interior of B. With that the wave field could also be predicted at the surface of any non-spherical source. At present, there is no doubt that the so called Rayleigh hypothesis (or Rayleigh conjecture) does not generally apply to arbitrarily shaped source configurations. Millar [4.3] and van den Berg [4.4] showed that the validity of the Rayleigh hypothesis depends on whether there are singularities in the wave field or not. Consider a minimal sphere B_1 with smaller radius than B but the same origin so that all singularities of the sound field are inside B_1 as depicted in Figure 1a).

Everywhere outside B_1 the Rayleigh hypothesis holds. Only if B_1 is completely inside D as illustrated in Figure 1b) the solution of the expansion can be analytically continued to the entire source surface. Consequently the hypothesis never holds if the surface has edges [4.4], [4.5]. And this, however, is in general the case for practically relevant sources. This means, that the NAH is not applicable in engineering practice unrestrictedly.

To overcome this problem, Wu [4.6] suggested the Helmholtz equation–least-squares (HELS) method. The applicability of this method was demonstrated for simply shaped vibrating bodies with smooth surfaces. Alternatively, the Helmholtz integral theory can be used to form an NAH description. This BEM-based NAH has been used successfully to reconstruct acoustic radiation from structures [4.8]. Wu [4.9] employed a combination of both methods in the combined Helmholtz equation–least-squares (CHELS) method. The outer domain between the measurement surface and the minimal sphere is solved with sound field reconstruction whereas the inner domain is calculated using a BEM-approach. For complex structures the number of nodes necessary to describe the acoustic field can be large, which makes the reconstruction process very time consuming.

The problem of sound field reconstruction is closely related to the handling of scattering by obstacles. In the publications on the modified Rayleigh conjecture, Ramm [4.10] has shown the sound field to converge overall on the surface of obstacles not fulfilling the Rayleigh hypothesis. With this in mind the question arises if there is an approximation of the sound field values directly on or close to the surface of arbitrary shaped vibrating bodies.

Hence, focus of this work package is on investigating the influence of the singularities in the sound field beside the fact that the field expansion is not uniformly convergent. With this knowledge a method will be proposed for an approximate prediction of the sound field not fulfilling the Rayleigh hypothesis. In this method the expansion is transformed into one that converges rapidly.

For the investigations a manageable virtual test rig is required. Such a test rig consists of a known source. It enables the determination of sound field parameters at any virtual surface surrounding the source. On that surface the sound field can be sampled. Since it

is known that the NAH reconstruction of the sound field is sensitive to the presence of noise it will be added artificially to the sampled data. In Section 2 a virtual test rig is developed employing the Kirchhoff-Helmholtz-Integral.

2 Modeling the test source

The virtual test rig developed in this section will be used in the same configuration for all investigations presented within this work package. The test rig is used for simulating the sound pressure on the measurement grid and for the assessment of the NAH results. Using the Kirchhoff-Helmholtz-Integral (KHI), the sound pressure at any point in the exterior field of a source can be calculated by integrating the monopole- and dipole-parts of any surface element of the source. For harmonic motion, the KHI is given by [4.11]

$$p\left(\vec{x}_0\right) = \frac{i\omega\rho_0}{4\pi}\int_S \frac{e^{-ikr}}{r} v_n dS + \frac{1}{4\pi}\int_S p\frac{\partial}{\partial n}\left(\frac{e^{-ikr}}{r}\right)dS\,. \tag{1}$$

Herein n is the normal vector to the surface *S* of the source and $r = |\vec{x}_S - \vec{x}_0|$ the distance between the surface position and the observation point $\vec{x}_0$.

As an appropriate geometry for the investigation a parallelepiped is chosen. The corners of the parallelepiped ensure that the condition for the validity of the Rayleigh hypothesis is violated for any source intercepting the minimal sphere. Consequently, the minimal sphere $B_1 = B$ encloses the vibrating body completely. For the sake of generality, all lengths and dimensions refer to the *x*-dimension of the source. The side lengths are given as $l_x = 1$, $l_y = l_x/3$ and $l_z = 2l_x/3$. For simplicity, this parallelepiped has a simple velocity distribution at one side and zero velocity at the other. A sinusoidal velocity distribution is applied on a source surface parallel to the x-z-plane generated by

$$v\left(x,z\right) = v_0 \cos\left(\frac{\pi x}{l_x}\right)\cos\left(\frac{\pi z}{l_z}\right), \tag{2}$$

with v_0 as velocity amplitude. This distribution suppresses velocity discontinuities at the edges. All walls of the source are assumed rigid except that one vibrating. A sketch of the test rig is shown in Figure 2 as a section at the equatorial plane. If the Kirchhoff-Helmholtz-Integral given in equation (1) is to be used for calculating the sound field

radiated from the test source, the velocity as well as the sound pressure on the surface of the source are required.

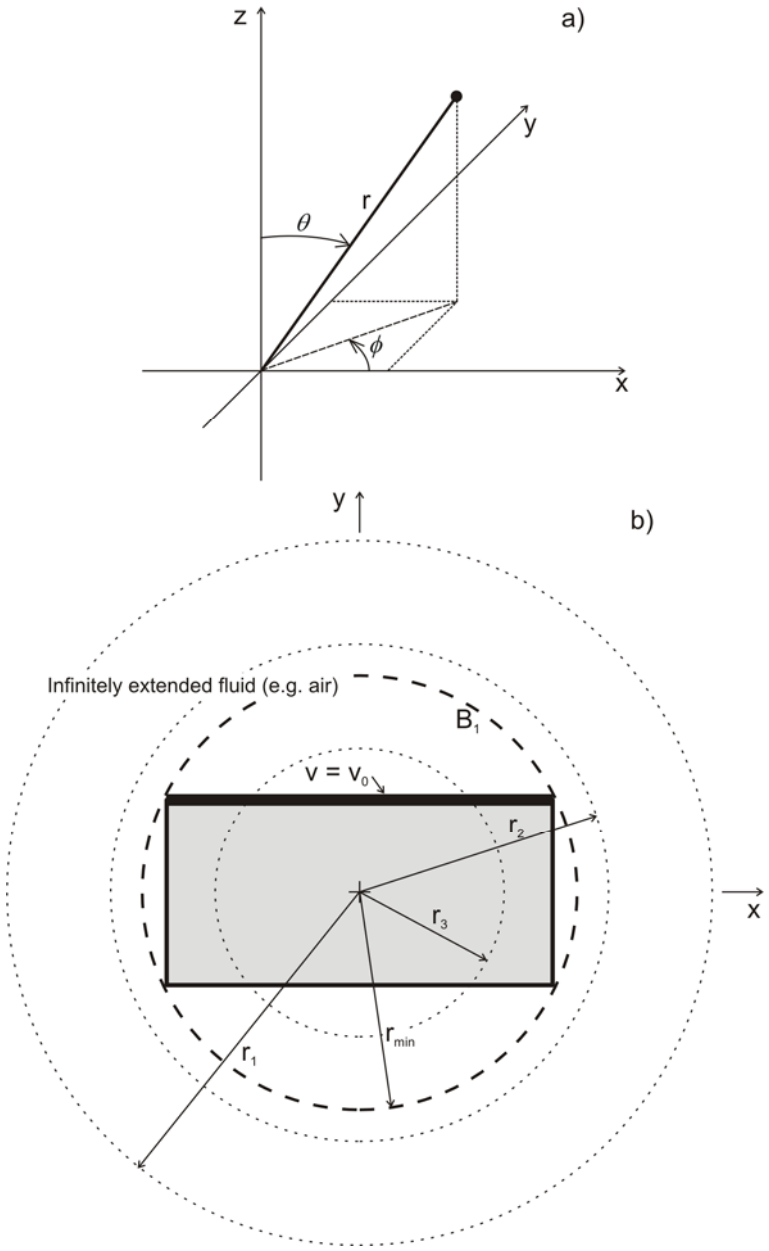

Figure 2: a) Spherical co-ordinate system. b) Virtual test rig at a section in the equatorial plane. The minimal sphere with radius $r_{\min}$ is drawn dashed.

The pressure can be calculated by employing a discretised form of the KHI. Accordingly, the source surface has to be decomposed into *N* surface elements S_j. The pres-

sure at the point $\vec{x}_0$, where $\vec{x}_0$ is a point on the source surface, can be approximated by summing over all discrete surface elements as

$$p_N(\vec{x}_0) = \sum_{j=1}^{N} A_j(\vec{x}_0) v_{n,j} + \sum_{j=1}^{N} B_j(\vec{x}_0) p_j \tag{3}$$

with

$$A_j(\vec{x}_0) = \frac{i\omega\rho_0}{2\pi} \int_{S_j} \frac{e^{-ikr}}{r} dS_j \tag{4}$$

and

$$B_j(\vec{x}_0) = \frac{1}{2\pi} \int_{S_j} \frac{\partial}{\partial n}\left(\frac{e^{-ikr}}{r}\right) dS_j \,. \tag{5}$$

This leads to a set of linear equations given by

$$(\mathbf{I} - \mathbf{B})\mathbf{p} = \mathbf{A}\mathbf{v} \tag{6}$$

where $\mathbf{I}$ is the identity matrix and $\mathbf{A}$, $\mathbf{B}$, $\mathbf{p}$ and $\mathbf{v}$ are of the forms

$$\mathbf{A} = \begin{bmatrix} A_1(x_1) & A_2(x_1) & \cdots & A_N(x_1) \\ A_1(x_2) & \ddots & & \vdots \\ \vdots & & \ddots & \vdots \\ A_1(x_N) & \cdots & \cdots & A_N(x_N) \end{bmatrix}, \quad \mathbf{B} = \begin{bmatrix} B_1(x_1) & B_2(x_1) & \cdots & B_N(x_1) \\ B_1(x_2) & \ddots & & \vdots \\ \vdots & & \ddots & \vdots \\ B_1(x_N) & \cdots & \cdots & B_N(x_N) \end{bmatrix} \text{ and}$$

$$\mathbf{p} = \begin{bmatrix} p_1 \\ \vdots \\ \vdots \\ p_N \end{bmatrix}, \quad \mathbf{v} = \begin{bmatrix} v_1 \\ \vdots \\ \vdots \\ v_N \end{bmatrix}. \tag{7}$$

For the off-diagonal elements the A_j and B_j can be calculated easily, whereas the diagonal elements have a singularity if the distance *r* between source position and obser-

vation point becomes zero. Although there are a lot of publications on solving the singularities in the BEM-literature a simple algorithm was developed to handle the problem. The integral for the off-diagonal elements can be approximated by assuming *r* constant over the surface element as

$$A_j = \frac{i\omega\rho_0}{2\pi}\frac{e^{-ikr}}{r}S_j \tag{8}$$

and

$$B_j = \frac{1}{2\pi}\frac{\partial}{\partial n}\frac{e^{-jkr}}{r}S_j . \tag{9}$$

In order to approximately calculate the diagonal elements of A_j, the rectangular surface S_j is replaced by a circular surface of the same area. By transforming the coordinate system, the integral in equation (4) changes to

$$\int_0^{2\pi}\int_0^{R} e^{-ikr}\,dr\,d\varphi = i\frac{2\pi}{k}\left(e^{-ik\sqrt{\frac{S_j}{\pi}}}-1\right), \tag{10}$$

which has no singularity. An approximate solution for the diagonal elements of A_j becomes

$$A_j = \rho_0 c\left(1-e^{-ik\sqrt{\frac{S_j}{\pi}}}\right). \tag{11}$$

The error of this approximation is below 1% for encountered values of $k\sqrt{S_j}$ compared with the exact solution of rectangular surface obtained by taking the principal value of the integral.

For calculating the diagonal elements of B_j this approximation can not be employed due to the derivative in normal direction. The derivative can be written as

$$\frac{\partial}{\partial n}\frac{e^{-ikr}}{r} = \frac{\partial r}{\partial n}\cdot\frac{\partial}{\partial r}\frac{e^{-ikr}}{r} \tag{12}$$

with

$$\frac{\partial}{\partial r}\frac{e^{-ikr}}{r} = \left(-\frac{1}{r^2} - \frac{ik}{r}\right)e^{-ikr}\,. \tag{13}$$

The distance *r* between source position $\vec{x}_S$ and observation point $\vec{x}_0$ is given by

$$r = \sqrt{\left(x_{0_x} - x_{S_x}\right)^2 + \left(x_{0_y} - x_{S_y}\right)^2 + \left(x_{0_z} - x_{S_z}\right)^2} \tag{14}$$

and one obtains

$$\frac{\partial}{\partial n}\frac{e^{-ikr}}{r} = \left(\vec{x}_0 - \vec{x}_S\right)\cdot\vec{n}\left[\frac{1}{r^3} + \frac{ik}{r^2}\right]e^{-ikr}\,. \tag{15}$$

This expression has a singularity for $\vec{x}_0 = \vec{x}_S$. Additionally, the dot product $b = \left(\vec{x}_0 - \vec{x}_S\right)\cdot\vec{n}$ goes to zero if the observation point drops on to the surface and both vectors become orthogonal.

The analytical solution of the integral is given by

$$F\left(r\right) = \int b\left[\frac{1}{r^3} + \frac{ik}{r^2}\right]e^{-ikr}dr = b\left[e^{-ikr}\left(-\frac{1}{2r^2} - \frac{ik}{2r}\right) + \frac{1}{2}k^2\,\mathrm{Ei}\left(-ikr\right)\right] \tag{16}$$

wherein $\mathrm{Ei}\left(z\right)$ is the exponential integral function. The limit for a finite and symmetrical integration interval $\left[-R, R\right]$ becomes

$$B_j = \frac{1}{2\pi}\lim_{b\to 0}\left(\left[F\left(r\right)\right]_{-R}^{R}\right) = 0 \tag{17}$$

if the dot product vanishes. Physically this integral term represents a dipole oriented perpendicular to the surface. Thus, its radiation in surface direction is zero, which corroborates the analytical consideration.

The given KHI formulations, however, does not consider the influence of the non differentiable source surface which deteriorates the accuracy of the results. For the exact determination of the radiated sound field also the simple discretisation chosen should be improved by using triangular or quadrilateral surface elements. The comparatively simple formulation presented in equation (1) to (7), nevertheless, provides results accurate enough for the present purpose. The detailed modelling of the source geometry is of subordinate relevance for comparing the radiated and the reconstructed field at different distances from the source surface.

By using equation (1) in conjunction with the known sound pressure and velocity distributions on the surface of the source, the pressure can be calculated at each field point outside the source. With this, on the one hand, a virtual measurement grid of sound pressure values can be generated. On the other hand, pressure and velocity values at arbitrary points can be used for assessing the validity of the NAH reconstruction. The main advantage of the KHI results is that these are not restricted by a minimal sphere limit like NAH.

3 Reconstruction of an acoustic field

In the following the reconstruction procedure for the acoustic field is developed. At first the formulae describing a spherical wave field are adopted to obtain the fundamentals of the Nearfield Acoustical Holography. Consider the sound radiation from an arbitrarily shaped sound source which satisfies the Helmholtz equation

$$\left(\nabla^2 + k^2\right) p = 0 \tag{18}$$

in an unbounded fluid with sound speed c and density ρ_0. The time dependence $e^{j\omega t}$ is suppressed for brevity and the spherical co-ordinates are indicated in Figure 2a). By considering only outgoing waves, the sound pressure on a sphere with the radius r can obtained as [4.1]

$$p\left(r,\theta,\phi\right) = \sum_{n=0}^{N}\sum_{m=-n}^{n} \frac{h_n^{(2)}\left(kr\right)}{h_n^{(2)}\left(kr_0\right)} P_{mn}\left(r_0\right) Y_n^m\left(\theta,\phi\right) \tag{19}$$

and the velocity accordingly as

$$v\left(r,\theta,\phi\right) = \frac{1}{i\rho_0 c}\sum_{n=0}^{N}\sum_{m=-n}^{n} \frac{h_n^{(2)\prime}\left(kr\right)}{h_n^{(2)}\left(kr_0\right)} P_{mn}\left(r_0\right) Y_n^m\left(\theta,\phi\right). \tag{20}$$

The wave field is expanded in terms of a finite series of spherical harmonics

$$Y_n^m\left(\theta,\phi\right) = \sqrt{\frac{\left(2n+1\right)\left(n-m\right)!}{4\pi\left(n+m\right)!}} P_n^m\left(\cos\theta\right) e^{im\phi}, \tag{21}$$

where $P_n^m\left(x\right)$ are the associated Legendre functions augmented by an orthonormalisation factor. The spherical Hankel functions of second kind $h_n^{(2)}\left(r\right)$ represent the outward radial propagation. $h_n^{(2)\prime}\left(r\right)$ is its derivative with respect to the argument. The series in (19) and (20) are truncated after $\left(N+1\right)^2$ expansion terms. When the source

strength $P_{mn}(r_0)$ is known, the sound pressure $p(\alpha)$ as well as the particle velocity $v(\alpha)$ with $\alpha \in D'$ can be determined at every point α in the three-dimensional sound field outside the source as well as on any point of the source surface as long as α lies outside the minimal sphere B_1.

For determining the source strength $P_{mn}(r_0)$ the sound field has to be decomposed in its spherical wave components. For a known pressure distribution on a sphere of radius r_0 the procedure can be written as

$$P_{mn}(r_0) = \int p(r_0, \theta, \phi) Y_n^m(\theta, \phi)^* \, d\Omega \tag{22}$$

where $(\ )^*$ indicates the complex conjugate and $d\Omega = \sin\theta d\theta d\phi$ is an angular element. If the sound pressure around the source is sampled at discrete positions the equation has to be discretised.

Alternatively, the wave components coefficients $P_{mn}(r_0)$ can be determined by solving a system of linear equations. By omitting the radial transform which is already included in the back transformation, equation (19) is modified to

$$p(r, \theta, \phi) = \sum_{n=0}^{N} \sum_{m=-n}^{n} P_{mn}(r) Y_n^m(\theta, \phi). \tag{23}$$

By merging the indices to $i = n^2 + n + m + 1$ and neglecting the r-dependence, $P_{mn}(r)$ converts to ψ_i. For the angular position (r, θ, ϕ) substituted by $\vec{\alpha}$ the equation simplifies to

$$p(\vec{\alpha}) = \sum_{i=1}^{I} \psi_i Y_i(\vec{\alpha}) \tag{24}$$

with $I = (N+1)^2$. For a number of J grid points at $\vec{\alpha}_j, j = 1 \ldots J$ the equation can be written in matrix form

$$\begin{bmatrix} p(\vec{\alpha}_1) \\ \vdots \\ p(\vec{\alpha}_J) \end{bmatrix} = \begin{bmatrix} Y_1(\vec{\alpha}_1) & \cdots & Y_1(\vec{\alpha}_J) \\ \vdots & \ddots & \vdots \\ Y_I(\vec{\alpha}_1) & \cdots & Y_I(\vec{\alpha}_J) \end{bmatrix} \cdot \begin{bmatrix} \psi_1 \\ \vdots \\ \psi_I \end{bmatrix} \tag{25}$$

or short

$$\mathbf{p} = \mathbf{Y} \cdot \boldsymbol{\psi} . \tag{26}$$

The wave expansion coefficients $\boldsymbol{\psi}$ are determined by least square fitting the equation (26) to the data $\mathbf{p}$ determined e.g. from the test set up. The least square fit is applicable if the equation is over-determined or quadratic. Otherwise equation (26) has to be solved by singular value decomposition (SVD).

Table 1: First 16 NAH expansion coefficients calculated with either integral method or least square method ($N = 12$, $kl_x = 4$).

n	*m*	*Integral (eq. (22))*	*Least Square (eq. (26))*
0	0	72,106 + 1,548i	72,069 + 1,548i
1	-1	0,315 + 15,914i	0,315 + 15,914i
1	0	0,002 - 0,012i	0
1	1	0,315 + 15,913i	0,315 + 15,914i
2	-2	-0,516 + 0,0248i	-0,516 + 0,0248i
2	-1	-0,001	0
2	0	-0,712 - 0,038i	-0,637 - 0,004i
2	1	0,001 + 0,001i	0
2	2	-0,516 + 0,024i	-0,516 + 0,024i
3	-3	0,002 + 0,073i	0,002 + 0,073i
3	-2	0	0
3	-1	0,001 - 0,004i	0 - 0,003i
3	0	-0,013 + 0,012i	0
3	1	-0,002 - 0,002i	0 - 0,003i
3	2	0	0
3	3	0,002 + 0,073i	0,002 + 0,073i

Table 1 shows the first 16 coefficients $P_{mn}\left(r_1 = 7l_x\right)$ for the test set-up calculated with either the integral formula (22) or the least square method (26). The configuration of the set up is detailed in Section 2. By comparing the results it can be seen that both methods deliver essentially the same results for the significant source components. This trend does not change also if the input data are distorted by adding random noise up to an SNR of 40 dB. For the investigations presented, the least square method has been employed.

It is worth noticing that the design of the sample grid determines the upper frequency limit of the NAH procedure. Commonly, the sound field is sampled at the crossings of a uniform longitude-latitude grid. The main disadvantage of this design is that the lattice points lie much denser near the poles than in the equatorial region. Especially for a limited number of microphones, such a point distribution is not suitable for the NAH application, bearing in mind that the number of sampling points defines an upper limit of the useful frequency range. In Ref. [4.12] an algorithm is presented to compute optimal facility locations on the unit sphere with high accuracy and an appropriate algorithm to calculate the corresponding weighting factors for application in equation (22). The algorithm aims at a minimisation of the maximum distance between adjacent grid points. The result of this procedure is a grid of sampling points with a better utilisation of the number of microphones available which increases the upper frequency limit by a factor of two [4.13], [4.14].

4 Shrinking of the reconstruction surface

The results of the NAH-reconstructed sound field, calculated from KHI-generated virtual measurements and the KHI-sound field results agree as long as $r_2 > \sqrt{(l_x/2)^2 + (l_y/2)^2 + (l_z/2)^2}$. Fulfilling this condition, the field is reconstructed outside the minimal sphere B_1. Figure 3 shows the results. For the calculation the pressure values are measured at 144 equally spaced microphone positions on a spherical surface of radius $r_1 = 7l_x$ and the sound field is reconstructed on radius $r_2 = 2l_x/3$ (see Figure 2).

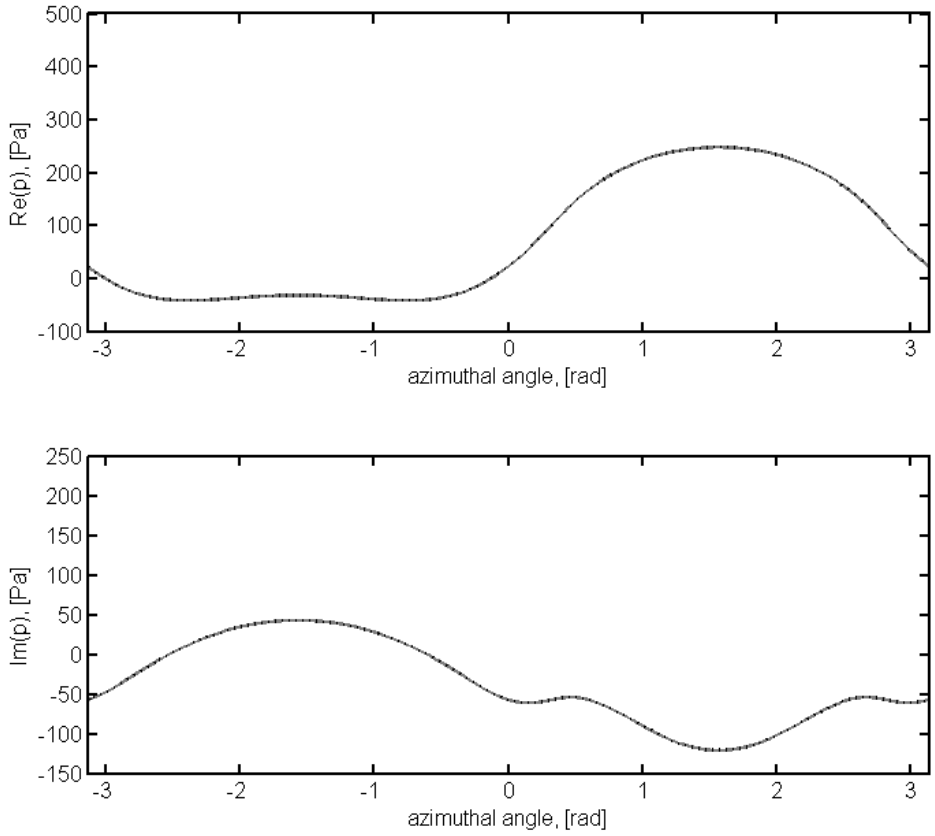

Figure 3: Reconstructed sound pressure (····) along a circle at the equator ($\theta = \pi/2$) of radius $r_2 > r_{\min}$ compared with the Kirchhoff-Helmholtz-Integral (—) result. ($kl_x = 4$, $r_2 = 0.66l_x$, $N = 12$)

If the condition for the Rayleigh hypothesis is violated by intercepting the test source at its edges with a reconstruction surface of radius $r_3 < \sqrt{(l_x/2)^2 + (l_y/2)^2 + (l_z/2)^2}$ an oscillation effect can be observed. As depicted in Figure 4 for $r_3 = 0.46 l_x$, the curve of the reconstructed field starts to oscillate around the true value. This oscillation becomes more significant, for smaller radii of the reconstruction surface. As expected, the solution does not converge if there are singularities in the field between measurement surface and reconstruction surface.

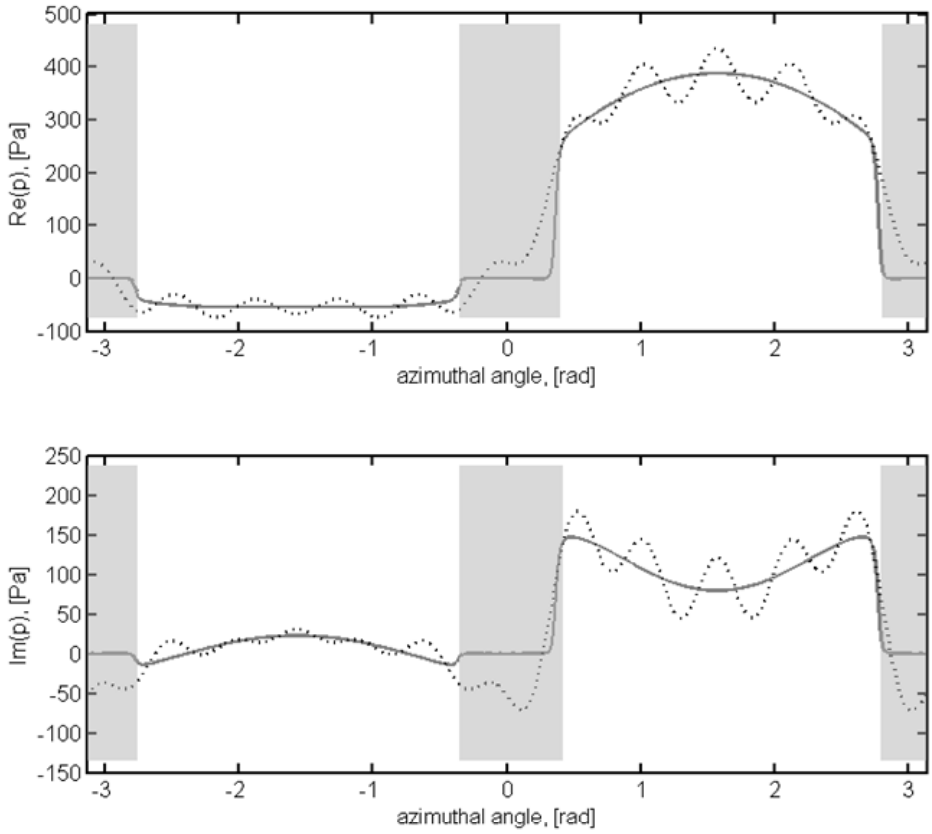

Figure 4: Comparison of sound pressures reconstructed from NAH (····) with actual values (KHI) (—) on $r_3 < r_{\min}$. Intercepted parts are marked grey. ($kl_x = 4$, $r_3 = 0.46 l_x$, $N = 12$)

This is also consistent with Ref. [4.15]. There it is shown that the partial wave expansion as given in equation (19) diverges for any point inside B_1. Although it is inherently impossible to obtain accurate local information (point values), as is evident from Figure

4, the solution contains the features of the global behavior. This corresponds to the propositions made in Ref. [4.10] regarding scattering. It is shown that the velocity reconstruction converges at least overall but not pointwise on the source surface for any obstacle shape.

Granted that there is a possibility to extract information about the field also from the non convergent description, the solution in the region inside B_1 can be improved at least for limited interceptions. If the non-convergent series, which in fact contains enough information about the true field, can be converted to a convergent series retaining the same information, the global information can be extracted such that the field can be reconstructed for any point.

In its broadest sense the convergence problem described is analogous to Gibbs phenomenon. Although the cause of Gibbs phenomenon is different, the problem resulting in the jump discontinuities is comparable to the NAH singularity problem. Thus it is expected that a resolution of the Gibbs phenomenon can be applied successfully also for the present problem. Such a resolution for problems in spherical co-ordinates is presented in Refs. [4.16] and [4.17]. It is based on converting the underlying regular Sturm-Liouville problem to a singular Sturm-Liouville problem, which converges rapidly. Assuming that the first $\left(N+1\right)^2$ coefficients of the spherical wave expansion can provide enough information to reconstruct the coefficients of an expansion based on a singular Sturm-Liouville problem, the prediction might be improved. This can be done by constructing a Gegenbauer expansion based on the known first few spherical harmonic coefficients. The convergence of the Gegenbauer series has been shown to be exponentially converging on any subinterval for which the function described by the harmonic coefficients is analytic [4.18]. The latter condition is fulfilled at least if one handles those sub-areas separately where the intercepting reconstruction surface is outside the source and which do not include singularities. A detailed mathematical proof is given elsewhere [4.16], [4.17] and will not be part of this paper. In the expansion, the Gegenbauer polynomials [4.19] $C_n^{(\alpha)}\left(x\right)$ for $\alpha \geq 0$ are orthogonal within the interval $\left[-1,1\right]$ with the weighting function $\left(1-x^2\right)^{\alpha-1/2}$. The goal is to recover the sound pressure $p\left(\theta,\phi\right)$ for ϕ in the subinterval $\left[\phi_1,\phi_2\right] \subset \left[0,2\pi\right]$ and a fixed $\theta_{const} \in \left[0,\pi\right]$. Adapted to the spherical problem, the Gegenbauer partial sum is defined by

$$\tilde{p}_m^{(\alpha)}\left(\theta_{const},\phi\right)=\sum_{l=0}^{m}\gamma^{(\alpha)}\left(l\right)C_l^{(\alpha)}\left(\xi\right). \tag{27}$$

For a pressure distribution $p_N\left(\theta,\phi\right)$, calculated using equation (19) up to the order $N<\infty$, the first m Gegenbauer coefficients are obtained from

$$\gamma^{(\alpha)}\left(l\right)=\frac{1}{\Psi_l^{\alpha}}\int_{-1}^{1}\left(1-\xi^2\right)^{\alpha-\frac{1}{2}}C_l^{(\alpha)}\left(\xi\right)p_N\left(\varepsilon\xi+\delta,\theta_{const}\right)d\xi \tag{28}$$

with the normalisation constants

$$\Psi_n^{\alpha}=\pi^{\frac{1}{2}}C_n^{(\alpha)}\left(1\right)\frac{\Gamma\left(\alpha+1/2\right)}{\Gamma\left(\alpha\right)\left(n+\alpha\right)} \tag{29}$$

and $0\le m\le N$ and $0\le\alpha\le N$. The parameters α and m should be optimized to reduce the error of the procedure. Details about the optimisation process are published elsewhere [4.16]. In the investigations presented the parameters have been set to $m=\alpha=N/4$ according to Ref. [4.16]. Note, that the result of the Gegenbauer expansion $\tilde{p}_m^{(\alpha)}$ is the new sound pressure field.

The angle ϕ in the subinterval $\left[\phi_1,\phi_2\right]$ has been transformed to ξ in $\left[-1,1\right]$. The relation between the local variable ξ and the angle ϕ with $\phi_1<\phi_2$ is defined by

$$\xi\left(\phi\right)=\frac{\phi-\delta}{\varepsilon} \tag{30}$$

with

$$\varepsilon=\frac{\phi_2-\phi_1}{2} \tag{31}$$

and

$$\delta=\frac{\phi_2+\phi_1}{2}. \tag{32}$$

The same scheme can be applied for θ in lateral direction for constant ϕ. Fully analogous, the velocity field $v_N(\theta,\phi)$ can be treated. The process is repeated for each closed subset of the reconstruction surface outside the source and free of singularities. Consequently, each subset gets its own set of Gegenbauer coefficients. It is worth mentioning that the procedure described is computationally reliable also when N is small.

5 Numerical example

Consider the radiation problem outlined in Section 2. The task is to reconstruct the acoustic field variables at points close to or on the source surface, starting from measurements of the sound pressure on a spherical measurement grid of radius $r_1 = 7l_x$. For a parallelepiped with a sinusoidal velocity distribution on one *x*-*z*-surface as described, the radiated sound pressure at the grid is calculated using the Kirchhoff-Helmholtz-Integral.

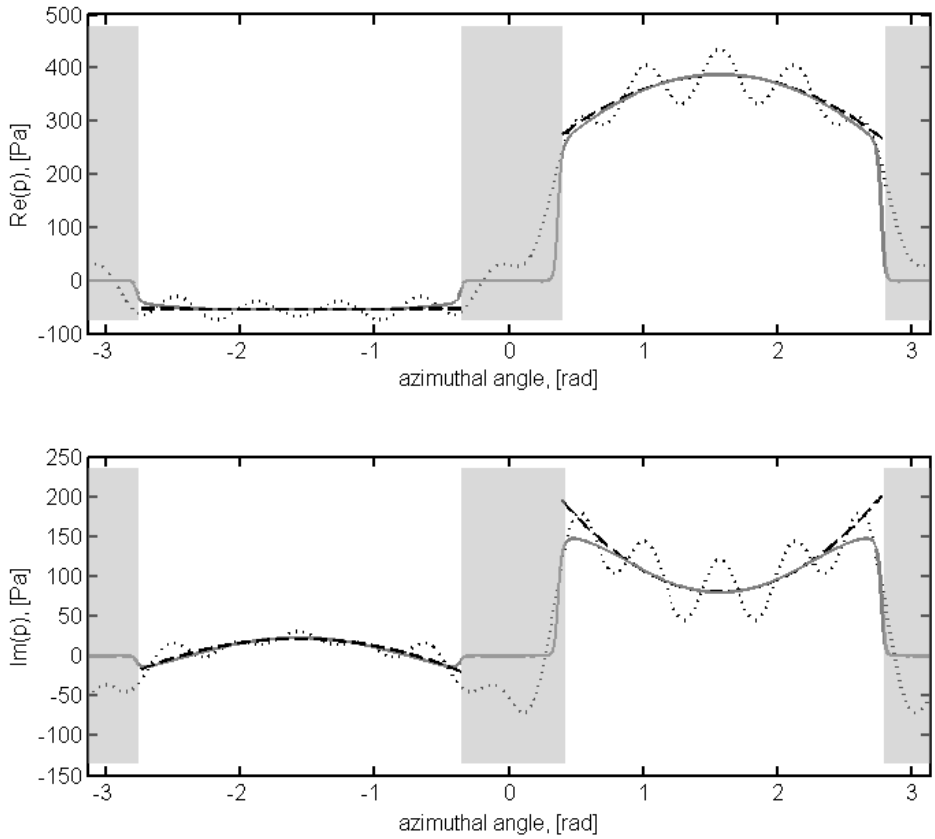

Figure 5: Comparison of sound pressures reconstructed from NAH with Gegenbauer correction (---) and without (····) with actual values (KHI) (—) on $r_3 < r_{\min}$. *Intercepted parts are marked grey. (*$kl_x = 4$, $r_3 = 0.46l_x$, $N = 12$*)*

For points on a closed subset of the reconstruction surface inside the minimal sphere but outside the source, the reconstruction has been performed in the following steps:

Step 1: The sound field is expanded in a truncated series of N spherical harmonic wave components. For the results shown in the following, the solution of the system of linear equations as described in equation (26) was used. An equally spaced measurement grid as described in Ref. [4.12] is used.

Step 2: By using equations (19) or (20) the sound field variables are reconstructed on a circular arc of radius r and fixed longitude or latitude respectively. The curve described by the arc must not intercept the source at any point. No singularities are on the curve.

Step 3: The dependent angle on the latitude or longitude interval is transformed to an interval $[-1,1]$ using equations (30) to (32).

Step 4: The $p_N(\theta,\phi)$ or $v_N(\theta,\phi)$ are expanded as truncated series of Gegenbauer polynomials. The resulting series converges exponentially.

The results shown in Figure 5 are calculated for the test rig sketched in Figure 2. The reconstructed sound pressure is depicted for a circle at the equatorial plane of radius $r_3 = 0.46 l_x$. Due to the interception, the Gegenbauer polynomial expansion is undertaken for two subintervals. To avoid any influence of symmetries of the test rig, in Figure 6 the results are also presented for a plane at slightly elevated latitude. As can be seen, the results are comparable to those of Figure 5. The curves show that the additional Gegenbauer polynomial expansion approximation eliminates the oscillation in each subinterval. With a maximum order of spherical wave components of $N = 12$, only 3 Gegenbauer coefficients are used for the approximation. The deviation of the approximation at the ends of each subinterval depends on the number of coefficients used. It is expected that a higher number of coefficients will improve the accuracy of the approximation. This improvement can be seen in Figure 7 for $N = 16$, which allows the use of 4 Gegenbauer coefficients. Hence, the approximation becomes more and more accurate the higher the number of useful wave components. It is worth noticing that by increasing the frequency as additionally shown in Figure 7, the oscillation effect diminishes. For the results shown in Figure 8 the measurement data for a set-up as used above are distorted by adding of random noise, with a signal-noise-ratio of 40 dB. This leads to a mathematically ill posed problem. To get stable results, thus, the maximum order of wave components has to be reduced to $N = 9$. Again, 4 Gegenbauer coeffi-

cients are used. By considering these constraints it is assumed that the least square fit used for determining the expansion coefficients as well as the Gegenbauer expansion are appropriate under practical conditions.

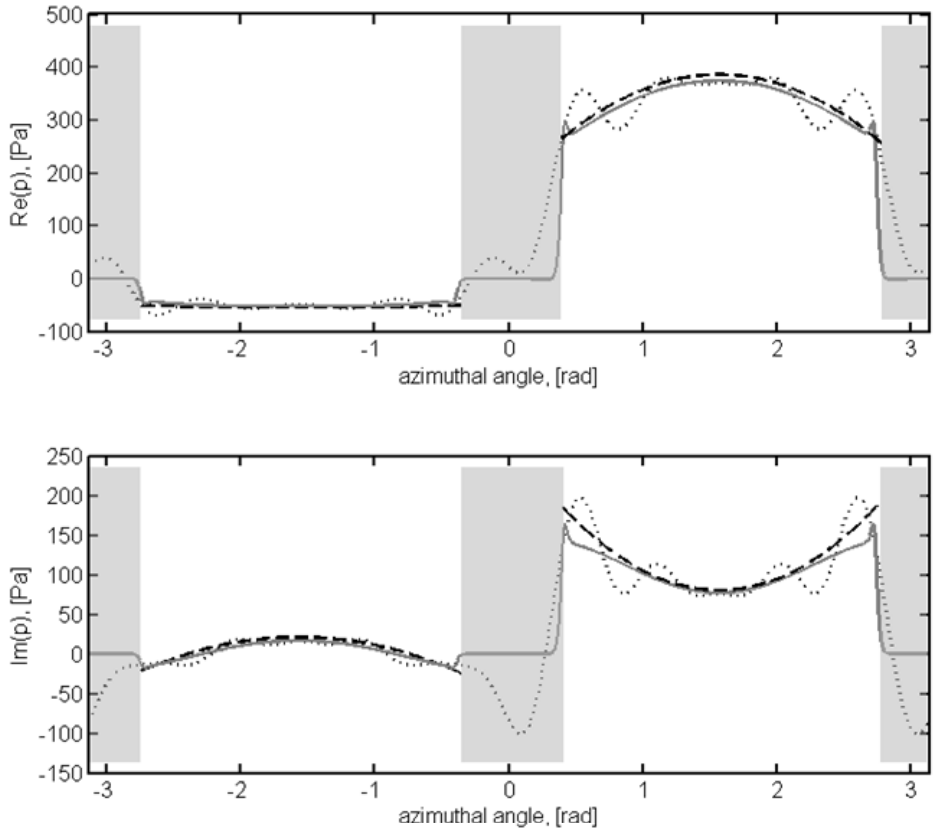

Figure 6: Comparison of sound pressures reconstructed from NAH with Gegenbauer correction (---) and without (····) with actual values (KHI) (—) on $r_3 < r_{\min}$. *Intercepted parts are marked grey.* ($kl_x = 4$, $r_3 = 0.46 l_x$, $N = 12$, $\theta = \pi/2 + 0.1$)

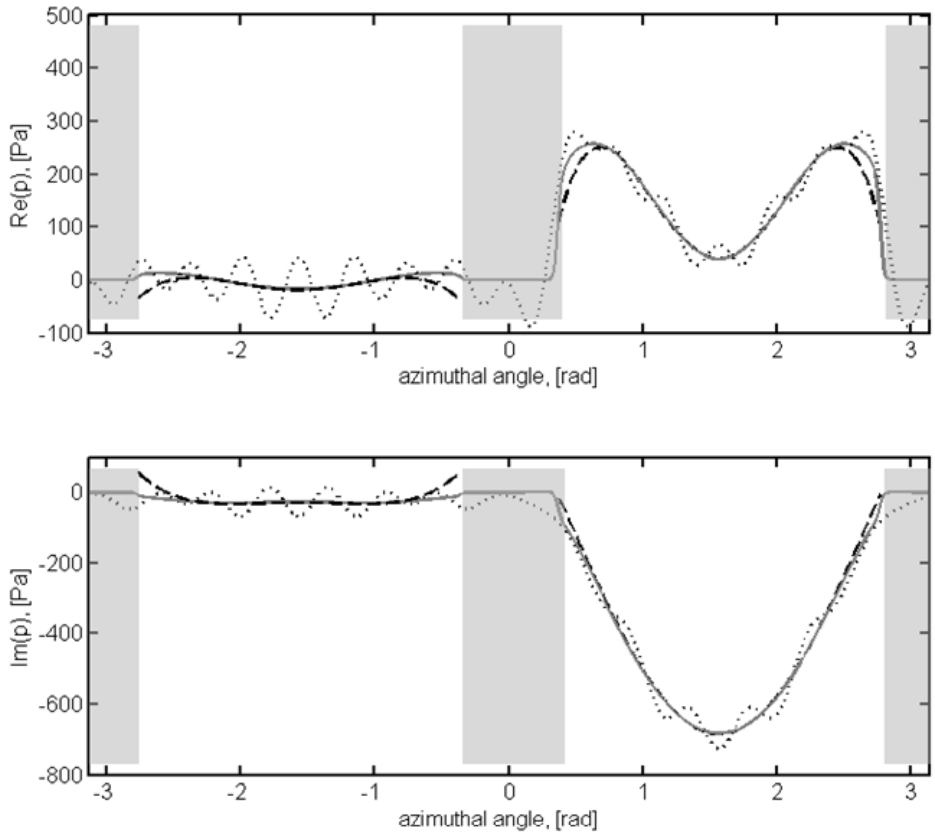

Figure 7: Comparison of sound pressures reconstructed from NAH with Gegenbauer correction (---) and without (····) with actual values (KHI) (—) on $r_3 < r_{\min}$. *Results are shown for an enlarged wave number range and a high number of wave components included. Intercepted parts are marked grey. (*$kl_x = 8$, $r_3 = 0.46 l_x$, $N = 16$*)*

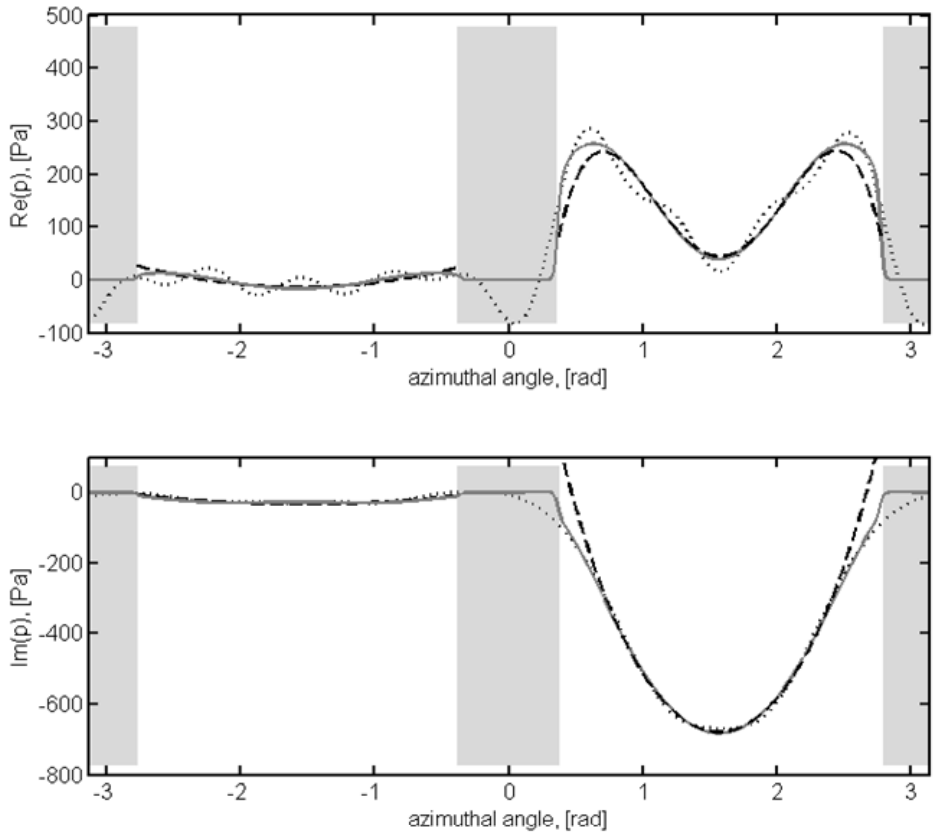

Figure 8: Comparison of sound pressures reconstructed from NAH with Gegenbauer correction (---) and without (····) with actual values (KHI) (—) on $r_3 < r_{\min}$. *Noise is added to the input data with a SNR of 40 dB. Intercepted parts are marked grey. (*$kl_x = 8$, $r_3 = 0.46 l_x$, $N = 9$*)*

6 Concluding remarks

A method is proposed to overcome the problems arising from singularities in conjunction with NAH sound field reconstruction in spherical co-ordinates. The occurrence of the singularities depends on the shape of the vibrating body and leads to a non-convergent solution of the field expansion. An oscillation of the reconstructed sound field variable around the true value arises. It is shown, however, that the incomplete solution contains enough information to recover the sound field approximately. By using a truncated series of Gegenbauer polynomials, the non-convergent spherical harmonic expansion from the NAH solution can be transformed to a rapidly convergent series. The oscillation is 'filtered' and the global information is used for an approximate reconstruction of the field over partial surfaces.

Based on the numerical analysis undertaken, it is argued that the method proposed is limited to high interception ratios. The interception ratio is defined as the ratio of reconstruction surface outside the source to the overall surface of the reconstruction sphere. This means that the method may fail when the interception ratio becomes too small. An improved prediction at the limits of each sub interval of the Gegenbauer expansion can be achieved with an increased number of wave components N included. An optimisation of N seems to be necessary as well as an investigation of the minimum interception ratio. All these limitations are frequency dependent and depend also on the character of the underlying radiation problem. For engineering practice, one can speculate that the smoother the source shape and the field distribution the less likely is the presence of singularities and the more accurate is the reconstruction as well as the approximation.

7 References

[4.1] M. Ochmann, “The Source Simulation Technique for Acoustic Radiation Problems,” Acustica **81**, 512-527 (1995).

[4.2] Lord Rayleigh, “On the Dynamical Theory of Gratings,” Proc. Roy. Soc., Ser. A **79**, 399-416 (1907).

[4.3] R. F. Millar, “The Rayleigh hypothesis and a related least-square solution to scattering problems for periodic surfaces and other scatterers,” Radio Science **8**, 785-796 (1973).

[4.4] P. M. van den Berg and J. T. Fokkema, „The Rayleigh Hypothesis in the Theory of Diffraction by a Cylindrical Obstacle,“ IEEE Trans. Ant. Prop. **AP-27**, 577-583 (1979).

[4.5] D. N. Ghosh Roy and E. G. Williams, “The Rayleigh Hypothesis and Near-Field Acoustical Holography,” Proc. 17th ICA, Rome, 2001.

[4.6] Z. Wang and S. F. Wu, “Helmholtz equation-least-square method for reconstructing the acoustic pressure field,” J. Acoust. Soc. Am. **102**, 2020-2032 (1997).

[4.7] E. G. Williams, *Fourier Acoustics, Sound Radiation and Nearfield Acoustical Holography*. (Academic Press, Inc., 1999).

[4.8] W. A. Veronesi and J. D. Maynard, “Digital holographic reconstruction of source with arbitrarily shaped surfaces,” J. Acoust. Soc. Am. **85**, 588-598 (1989).

[4.9] S. F. Wu, “On reconstruction of acoustic pressure fields using the Helmholtz equation least squares method,” J. Acoust. Soc. Am. **107**, 2511-2522 (2000).

[4.10] A. G. Ramm, “Modified Rayleigh conjecture and applications,” J. Phys. A **35**, L357-L361 (2002).

[4.11] A. D. Pierce, *Acoustics: An introduction to its physical principles and applications*. (McGraw-Hill, 1981).

[4.12] J. Fliege and U. Maier, "A Two-Stage Approach for Computing Cubature Formulae for the Sphere," Ergebnisberichte Angewandte Mathematik, No. 139T. Fachbereich Mathematik, Universität Dortmund, 44221 Dortmund, Germany, (1996). An online version is available at <www.mathematik.uni-dortmund.de/lsx/research/projects/fliege/nodes/nodes.html > (Last viewed on April 12, 2007).

[4.13] M. Taylor, “Cubature for the Sphere and the Discrete Spherical Harmonic Transform,” SIAM Journal of Numerical Analysis, **32**, No. 2, 667-670 (1995).

[4.14] R. Duraiswami and D. Zotkin and Z. Li and E. Grassi and N. Gumerov and L. Davis, “System for Capturing of High Order Spatial Audio using Spherical Microphone Array and Binaural Head-Tracked Playback over Headphones with Head Related Transfer Function cues,” Convention Paper presented at the AES 119th Convention, New York (2005).

[4.15] D. Colton and R. Kress, *Inverse Acoustic and Electromagnetic Scattering Theory*. (Springer Verlag, 1992).

[4.16] A. Gelb, “The Resolution of the Gibbs Phenomenon for Spherical Harmonics,“ Mathematics of Computation, **66**, No. 218, 699-717, (1997).

[4.17] D. Gottlieb and C. Shu, “On the Gibbs Phenomenon and its Resolution,” SIAM Rev. **39,** No. 4, 644-668, (1997).

[4.18] D. Gottlieb and C. Shu, “On the Gibbs Phenomenon IV: Recovering Exponential Accuracy in a Subinterval from a Gegenbauer Partial Sum of a Piecewise Analytic Function,” Mathematics of Computation, **64**, No. 211, 1081-1095, (1995).

[4.19] M. Abramowitz and I. A. Stegun, *Handbook of Mathematical Functions*. (Dover Publications, Inc., 1965).

Concluding remarks

In the study presented different aspects are investigated of sound propagation inside a partially open enclosure densely packed with active and passive installations. Primarily the work is aimed at predicting the sound field at the interfaces of the enclosure to the adjacent fluid space to ensure a subsequent modelling of sound radiated from the system. The prediction procedure is subdivided into the description of the sound sources inside the enclosure and the prediction of the transfer impedance linking the sound sources to the sound field at the interface to the adjacent fluid.

Depending on the relation between wavelength and the geometrical dimension of the system the sound field structure inside the enclosure is found to vary markedly with frequency. Consequently, three distinct frequency ranges are distinguished: At low frequencies the field is quasi statically and can be described as lumped system. It is shown that the acoustic behaviour is mainly affected by the free fluid volume and the mass plugs at the openings. At intermediate frequencies a modal behaviour arises. Distinct eigenfrequencies occur. At high frequencies the modal density rises and the field is increasingly diffuse. Statistical analysis tools like SEA become applicable.

The SEA modelling, which presumes diffuse field conditions, is supplemented by an approach including the influence of source and receiver positions close to boundaries or field discontinuities. Therefore a correction based on spherical Bessel functions is included in the SEA. This correction considers the first order reflections by including the corresponding image sources. It is also shown that this approach is applicable for structure-borne sound on a simply supported plate. By using the first order image source correction the results of the SEA modelling are substantially improved compared to an elementary SEA calculation.

From testing the applicability of common analysis tools it is shown a lack of appropriate analysis tools for the intermediate frequency range, which also provide information about the reliability of the analysis results. Two novel approaches are presented to predict the sound field in a frequency region of low modal density. The approaches are based on probabilistic descriptions of the system geometry, which appear promising with regard to the engineering practice.

It is shown that the “spine” of the acoustical behaviour can be extracted by either modelling the remaining free fluid space or the installations inside the enclosure. Although

the validity limitations of the approaches presented are different, both approaches produce similar results in the frequency region where the modal behaviour first occurs. At those frequencies, consistently, a local maximum in the “spine” curve is observed. The phase of the transfer impedance is shown to be dependent only on the shortest distance between source and receiver position.

Strategies are presented for integrating the sound sources into the modelling. It is revealed, that beside the fact that the position of the source is relevant in the statistical range at high frequencies, the correlation between different sources inside the enclosure is not negligible. For the coupling between source characterisation and sound propagation it is suggested to use a decomposition of complex shaped sound sources into multipoles of different order. The decomposition in terms of spherical Nearfield Holography (NAH), however, is found to be limited to simple, nearly spherical, source geometries. For complex shaped sound sources, not fulfilling the validity conditions of the Rayleigh hypothesis a method using a truncated series of Gegenbauer polynomials is proposed to overcome the problems arising from singularities in the sound field.

Different investigations are used to assess the validity as well as the applicability of the approaches presented. The findings on the salient physics are verified by comparing analytical results with those of a dedicated experiment. The validity of the simplifications is demonstrated by comparing the results with those measured in an engine compartment of a passenger car. Consistently, the same salient physical behaviour is revealed for the simplified model and the full-scale assembly. The validity and applicability of the probabilistic approaches describing the sound field at intermediate frequencies is demonstrated by comparing the results with those from a numerical calculation using FEM.

In the work presented, a set of tools is offered, which is aimed mainly at the requirements of the design engineer for calculating the sound field parameter and, in addition, predicting the reliability of the results. All tools used were selected or designed with a view towards a minimal calculation effort.